

Some pages of this thesis may have been removed for copyright restrictions.

If you have discovered material in AURA which is unlawful e.g. breaches copyright, (either yours or that of a third party) or any other law, including but not limited to those relating to patent, trademark, confidentiality, data protection, obscenity, defamation, libel, then please read our [Takedown Policy](#) and [contact the service](#) immediately

COALESCENCE OF SECONDARY DISPERSIONS.

by

David George Austin

A thesis submitted to the University of Aston  
in Birmingham for the degree of Doctor of Philosophy.

Department of Chemical Engineering  
The University of Aston in Birmingham.

# COALESCENCE OF SECONDARY DISPERSIONS

## SUMMARY

A thesis submitted by David George Austin to the Faculty of Engineering, University of Aston in Birmingham, for the Degree of Doctor of Philosophy. March 1979.

A study has been made of the coalescence of secondary dispersions in beds of woven meshes. The variables investigated were superficial velocity, bed depth, mesh geometry and fibre material; the effects of presoaking the bed in the dispersed phase before operation were also considered.

Equipment was designed to generate a 0.1% phase ratio toluene in water dispersion whose mean drop size was determined using a Coulter Counter. The coalesced drops were sized by photography and a novel holographic technique was developed to evaluate the mean diameter of the effluent secondary drops.

Previous models describing single phase flow in porous media are reviewed and it was found that the experimental data obtained in this study is best represented by Keller's equation which is based on a physical model similar to the internal structure of the meshes.

Statistical analysis of two phase data produced a correlation, for each mesh tested, relating the pressure drop to superficial velocity and bed depth.

The flow parameter evaluated from the single phase model is incorporated into a theoretical comparison of drop capture mechanisms which indicated that direct and indirect interception are predominant. The resulting equation for drop capture efficiency is used to predict the initial, local drop capture rate in a coalescer.

A mathematical description of the saturation profiles was formulated and verified by average saturation data. Based on the Blake-Kozeny equation, an expression is derived analytically to predict the two phase pressure drop using the parameters which characterise the saturation profiles. By specifying the local saturation at the inlet face for a given velocity, good agreement between experimental pressure drop data and the model predictions was obtained.

Key Words :

Coalescence, Holography  
Porous Media, Pressure Drop,  
Secondary Dispersion.

ACKNOWLEDGEMENTS.

The author would like to express his gratitude to:-

Professor G.V.Jeffreys, my supervisor and colleague, for his invaluable help and guidance throughout the project and for providing the facilities for this research.

The members of the Technical Staff of the Department of Chemical Engineering.

The Science Research Council for providing a scholarship during the first year of the project.

Mrs.Marie E. Haddleton for competently typing the thesis.

DEDICATED TO  
ONE OF MY STUDENTS.

<u>CHAPTER 1</u>	<u>INTRODUCTION</u>	1
<u>CHAPTER 2</u>	<u>FORMATION OF SECONDARY DISPERSIONS.</u>	4
2.1	Introduction.	5
2.2	Theory of Dispersion formation.	5
2.2.1	Subdivision of a bulk phase.	8
2.2.2	Formation by nucleation and growth.	10
2.3	Preparation of secondary dispersions.	10
2.3.1	Critical emulsification.	11
2.3.2	Emulsification by condensation.	11
2.3.3	Emulsification by mechanical dispersion.	13
2.3.4	Recently developed techniques.	17
2.4	Industrial occurrence of secondary dispersions.	19
2.4.1	Effluent from ocean going ships.	19
2.4.2	The oil industry.	20
2.4.3	Miscellaneous sources.	21
<u>CHAPTER 3</u>	<u>SEPARATION OF SECONDARY DISPERSIONS.</u>	22
3.1	Stability of secondary dispersions.	23
3.2	Treatment of secondary dispersions.	24
3.2.1	Chemical coagulation.	24
3.2.2	Centrifugation.	25
3.2.3	Electrostatic coalescers.	26
3.2.4	Heating	27
3.2.5	Air flotation	27
3.2.6	Coalescence in Porous Media	28
<u>CHAPTER 4</u>	<u>COALESCENCE IN FIBROUS BEDS.</u>	30
4.1	Effect of operating conditions.	31
4.2	System characteristics.	34

<u>CHAPTER 5</u> <u>MECHANISMS OF DISPERSION COALESCENCE.</u>	39
5.1 Introduction.	40
5.2 Drop Capture	40
5.2.1.1. Indirect interception.	42
5.2.1.2. Hydrodynamic retardation.	46
5.2.2. Direct interception.	47
5.2.3. Inertial impaction.	48
5.2.4. Sedimentation.	49
5.2.5. London-Van der Waal's forces.	49
5.2.6. Electrical double layer forces.	51
5.2.7. Diffusion.	53
5.3 Coalescence Processes.	55
5.3.1. Coalescence sites.	55
5.3.2. Drop passage through interstices.	57
5.4 Dispersed phase flow regime.	60
5.4.1. Drop redispersion.	60
5.4.2. The travelling drop hypothesis.	62
5.4.3. Critical drop diameter.	63
5.4.4. Dispersed phase continuum model.	64
5.5 Saturation profiles.	65
5.6 Exit drop release.	68
<u>CHAPTER 6</u> <u>EXPERIMENTAL WORK.</u>	71
6.1 Equipment design.	72
6.2 Coalescer design.	77
6.3 Packing selection and preparation.	85
6.4 Liquid system description.	91
6.5 Pressure drop measurement.	92
6.6 Operating procedure.	93
6.7 Average saturation determination.	95
6.8 Experimental design.	95
6.8.1. Mesh properties.	96
6.8.2. Operating conditions.	98

<u>CHAPTER 7</u>	<u>DETERMINATION OF DROP SIZE DISTRIBUTIONS</u>	100
7.1	Introduction.	101
7.2	Analysis of the effluent primary dispersion.	101
7.3	Characterisation of the inlet dispersion.	102
7.4	Effluent secondary dispersion.	107
7.5	The holographic technique.	108
7.5.1	'Off-axis' holography.	108
7.5.2	'In-line' holography.	109
7.6	Hologram recording.	111
7.6.1	The light source.	111
7.6.2	Test section design.	116
7.6.3	Selection of photographic recording material	118
7.7	Development of holograms.	120
7.8	Hologram reconstruction.	121
7.9	Data acquisition.	125
<u>CHAPTER 8</u>	<u>EXPERIMENTAL RESULTS.</u>	128
8.1	Inlet drop size.	128
8.2	Coalesced drop size.	129
8.2.1	Stainless steel meshes.	129
8.2.2	Nylon meshes.	132
8.2.3	Observation of drop release sites.	136
8.2.4	Effluent secondary drops.	139
8.3	Separation efficiency.	141
8.4	Average saturation data.	144
<u>CHAPTER 9</u>	<u>ANALYSIS OF PRESSURE DROP DATA.</u>	148
9.1	Single phase flow pressure drop.	149
9.2	Fluid flow equations.	151
9.3	Analysis of single phase pressure drop data.	155
9.4	Comparison of single phase flow models.	156

9.5 Transient pressure drop.	161
9.6 Two phase pressure drop.	167
9.7 Quantitative analysis of data.	174
<u>CHAPTER 10 MODEL OF DISPERSION COALESCENCE.</u>	176
10.1 Prediction of filter coefficient.	177
10.1.1. Vinson and Churchill equation.	177
10.1.2. Spielman and Goren equation.	177
10.1.3. Sherony and Kintner equation.	179
10.1.4. Rosenfeld and Wasan equation.	180
10.2 Theoretical comparison of capture mechanisms.	181
10.3 Rate of drop capture.	190
10.4 Formulation of a mathematical model.	193
10.4.1. Preliminary considerations.	193
10.4.2. Mathematical description of saturation profiles.	199
10.5 Two phase pressure drop prediction.	202
10.5.1. Previous models.	202
10.5.2. Derivation of proposed equation.	203
10.6 Testing the model.	207
10.6.1. Evaluation of parameters from saturation data.	207
10.6.2. Comparison with experimental data.	207
10.7 Queueing drop model.	211
10.7.1. Derivation of queue length equation.	211
10.7.2. Filter coefficient.	216
<u>CONCLUSIONS.</u>	222
<u>RECOMMENDATIONS FOR FURTHER WORK.</u>	228

APPENDIX A.	Determination of the Hamaker constant.	232
APPENDIX B.	Calculation of critical diameter for drop release.	233
APPENDIX C.	Equipment design.	236
APPENDIX D.	Properties of Packing Materials.	239
APPENDIX E.	Physical properties of liquid system.	245
APPENDIX F.	Average saturation determination.	250
APPENDIX G.	Hologram development procedure and processing solutions.	252
APPENDIX H.	Tabulated experimental data.	253
APPENDIX I.	Derivation of algorithm for tortuosity factor.	261
APPENDIX J.	Computer program for analysis of single phase pressure <b>drop</b> data.	263
APPENDIX K.	Computer program for analysis of transient pressure drop data.	269
APPENDIX L.	Computer program for evaluation of capture mechanism contributions.	279
APPENDIX M.	Formulation of equation to describe critical <b>trajectory</b> of a drop approaching a cylindrical collector.	285
	M.1 London attractive force.	285
	M.2 Hydrodynamic interaction functions.	287
	M.3 Solution of trajectory equation.	289
APPENDIX N.	Computer program to calculate initial drop capture rate in coalescer.	296
APPENDIX O.	Evaluation of specific surface for coalescer containing drops of dispersed phase.	298
APPENDIX P.	Integration of pressure drop equation.	300
APPENDIX Q.	Prediction of pressure drop using mathemat- ical model.	303
	Q.1 Computer program.	304
	Q.2 Output for constant inlet saturation.	305
	Q.3 Output for fitted values of inlet saturation.	308
	<u>NOMENCLATURE.</u>	311
	<u>REFERENCES.</u>	316

CHAPTER 1  
INTRODUCTION

§

The increasingly stringent restrictions recently imposed upon all types of effluent discharge have promoted commercial interest in coalescence and similar methods of phase separation. As well as shore pollution by sea-borne contaminants, inland pollution of permeable strata may result in the fouling of watercourses, thus limiting water resources.<sup>1</sup> Ecological effects upon plants, animals and ultimately man are also cause for concern with respect to pollution. Equally serious is the fact that, during research to ascertain the extent of our natural oil resources, it has been indicated that supplies of this internationally vital commodity could be exhausted by the close of the century. Increasing demands, together with the current trend of rising oil prices, therefore accentuate the obvious advantages to be gained from combining a solution of the pollution problem with the recovery of oil, or any other valuable material, for re-use.

In addition, the capacity of all forms of liquid extraction equipment is limited by the behaviour of small droplets within the plant. Effective mass transfer is only obtained with a large number of small droplets, but, following the extraction operation, rapid coalescence of the drops is desirable. This reduces the residence time and alleviates the possibility of poor phase separation which would decrease the capacity and efficiency of the process. Models predicting coalescence rates based upon the physical properties of the system and operating conditions are therefore essential to improve design techniques.

The separation of primary dispersions is generally easily accomplished by gravity settling but the required residence time for secondary dispersions, which may consist of drops down to  $1 \mu\text{m}$  diameter, is often prohibitive for this method

to be effective. Consequently, it is necessary to increase the settling rate, which can be achieved by promoting intimate contact between constituent drops thereby encouraging coalescence to occur. Passing the dispersion through a porous packing is an attractive method since it is efficient, inexpensive and continuous. Drops are captured within the bed, where they are retained to induce coalescence, and eventually, are released as larger primary drops. Because the drops are not permanently retained, the bed usually operates under steady state conditions except in cases where particulate material, present in the feed dispersion, causes a rapid deterioration in the efficiency and operating life of the device.

Practical design of coalescers is usually based on trial and error procedures because the mechanisms of coalescence in porous media are not fully understood. The objective of this investigation was to analyse the mechanisms of drop capture and two phase flow in a coalescer in order to develop a mathematical model for the efficiency, represented by the filter coefficient and the energy requirements, measured by the pressure drop across the bed. Also, a series of experiments, have been completed using packings of accurately known geometrical characteristics to establish the effects of operating conditions and bed properties and to evaluate the proposed theoretical model.

CHAPTER 2  
FORMATION OF SECONDARY DISPERSIONS.

## 2.1. INTRODUCTION.

When one phase in a liquid/liquid system is dispersed as discrete drops, the dispersion produced can exhibit widely differing physical and chemical properties depending upon the drop size. The latter is therefore extensively employed to categorise particular dispersions which may be broadly divided into primary dispersions, secondary dispersions and colloids or emulsions. Exact definitions of the ranges of these dispersion types in terms of drop size have not been elucidated. However, most previous workers in the field of secondary dispersions have arbitrarily defined such ranges without sufficient justification, apparently for theoretical and/or experimental convenience. Such arbitrary definitions of a secondary dispersion must be considered as over-simplifications especially when a theoretical description of the phenomenon of coalescence is attempted. The reason for this is that before coalescence, the dispersion may behave as a colloidal system; during coalescence growth of the drops occurs by different mechanisms depending partly upon the coalescence medium selected. Finally as the larger drops leave the coalescence medium, they will behave as primary dispersions. However, to place secondary dispersions into broad perspective, the approximate ranges of the three types of dispersion are illustrated in Fig. 2.1.

## 2.2. THEORY OF DISPERSION FORMATION.

A fundamental understanding of the basic processes of dispersion and coalescence can be gained by consideration of colloidal systems. Colloids may be defined as systems in which a significant proportion of the dispersed phase molecules lie in or are associated with interfacial regions. Because of the excess energy associated with the formation

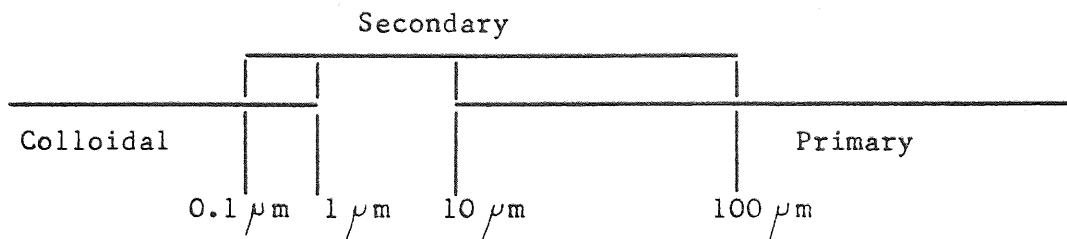


Fig 2.1. Classification of Dispersions by Drop Size.

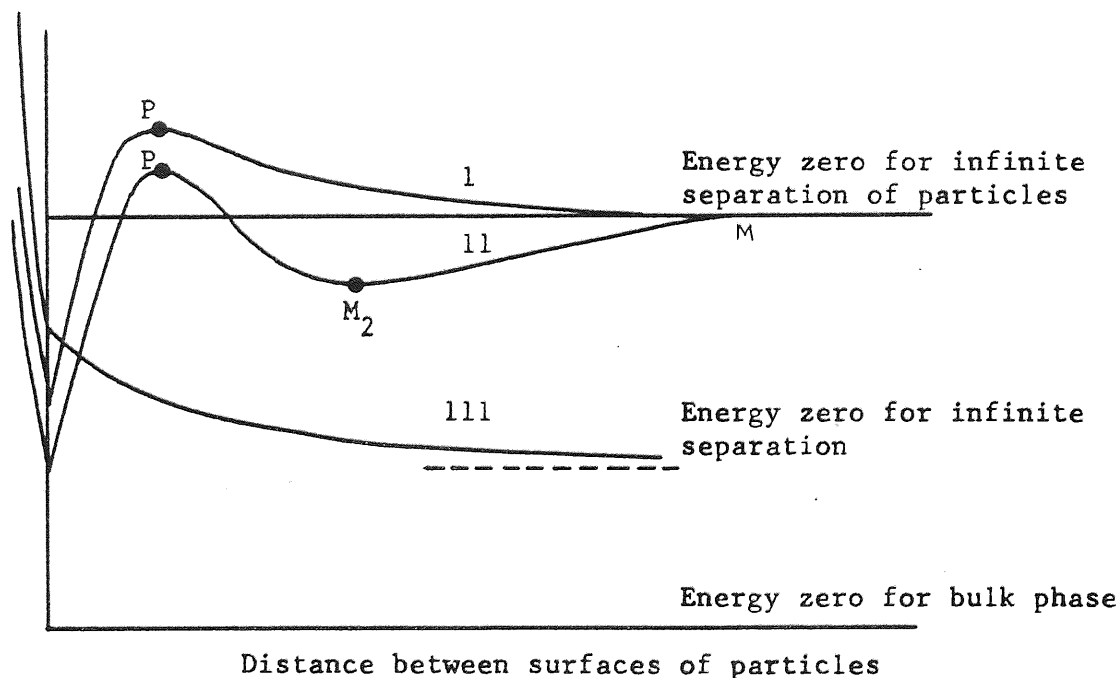


Fig 2.2.

Mutual potential energy of two colloidal particles as a function of the distance of separation between their surfaces:

- 1. curve with primary maximum P and primary minimum M<sub>1</sub>
- II. curve with primary maximum P, primary minimum M<sub>1</sub> and secondary minimum M<sub>2</sub>
- III. curve for spontaneous (unactivated) dispersion

of new surfaces, subdivision of a liquid within another liquid always increases the energy of the system and the dispersed phase is thermodynamically unstable (or metastable) with respect to the bulk phase. The energy is also modified by interactions between the surfaces and the phase in which it is immersed. Depending on the magnitude of the energy associated with such interactions, the dispersed colloid may remain unstable (or metastable) with respect to the bulk phase (lyophobic dispersion) or may become thermodynamically stable (lyophilic dispersion). When two particles in a lyophobic dispersion collide, they may adhere to one another; if the system is metastable only a fraction of the collisions will result in adhesion. The metastability of lyophobic colloids thus arises from the existence of an energy barrier which has to be surmounted before the two particles can adhere. This barrier may exhibit two characteristic forms as shown in Fig.2.2.<sup>2</sup>

With reference to Fig 2.2, in case I, a collision in which the associated kinetic energy is sufficient to carry the system over the potential energy barrier (primary maximum, P) into the minimum M, (primary minimum) will result in association of the droplets i.e. coagulation; if the potential energy barrier is high in comparison with thermal kinetic energies, the particles will repulse one another and the dispersion will remain stable indefinitely.

In case II, a third possibility arises in which the two droplets may become associated in a state represented by  $M_2$ , the secondary minimum corresponding to flocculation. They may later either dissociate or pass over into the primary minimum. Two droplets associated in the primary minimum may remain in this state or may coalesce to form a larger

droplet of lower surface energy, as when an emulsion breaks.

If the interaction curve between two droplets has the form shown in case III, the dispersed state is stable, at constant particle size, so that dispersion of the particles occurs spontaneously.

The form of the curves in Fig 2.2 depends on the size of the drops or particles involved. Therefore, even for the simplest case of monodisperse colloids, it is necessary to consider systems whose energies depend both on particle size and distance of separation, and so may be represented by a three-dimensional surface such as that shown very schematically in Fig 2.3. However, the shapes and characteristic features of such surfaces depend on many other parameters besides size. Continuous phase properties, dispersed phase concentration, electrical state of the interface, structure and chemical state of the dispersed phase and the presence of adsorbed films at the interface are among the more important factors. The surface illustrated in Fig.2.3 is therefore only one three-dimensional section of a multi-dimensional hyper-surface, but is adequate for a basic description of the phenomena of dispersion and coalescence. Secondary dispersions may, in principle, be formed in two ways. Firstly, by mechanically breaking down a bulk phase to colloidal dimensions and dispersing the particles as formed or secondly by building up colloidal particles from molecular units.

#### 2.2.1. Subdivision of a Bulk Phase.

A liquid phase may be subdivided into droplets of colloidal size by mechanical means, i.e. emulsification. This process may be represented in Fig.2.3 by routes B - C or  $BM_1P_1M_2C$  depending upon the method of emulsification.

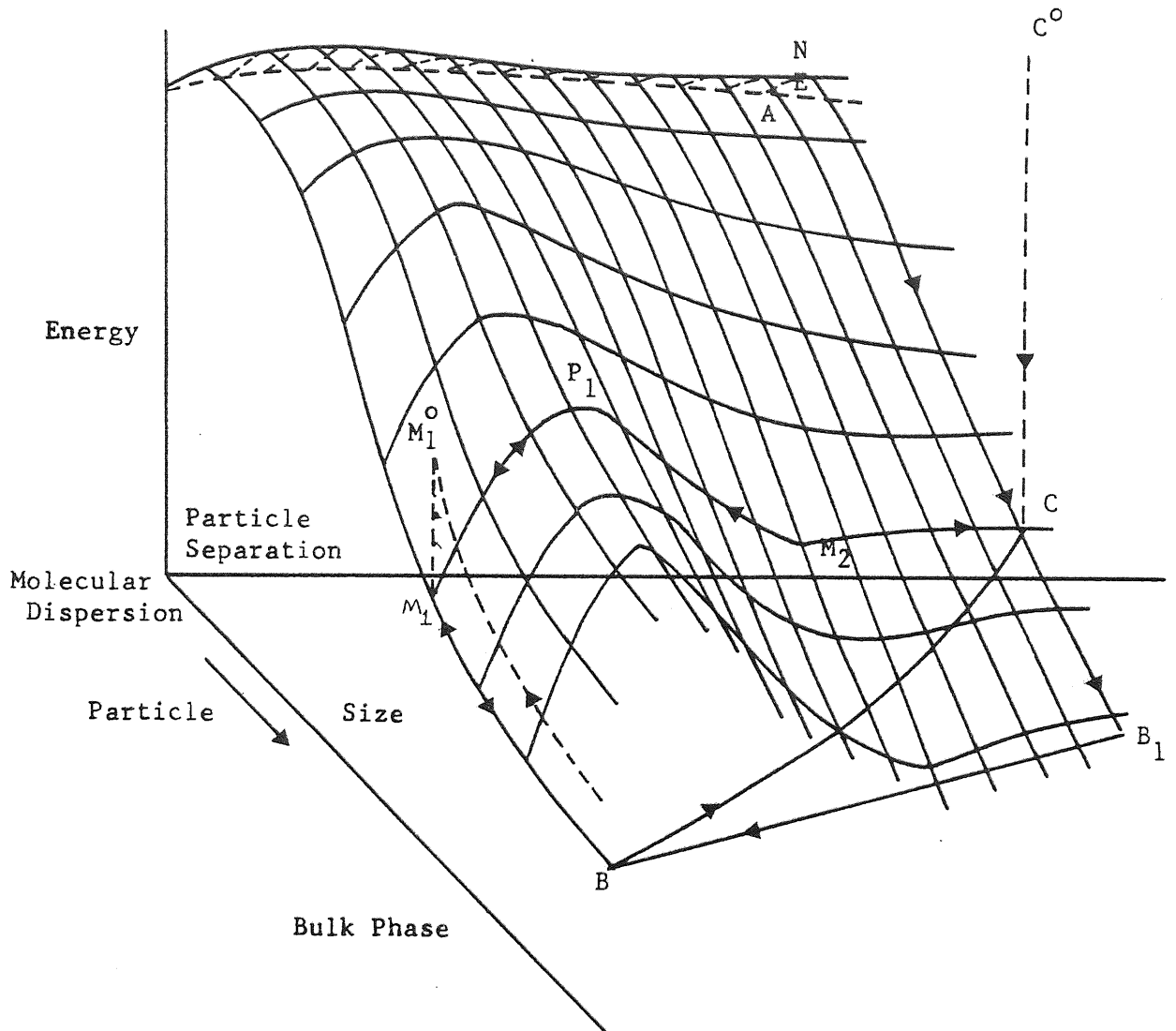


Fig. 2.3

Mutual potential energy surface of two colloid particles of a lyophobic colloid in a liquid medium as function of distance of separation and size of particles, showing routes by which colloid state C can be reached by (i) comminution, routes BC or  $BM_1P_1M_2C$  or (ii) by nucleation and growth, ANC; and routes by which coagulation can occur (i)  $CB_1B$  and (ii)  $CM_2P_1M_1B$ . Note that the reverse route CNA in which a colloid would disperse to the molecular state does not in general occur spontaneously. (The short range repulsion "cliff" adjacent to the left hand face of the diagram is omitted for clarity.)  $M_1^o$  and  $C^o$  are points representing energies in a vacuum environment.

The route B - C applies when the drops are already dispersed in the continuous phase and route  $BM_1P_1M_2C$  is taken when the dispersed phase is introduced as a continuum into the continuous phase after which, thermal motions or mechanical disturbance will take the system to the dispersed state C if the activation energy over the path  $M_1P_1$  is sufficiently low.

### 2.2.2. Formation by Nucleation and Growth.

The building-up of colloidal particles to C (Fig 2.3) from atomic or molecular units at A involves following the path AENC. The formation of an embryo, at E, of new phase in an existing bulk phase involves an increase in energy, which when the embryo reaches a critical size, passes through a maximum. This corresponds to the nucleus, N. Thereafter, the decrease in surface energy which accompanies growth acts as a driving force for spontaneous growth of the nucleus. However, if a large number of nuclei are present and the bulk phase is of limited extent, then growth involves the depletion of the bulk phase of the components of the growing particles, whose ultimate size (at C) is thus limited by the amount of material available. Since not all nuclei are formed simultaneously, they will have been growing for different times when growth ceases and consequently the final dispersion will be polydisperse.

### 2.3. PREPARATION OF SECONDARY DISPERSIONS.

In addition to a classification of dispersions based upon the energy changes and mechanisms of their formation as described in Section 2.2, Bikerman<sup>3</sup> adopts a similar classification relating to the practical aspects of formation. The latter considers critical emulsions, emulsions produced by condensation and emulsions produced

by mechanical dispersion.

### 2.3.1. Critical Emulsification.

If two liquids are completely miscible above an 'upper critical dissolution temperature' and partially miscible below this temperature, then heating a mixture of the two liquids to the vicinity of the 'upper critical dissolution temperature' often causes appearance of critical opalescence due to the formation of an emulsion. Also, some systems exhibit a 'lower critical dissolution temperature' when cooling from room temperature is required to achieve partial miscibility. Such emulsions are fairly stable at the critical temperature due to similar densities and interfacial tensions of the dispersed and continuous phase.

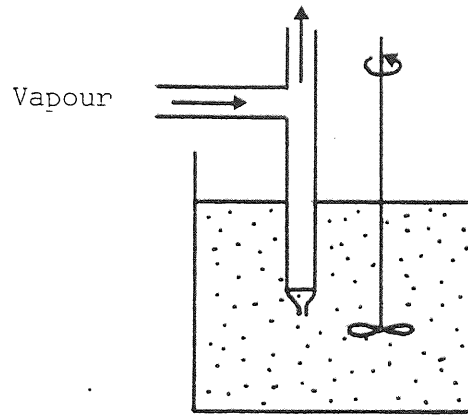
However, the strong temperature and system dependencies inherent in this method of formation render it unsuitable for most practical purposes.

### 2.3.2. Emulsification by Condensation.

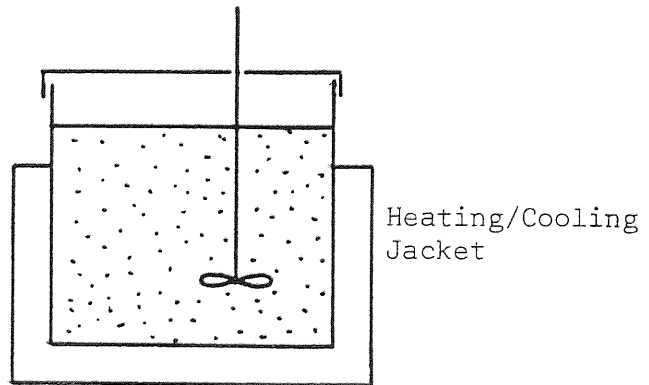
This process is achieved by nucleation and growth as described in Section 2.2. The nuclei may be natural impurities of dust or smoke, or may be ions and other seeds that are artificially introduced. Even in the absence of foreign matter, the nuclei may be spontaneously formed by the aggregation of molecules into droplets of sub-micron size. There are two basic types of emulsification by condensation as illustrated in Fig.2.4 namely vapour injection and the freeze-heat technique.

Vapour injection consists of injection of a super-saturated vapour of the dispersed phase using a jet orifice which is submerged in the continuous phase containing a suitable emulsifier. In this process, the vapour condenses as micron-sized droplets, whose size and size

To measurement and control of pressure and temperature



(a) Vapour Injection



(b) Freeze-Heat Technique

Fig. 2.4 Emulsification by Condensation

distribution is determined by the temperature and pressure of the injected vapour and the diameter of the orifice <sup>4</sup>. Careful seeding usually produces a fairly monodisperse emulsion and subsequently this technique has been modified for controlled aerosol formation.

The freeze-heat technique or precipitation is often manifested, under uncontrolled conditions as clouding of either organic or aqueous bulk phases. Meissner and Chertow <sup>5</sup> developed this technique for emulsification which relies upon the temperature dependence of mutual solubility of two liquid phases. This method involves varying the temperature of an agitated mixture of the organic and aqueous phases in a sealed system containing an emulsifier until condensation occurs. This technique has been extensively employed in the laboratory for evaluation of emulsion stabilisers <sup>6,7,8</sup>. Hermanie and van der Waarden <sup>9</sup> have shown that monodisperse systems are produced by this technique but rapidly become heterodisperse once formed. The method is extremely sensitive to temperature and the geometry and materials of the equipment used <sup>10</sup>.

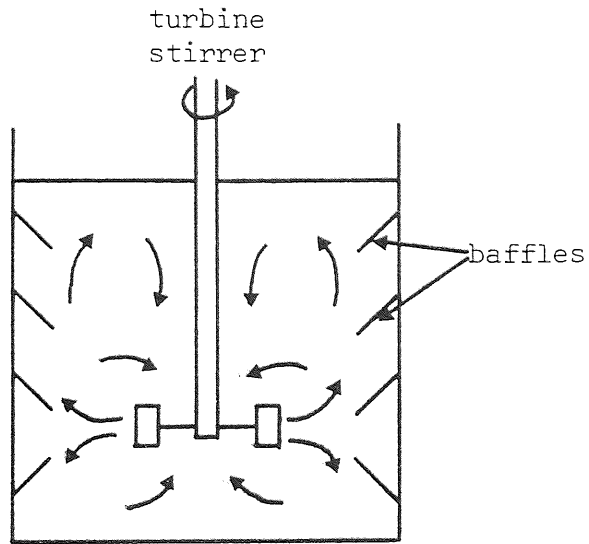
Condensation methods have not grown beyond the stage of laboratory development due to the complexity of the equipment required to adequately control the conditions of formation. However, several practical techniques have been evolved to disrupt the interface between two bulk phases efficiently into many small droplets. Thus the dispersion approach is commonly used in industrial and laboratory preparation of emulsions for which a wide range of emulsification equipment has been developed.

### 2.3.3. Emulsification by Mechanical Dispersion.

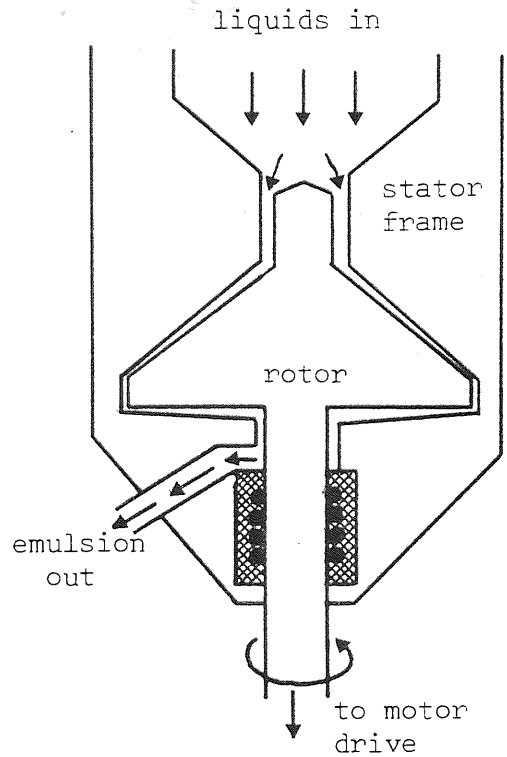
Mechanical dispersion is based on a two-stage

mechanism. In the first stage, a droplet is deformed in a way characteristic of the system as a whole, and adopts a cylindrical conformation. These cylinders, once formed, become unstable when their length exceeds their circumference. The second stage of spontaneous break-up which then follows, the Rayleigh disproportionation, results in the formation of a number of smaller drops. The effect of system parameters on this elementary emulsification process has recently been studied by Carroll and Lucassen<sup>11</sup>. The extensive deformation of large drops, necessary for initiation of the above process, is achieved by several different methods in practice. The second stage of emulsification may be delayed when external forces are continuously acting on the deformed drops during agitation. However, if agitation ceases then spontaneous break-up occurs. This advantage of interrupting agitation is employed in Brigg's method of preparing emulsions<sup>4</sup> in which polydisperse systems of 50-100  $\mu\text{m}$ . are produced by intermittently shaking the two bulk phases, with rest periods between shakes. Ford and Furmidge<sup>12</sup> have applied this technique to the study of oil-soluble emulsifiers because of its simplicity.

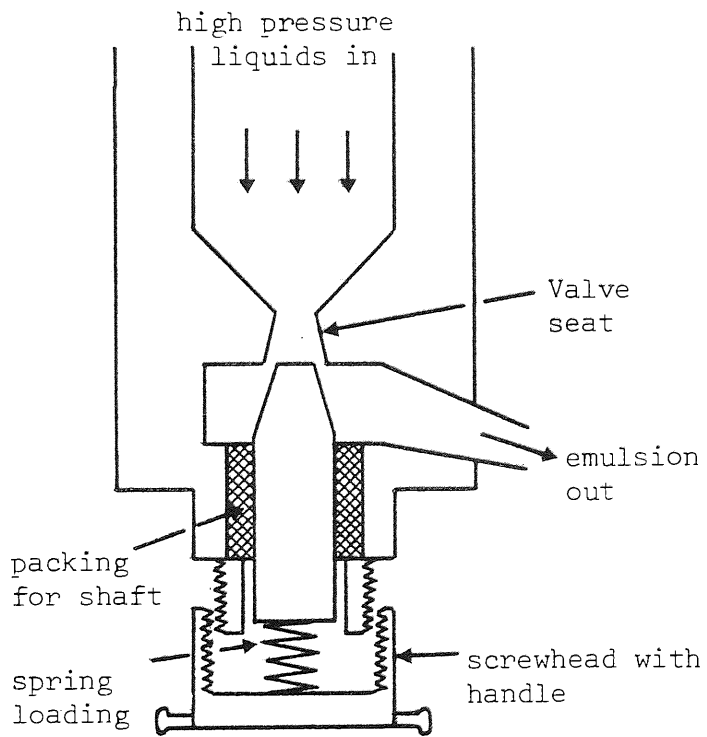
However, it is usually desirable to produce smaller droplets in a short time which necessitates the application of large velocity gradients using such techniques as illustrated by Fig 2.5. One method of attaining the required shear rate is to use a turbine rotor in a baffled tank. Careful design of the geometry and materials of the mixer produces a homogeneous turbulent flow field capable of reducing the drop diameter to as low as 5  $\mu\text{m}$ . The properties of the prepared dispersion also depend upon the agitator speed and the physical properties of the bulk



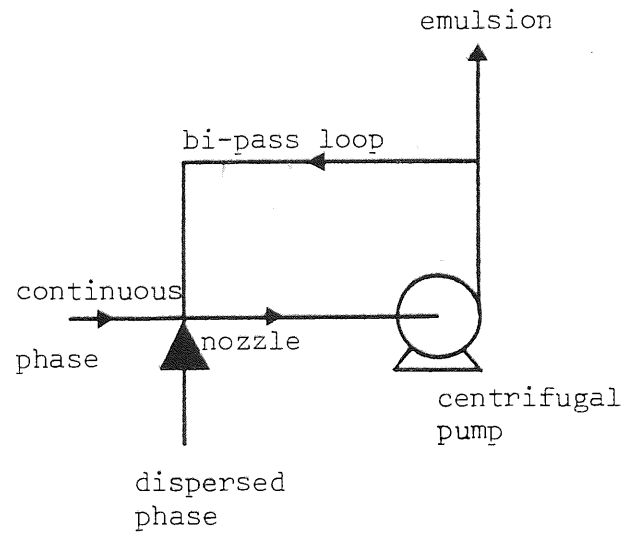
(a) Mixer



(b) Colloid Mill



(c) Homogeniser



(d) Centrifugal Pump

Fig. 2.5. Mechanical methods of emulsification

phases<sup>13</sup>.

In a colloid mill or blender, emulsification of the liquids is carried out under strong shearing flow between a high speed rotor and a stator surface. The velocity gradient associated with a rotor gap of 0.025 mm and rotor speed of up to 20,000 r.p.m., which may be adjustable to suit the bulk phase viscosities, can produce drops of  $2\ \mu\text{m}$  diameter. Besides laboratory use of this equipment to study emulsion characteristics<sup>14</sup>, commercial units of this type are readily available of varying materials of construction selected on the basis of the liquids to be emulsified<sup>4</sup>.

Deformation of drops in a homogenizer is achieved by forcing the bulk phases, which have previously been mixed, through a small orifice under pressures of approximately 350 bar. The orifice, which can be adjustable, may be about  $10^{-8}\ \text{m}^2$  in area and droplets of  $1\ \mu\text{m}$  can be easily produced. Alternatively sub-micron droplets can be produced by repeated passes of the dispersion through an orifice at lower pressures of about 2 bar<sup>15</sup> and larger drops formed by a single pass through larger diameter capillaries at low pressures<sup>16</sup>.

Emulsification of viscous liquids by mechanical dispersion often necessitates cooling of the equipment because the temperature rise associated with high shear rates may be detrimental to heat sensitive fluids.

A simple but effective method of producing secondary hazes continuously is to pass the bulk phases through a centrifugal pump which is associated with a bi-pass circuit. Polichronakis<sup>17</sup> has investigated the characteristics of dispersions formed in this manner which typically produce a mean drop size of about  $20\ \mu\text{m}$ . Also recent research work<sup>18</sup> has investigated the possibility of

17

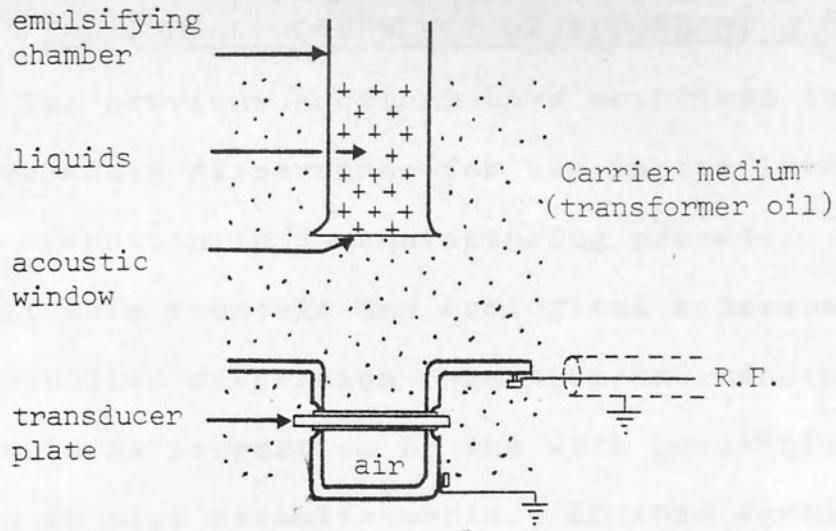
secondary dispersion formation by pumping the dispersed phase through a 'micromesh' distributor.

#### 2.3.4. Recently Developed Techniques.

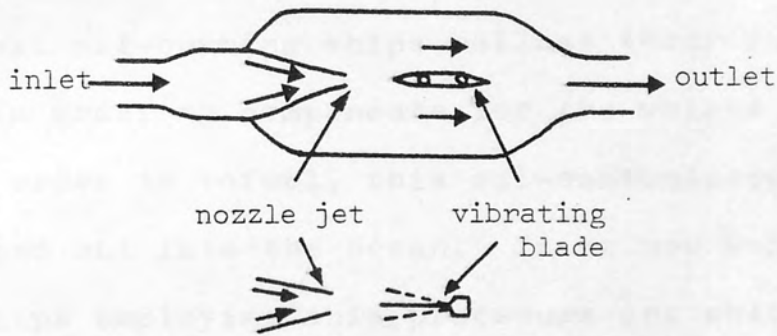
The sonic, ultrasonic and electrical methods of emulsification, while not capable of rendering the other methods obsolete, are supplementary techniques which are especially valuable under certain conditions and have been adopted for industrial use <sup>4</sup>.

In sonic and ultrasonic techniques, electrical energy is converted into mechanical vibrations in the audio or radio frequency range, by the use of electro-mechanical transducers. The three most commonly used generators are illustrated in Fig.2.6. The characteristics of the dispersions formed by sonic and ultrasonic vibrations are little different to those produced by conventional techniques but emulsions containing a high volume fraction (30%  $\frac{V}{V}$ ) of the dispersed phase may be obtained without the use of any surface active agent. However, the chief disadvantage is that the method is most efficient at the lower frequencies in the audio range and the use of high intensity sound waves is objectionable on physiological and sociological grounds.

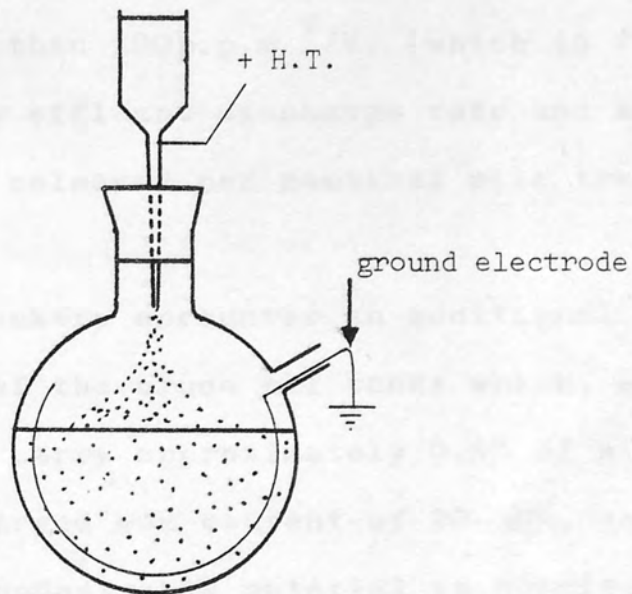
The electric dispersion method is employed for production of high concentration, monodisperse emulsions on the laboratory scale. The basic equipment is illustrated in Fig 2.6 in which application of an appropriate high voltage (about 8 kV) between the bulk dispersed and continuous phases produces an aerosol of the dispersed phase which passes into the bulk continuous phase. Monodisperse emulsions having a mean drop diameter of 1  $\mu\text{m}$  are feasible but difficulties may be encountered as a result of the electrostatic charges on the drops and also when



(a) Emulsification using a piezoelectric generator



(b) Ultrasonic emulsification



(c) Electric dispersion of liquids

Fig. 2.6. Emulsification using electromagnetic transducers

dealing with high viscosity fluids.

#### 2.4. INDUSTRIAL OCCURRENCE OF SECONDARY DISPERSIONS.

The previous sections have described the production of secondary dispersions for use in the laboratory or as a unit operation in a manufacturing process. However, the undesirable economic and ecological consequences of uncontrolled dispersion formation in industry are responsible for a large proportion of the work presently being undertaken in many establishments. In this section, the principal offending sources of unwanted emulsion formation will be briefly described.

##### 2.4.1. Effluent from Ocean Going Ships.

Most oil-burning ships ballast their fuel tanks with water in order to compensate for the weight of fuel used and in order to refuel, this oil-contaminated water has to be pumped out into the ocean. It is now well established that ships employing this procedure are obliged to process the effluent in some form of oil/water separator before discharge<sup>19</sup>. Oil discharge requirements at sea are quoted<sup>1</sup> as less than 100p.p.m  $V/V$ . (which is regarded as innocuous) at any effluent discharge rate and a limit of 60 litres of oil released per nautical mile travelled is also imposed.

Crude oil tankers encounter an additional problem during cleaning of the crude oil tanks which, after unloading, still carry approximately 0.4% of a full cargo, which has an enlarged wax content of 20-30%, as a residue. Removal of this undesirable material is completed employing sea-water jet washers which produce a secondary oil-in-water dispersion. The washings are then transferred to a tanker-cleaning station when the tanker is in dock<sup>20</sup> or alternatively to a 'slop tank' from which they are discharged

to the ocean in three basic steps known as the 'Load on Top' system. Creaming of the dispersion then occurs to some extent to produce three 'phases'. Phase I contains about 30 p.p.m.  $V/V$  oil and is discharged at high flowrates; Phase II, which contains approximately 100 p.p.m.  $V/V$  is released at lower flowrates and phase III, whose oil content varies from 500 to 4000 p.p.m.  $V/V$  is discharged at minimal rates. It is during this latter stage that an efficient coalescer is required to alleviate discharge of large amounts of crude oil.

Also when a large quantity of crude oil is spilt on the sea, four main effects can be observed: first, the more volatile components evaporate; second, water-soluble materials are leached out of the oil; third the slick spreads rapidly over the surface and finally, a persistent water-in-oil emulsion is formed <sup>21</sup> commonly referred to as 'chocolate mousse'. These dispersions hinder conventional methods of slick clean-up and severely retard the natural means of dispersal of the slick by biodegradation.

#### 2.4.2. The Oil Industry.

Recently, increased demands for hydrocarbons have necessitated the acceptance of lower quality crudes containing inorganic salts dissolved in both 'free' and emulsified water. Removal of these salts is essential to alleviate corrosion in oil refineries and to minimise general contamination of refinery products <sup>22</sup>.

Also, oil-well steam injection facilities are being installed in a number of low-gravity oil fields to stimulate oil production. <sup>23</sup> Dehydration involving dispersion removal is therefore necessary and in most cases, the waste water from this and other refinery processes must be cleaned before disposal.

### 2.4.3. Miscellaneous Sources.

Obnoxious effluents also emanate from most industrial operations which use oil as a lubricant or process fluid and the steel and motor industries are particularly prone to this type of problem <sup>24</sup>. The wool industry also experiences similar difficulty in the treatment of its scouring wastes <sup>25</sup>.

The contamination of aviation fuel by water is a critical problem with respect of combustion difficulties, corrosion, organic fouling and ice formation at high altitudes. Removal of the dispersed phase is further complicated by the presence of additives in the fuel eg. corrosion inhibitors and biocides which often possess surface active properties <sup>26</sup>.

In solvent extraction operations, the coalescence of primary drops by the stage-wise mechanism is often responsible for the formation of 'satellite' drops which constitute observed secondary fogs. The presence of the latter results in reduced efficiency and contamination of the process streams.

In conclusion, this section illustrates the many and varied areas of undesirable occurrence of secondary dispersions and emphasizes the obvious reasons for their efficient removal. It can also be realised that the various methods of dispersion preparation rely upon similar conditions under which unwanted formation of dispersions occurs in industrial processes.

Apparatus for the study of the stability of emulsions is described in detail in the literature. The apparatus is similar to that used by Taylor and Goldthorpe (1931) and the apparatus is shown in Figure 2.1. The apparatus consists of a cylindrical vessel of stainless steel with a diameter of 10 cm and a height of 15 cm. The vessel is fitted with a stirrer and a thermometer. The stirrer is driven by a motor and the speed of rotation is adjustable. The thermometer is used to measure the temperature of the emulsion. The apparatus is used to study the stability of emulsions by measuring the rate of creaming or sedimentation.

The rate of creaming or sedimentation is measured by measuring the height of the cream or sediment layer at various times. The height of the cream or sediment layer is measured by a ruler. The rate of creaming or sedimentation is expressed as a percentage of the original height of the emulsion. The rate of creaming or sedimentation is affected by many factors, such as the size of the dispersed particles, the viscosity of the continuous phase, and the density difference between the dispersed and continuous phases.

### CHAPTER 3

#### SEPARATION OF SECONDARY DISPERSIONS

The separation of secondary dispersions is a complex process. It involves the interaction of many factors, such as the size of the dispersed particles, the viscosity of the continuous phase, and the density difference between the dispersed and continuous phases. The separation of secondary dispersions is affected by many factors, such as the size of the dispersed particles, the viscosity of the continuous phase, and the density difference between the dispersed and continuous phases. The separation of secondary dispersions is a complex process. It involves the interaction of many factors, such as the size of the dispersed particles, the viscosity of the continuous phase, and the density difference between the dispersed and continuous phases.

This degradation of emulsions involves many general phenomena, namely creaming, phase inversion and complete demulsification. This classification is given in Figure 2.2. The phenomena represent somewhat different stages, though the borderline between them is not well defined.

Creaming occurs when the system separates into two phases, one having a higher concentration of the dispersed phase and one lower than that of the original dispersion. The rate of creaming is affected by many factors, such as the size of the dispersed particles, the viscosity of the continuous phase, and the density difference between the dispersed and continuous phases.

### 3.1. STABILITY OF SECONDARY DISPERSIONS.

A secondary dispersion is unstable if, in a significant proportion of collisions between droplets, association occurs, and the aggregations so formed continue to grow by further collisional processes until they are of such a size that Brownian Motion is no longer sufficient to overcome the tendency, arising from density differences, for bulk separation to occur.

The phase which separates out may have various forms depending on the type of system considered. With reference to Fig 2.3 if the secondary minimum is sufficiently deep, an associated state with a loose open structure is formed in which the droplets are spread at distances of the order of  $0.1 - 1 \mu\text{m}$ . This stage is termed flocculation. The height of the primary maximum controls the rate at which droplets transfer to the primary minimum corresponding to a separation of a few nanometers at most. If the activation energy for this process is not too high, the aggregated state may transform to a more compact structure by coagulation. Whether flocculation is an intermediate stage in the overall coagulation process depends on the relative positions of the secondary minimum and primary maximum points. This is represented by the path  $CM_2P_1M_1B$  on Fig 2.3.

This degradation of emulsions manifests itself as three general phenomena, namely creaming, phase inversion and complete demulsification. This classification is convenient because the phenomena represent somewhat different situations, though the borderline between them is not well defined.

Creaming occurs when the system separates into two emulsions, one having a higher concentration of the dispersed phase and one lower than that of the original dispersion. Slow sedimentation of the emulsified droplets produces a high

internal phase ratio emulsion in which they pack together as some transition form between spheres and polyhedra<sup>27</sup>. However the drops remain separate during contact unlike primary drops<sup>28</sup> which undergo coalescence as dispersion bands are formed.

Phase inversion is the instability developed when an emulsion suddenly reverts from O/W to W/O type or vice versa and may occur when the concentration of the dispersed phase reaches about 75%. This corresponds to the volume fraction occupied by a close packing of a number of rigid spheres of equal size.

Demulsification is the complete break up of an emulsion into its component parts. It is found in many systems that two stages may be distinguished in the break up. Firstly the drops adhere to one another to form clusters with a relatively thick film of continuous phase between them (flocculation). These clusters are easily redispersed by slight agitation. The intervening film drains and mutual fusion of the drops (coalescence) takes place to form larger drops and eventually bulk liquid.

### 3.2. TREATMENT OF SECONDARY DISPERSIONS.

It is well known that in order to prepare an emulsion having a useful and persistent concentration of dispersed phase, it is essential to add a third component of a particular type to bestow a measure of stability. Also, industrially occurring secondary dispersions are frequently contaminated with compounds which have a stabilising effect.

#### 3.2.1. Chemical Coagulation.

The separation of stabilised oil-in-water emulsions can be achieved by suitable chemical treatment which neutralises surface charges on the drops or dissolves the protecting film surrounding each drop depending on the nature of the emulsifying agent. Inactivation of the latter may be accomplished by

the addition of chemical coagulating agents such as aluminium, ferric or calcium salts<sup>29</sup>. The use of organic polyelectrolytes<sup>30</sup> is also widely recognised as a practical and often efficient technique. Demulsifying agents are very specific in their action and no universal compound has been found effective for treating the different types of emulsion.

In cases where either the dispersed or continuous phases are valuable, possible contamination of the liquid system by chemical additives is a disadvantage of this method. Also, as additives may be surface active, they reduce the interfacial tension between the phases of the dispersion leading to formation of very small drops and may be adsorbed onto the surfaces of coalescer elements thus inhibiting efficient operation<sup>26</sup>. Consequently, chemical coagulation is often employed in conjunction with flotation processes<sup>24</sup> when recovery of the dispersed phase is not mandatory.

Chemical treatment suffers from the disadvantages of high cost and technical and practical limitations in its application because the rate of separation is very sensitive to the presence of impurities, degree of aeration and variation in the type and intensity of agitation during the flocculation stage.

### 3.2.2. Centrifugation.

The settling velocity of secondary drops under steady, unhindered conditions is given by Stokes' Law,

$$u = \frac{gd^2 (\rho_d - \rho_c)}{18\mu_c} \quad 3.1$$

Increasing the settling rate may be conveniently discussed in terms of which of the variables in equation 3.1 are modified by application of the different techniques.

The acceleration due to gravity,  $g$  is enhanced by the application of centrifugal force in a centrifuge or hydro-

cyclone. Centrifuges are particularly effective in separating two liquids of low density difference, high continuous phase viscosity or small drop size and the presence of particulate matter does not present any practical problems. However, centrifuges are relatively expensive, having high capital and operating costs, so that their use has been restricted to military applications such as the purification of aviation fuel. The efficiency of a centrifuge depends on the residence time, which is generally short and dependant on flowrate, and therefore this technique finds application in pharmaceutical and radiological processes. The hydrocyclone is not very efficient because the turbulence created by the high flow rate tends to shear and break the dispersed oil phase into a still finer dispersion .

30

### 3.2.3. Electrostatic Coalescers.

An alternative means of supplementing buoyancy forces is to subject the drops in a dispersion to electrostatic forces. Electrical methods of inducing coalescence are based on one of two mechanisms; namely, due to forces exerted on drops having net charges (electrofining), and the forces between neutral drops resulting from their acquiring induced dipoles in an a.c. or d.c. field. For dispersions containing uncharged drops, dipole coalescence is the operative mechanism<sup>31</sup> for phase ratios above 0.1% but the efficiency decreases rapidly as concentration decreases because the mutual attractive force between droplets is inversely proportional to the fourth power of their separation. Therefore operation of electrostatic coalescers is usually conducted with a minimum of 3%<sup>v/v</sup> of the dispersed phase to ensure satisfactory coalescence.

32

This technique is only suitable for the separation of W/O dispersions where the continuous phase is relatively non-

conductive and has been applied extensively to the separation of emulsions generated during the desalting of crude oil.<sup>32</sup> Typically, a crude oil may contain approximately 5% v/v of water after desalting which may be reduced to no less than 0.1% so that electrostatic coalescers are unsuitable for applications where high separation efficiencies are required. They also possess the disadvantage of high capital costs but are simple and readily adaptable to automatic operation.

#### 3.2.4. Heat Treatment.

Raising the temperature of a dispersion increases the settling rate by reducing the continuous phase viscosity and may also increase the density difference. This method is often used in conjunction with chemical coagulation<sup>24</sup> since it increases the rate of reaction caused by demulsifying agents. However, the high energy consumption renders this technique uneconomical for the treatment of large quantities of dispersion.<sup>30</sup>

#### 3.2.5. Air Flotation.

The treatment methods so far described rely primarily on the mechanism of gravity and phase separation occurs by inter-drop or drop/interface coalescence. Despite the steady improvement in settler design from the initial American Petroleum Institute (A.P.I.) design<sup>33</sup> through to sophisticated tilted plate arrangements<sup>34</sup>, gravity separation becomes very inefficient when the drop diameter falls below 60  $\mu\text{m}$ . Consequently the dispersed phase concentration may not be reduced to less than about 150 p.p.m. by gravity methods. With the increasingly tight discharge standards now being imposed and the more recent needs for water recycling, much lower oil levels in discharged effluents are now required. To achieve these levels, secondary separation processes have been

developed which operate by capture of the secondary drops and encouraging them to maintain contact until coalescence takes place.

Air flotation systems cause the suspended drops to be captured by rising air bubbles of 10 to 100  $\mu\text{m}$  diameter and the agglomerates formed float to the surface of the liquid where they can be separated. This method finds extensive application in the treatment of oily wastes from refineries, petrochemical plants and steel mills<sup>35</sup> where quantities of up to 80,000  $\text{m}^3$  per day are purified to a dispersed phase concentration of about 20 p.p.m.<sup>36</sup> Flotation processes operate more efficiently when the effluent is pretreated with flocculating agents providing that it is not necessary to recover the dispersed phase from the 'float' which may be contaminated by addition of chemical coagulants.

Generation of the air bubbles may be achieved by chemical reactions, electrolytic methods or by injection of air through a distributor of very small pore size<sup>37</sup> but dissolved air flotation is the principal method of application due to its simplicity, capacity and versatility. The most common system involves pressurising a side stream of clarified effluent, followed by aeration and finally mixing with the pretreated waste product; this releases the pressure causing the evolution of air bubbles.

### 3.2.6. Coalescence in Porous Media.

Legislation often necessitates reduction of the dispersed phase concentration to less than 5 p.p.m.<sup>38</sup> and causing the dispersion to flow through mats, screens, granular media or fibrous packings is an efficient means of achieving this. Coalescers involve capture of suspended drops by the solid phase of the packing or by previously captured dispersed phase;

after coalescence, the dispersed phase migrates to the downstream face of the packing where large drops are released to be separated from the effluent by gravity.

Beds of glass fibre were used as early as 1949 for coalescence of emulsions in commercial processes, eg. in the desalting of crude oil<sup>22</sup>. Since then, a wide variety of porous media have been investigated including pebble beds<sup>40</sup>, ungraded gravel beds and stainless steel gauzes<sup>19</sup>. However, fibrous beds have been used successfully for the treatment of oil dispersions<sup>42</sup>, and removal of water from aviation fuel<sup>43,44,45</sup>.

Recently<sup>46</sup>, a polymeric material has been formed into an open-pored, three-dimensional, non woven structure and this base is impregnated with highly oleophilic particles to form 'epitropic' fibres of high surface roughness. Packings produced using this media are the basis of the I.C.I. 'Flofoil' process for the treatment of oil in water dispersions. The added advantage of using a base medium is that the packing near the exit face may be rendered hydrophilic to minimise 'foaming' or 'graping' release patterns (see Section 5.6) which form water globules, encased in an oil film. These possess neutral buoyancy forces resulting in poor separation efficiency.

Commercial designs of emulsion separating equipment nowadays incorporate coalescers in a three stage process<sup>47,48</sup>. After gravity settling and straining, to remove particulate matter, the dispersion is passed through a cylindrical coalescing element. Entrainment of coalesced drops is prevented by installation of a surface coalescer which consists of a porous membrane preferentially wetted by the continuous<sup>49</sup> phase.

2.3. Effect of Temperature on Coalescence

The effect of temperature on coalescence was investigated by measuring the pressure drop across a fibrous bed.

The results of fiber glass beds are not shown as coalescing was studied by Lewis and Kitchin.

They found that coalescence efficiency was improved by

(i) Decreasing superficial velocity in the range  $0.01 \times 10^{-2}$  to  $1.0 \times 10^{-2}$  m/s.

(ii) Decreasing the water to air ratio in the range 0.1 to 0.5.

(iii) Increasing the temperature to 300 K and found that the optimum temperature since operation above 400 K was

industrial air.

CHAPTER 4

COALESCENCE IN FIBROUS BEDS

(iv) Increasing fiber packing density from 140 to 240 kg/m<sup>3</sup>.

(v) Increasing bed depth, 10.7 x 10<sup>3</sup> m was reported relative to the concentration of salt in air to 0.1 g/m<sup>3</sup>.

These workers and Hayes et al., who conducted a study on a crude oil separating unit of a steel mill refinery, concluded that coalescing by glass fibers was comparatively attractive.

From a study using water vapor as a gas, Lewis et al. (1972) claimed that water coalescence was improved at a certain critical velocity range. The authors also mentioned that the critical velocity range was dependent on the fiber diameter and the water to air ratio.

#### 4.1 EFFECT OF OPERATING CONDITIONS

Previous studies of secondary dispersions will now be discussed to establish the preferred features of a coalescing bed.

The feasibility of fibre glass coalescers for crude oil desalting was studied by Burtis and Kirkbride<sup>50</sup>.

They found that coalescence efficiency was improved by,

(i) Decreasing superficial velocity in the range  $0.66 \times 10^{-2}$  to  $0.027 \times 10^{-2}$  m/s.

(ii) Decreasing the water to oil ratio in the range 0.3:1 to 0.2:1.

(iii) Increasing the temperature; 408 K was found to be the optimum temperature since operation above 450 K was impractical due to the high pressure required to prevent vapourisation.

(iv) Increasing fibre packing density from 140 to 240 kg/m<sup>3</sup>.

(v) Increasing bed depth;  $12.7 \times 10^{-2}$  m was capable of reducing the concentration of salt in oil to 30 p.p.m. These workers and Hayes et al<sup>22</sup>, who conducted a 58 week trial on a crude oil desalting unit of a full scale refinery, concluded that desalting by glass fibre beds was commercially attractive.

From a study using water-in-oil emulsions Voyutskii et al<sup>51</sup> claimed that water separation only occurred below a certain critical velocity; below this velocity coalescence depended upon total fibre contacting surface rather than on pore size. Gudsen<sup>52</sup> separated petroleum

fractions dispersed in water using a mixed fibrous bed of cotton and glass wool and also identified a critical separation velocity below which complete separation was possible.

Farley and Valentin<sup>19</sup> investigated the coalescence of high viscosity oils, with viscosities of 3.5 to 20.0 Ns/m<sup>2</sup>, with application to ballast water treatment. The oils were dispersed in water by pumping. A number of beds were used including porous porcelain, activated alumina and fibre glass as water wetted solids, and polypropylene, polystyrene and steel gauze as oil wetted solids. Effluent oil content was determined by light absorption following extraction with chloroform. As would be expected it increased with increase in superficial velocity, decrease in bed thickness and decrease in oil viscosity. It was considered more efficient to split the total packing thickness into two beds in series, with an intermediate oil take off, the second bed having twice the thickness of the first.

Sareen et al<sup>39</sup> observed visually the performance of single fibres (cotton, polypropylene, glass and p.t.f.e.) and mixed fibres (cotton-glass fibre bed and cotton-Dynel fibre bed) in coalescing several oil-in-water emulsions. The superficial velocity was varied from  $0.1 \times 10^{-2}$  to  $1.8 \times 10^{-2}$  m/s and the dispersed phase viscosity from  $1.4 \times 10^{-3}$  to  $137 \times 10^{-3}$  Ns/m<sup>2</sup>; dispersed phase concentration was in the range 2% to 5% by volume. Coalescence performance improved with decrease in fibre diameter and increase in bed length, but there was a

practical limit to the maximum bed depth. While residence time in the bed increased, the coalescence was better but there was a corresponding increase in pressure drop. Furthermore, redispersion of the coalesced drops occurred due to channels being formed within the bed. Coalescence performance decreased with increase in dispersed phase viscosity but then became constant at values above  $90 \times 10^{-3} \text{ Ns/m}^2$ . A critical separating velocity was also identified. Photomicrographs of exit drops indicated that a drop would break away from the fibre after attaining an equilibrium size; when the superficial velocity was higher than the critical velocity a retained drop was carried away before attaining the equilibrium size. These results were later confirmed by Davies and Jeffreys <sup>41</sup>.

Essentially 100% oil separation efficiency was achieved by Langdon et al <sup>42</sup> at a superficial velocity of  $1 \times 10^{-2} \text{ m/s}$  using a coalescer made from phenol-formaldehyde coated glass fibre  $3.2 \times 10^{-6} \text{ m}$  in diameter. Both inlet and effluent oil content were determined by a light reflectance technique. The pressure drop during the run increased from  $13.8 \times 10^3$  to  $172.4 \times 10^3 \text{ N/m}^2$  due to oil accumulation in the bed and, to a lesser extent, to mechanical degradation of the fibres. The possibility of solids contamination was ruled out. Because of the differential increase in pressure efficiencies were in fact determined under unsteady-state conditions. If solid contaminants were present, they would be deposited in the bed causing a gradual but permanent decrease in voidage. This cannot be avoided and replacement or intermittent back washing of the bed would eventually become necessary. Thus the bed ought not to be

used as a filter as suggested by Hazlett<sup>53</sup>.

To simulate the flow through fibrous beds, Vinson and Churchill<sup>54</sup> used photo-etched screens to separate a 0.05% oil-in-water emulsion with an average drop size of  $3 \times 10^{-6}$  m. The emulsion was prepared using a homogenizer and drop size estimated by a light scattering technique. Coalescence efficiency decreased with increase in superficial velocity, from  $0.025 \times 10^{-2}$  to  $2.08 \times 10^{-2}$  m/s, increase in screen filament width, from  $8.5 \times 10^{-6}$  to  $31.4 \times 10^{-6}$  m, and increase in aqueous phase viscosity from  $0.9 \times 10^{-3}$  to  $9.4 \times 10^{-3}$  Ns/m<sup>2</sup>. A correlation developed for fractional drop removal is discussed in more detail in Section 10.1.

#### 4.2 SYSTEM CHARACTERISTICS

Whether or not the packing should be preferentially wetted by the dispersed phase has been the subject of much discussion. Voyutskii et al<sup>51</sup> concluded that for best performance the fibre should be sufficiently 'water-wetted' to coalesce the water, but not so 'wetted' as to become clogged by the accumulation of water. The appearance of a secondary dispersion in the effluent was attributed to excess water wetting. In a second study<sup>55</sup> a mixed packing of viscose and wool fibres exhibited improved coalescence performance compared with single fibre material.

Sareen et al<sup>39</sup> using a photomicrographic technique, concluded that preferential wetting was not the controlling factor since drops that adhered to the fibre did not wet it. The results were justified by the relative surface roughness

of the fibres used. A similar conclusion was reached by Davies and Jeffreys<sup>41</sup>. Since droplet sizes were much smaller than the equilibrium drop size, droplets that adhered to the packing would be spherical regardless of material. However, surface roughness was considered extremely important.

For coalescence to take place, Burtis and Kirkbride<sup>50</sup> concluded that the packing must be preferentially wetted by the dispersed phase. Hazlett<sup>53</sup> accepted this principle to explain the attachment mechanism.

Farley and Valentin<sup>19</sup> concluded that water wetted packings were far superior to oil wetted ones for the separation of oil from water. The latter held the drops too tightly and did not allow coalesced drops to leave the packing; this resulted in their finally being broken up into clouds of small droplets by the water stream.

Langdon et al<sup>56</sup> considered the separation performance of a packing to be mainly determined by its wetting properties. An improved element with well defined and stable wetting characteristics could be achieved by using a packed bed composed of two materials, one essentially hydrophobic and the other essentially hydrophilic.

From this brief review of previous work on fibre wetting phenomena it is clear that there is a lack of understanding as to the effect of the nature of the coalescing media on the coalescence process. The consensus is however that preferential 'wetting' of the packing by the dispersed phase is not critical, but surface roughness is extremely

important. Suggestions that improved coalescer performance achieved by dipping the bed in the dispersed phase, i.e. 'priming', is due to prewetting effects are unproven. The phenomenon is more probably due to filling up the 'active sites' in the bed, i.e. increasing the hold up of the dispersed phase which is a major factor affecting the ultimate effectiveness of the coalescer.

As would be anticipated system interfacial tension is important in the operation of a coalescer element. Generally, the higher the interfacial tension, the easier is the separation. Values as low as  $20 \times 10^{-3}$  N/m can be separated satisfactorily, but below this value separation becomes increasingly difficult <sup>45</sup>. Rose <sup>51</sup> confirmed this from a study of nine different water-organic dispersions. Sareen et al <sup>39</sup> found that, during the separation of oil in water emulsions, for an interfacial tension value of  $20 \times 10^{-3}$  N/m incomplete coalescence was observed for water soluble surfactants while coalescence was complete with oil soluble surfactants for values as low as  $3.52 \times 10^{-3}$  N/m.

Some theories have been presented as to how surfactants poison coalescer elements. Bartle <sup>45</sup> suggested adsorption of the surfactant by the element. This would cause re-emulsification of the dispersed phase present on the media. Osterman <sup>26</sup> suggested there was adherence of the surfactant to the media thus allowing the emulsion to pass through unaffected due to the change in fibre wettability. Lindenhofen <sup>58</sup> disproved the above theories experimentally and suggested that the surfactant film at the oil-water

interface, water dispersed, may present a mechanical or electrical barrier to the coalescence of water droplets in the media. Flushing the element with Iso-propyl alcohol improved its coalescence performance and lowered its pressure drop. More recently <sup>59</sup> he suggested that commercial coalescers, which normally have a cotton outer wrapping or 'sock', malfunction due to the sock's adsorption of surfactant from the continuous phase when dispersed phase, i.e. water wetted, causing a high surfactant concentration at the release point. By coating the sock with a fluorocarbon resin a hydrophobic surface was produced and this operated normally even if poisoning was attempted. These results support the theory first presented by Hazlett <sup>53</sup> that poisoning is caused by interference with the detachment process at the point of release of the coalesced water drops from the sock.

From a study of the effect of the sodium sulphonate surfactant on fibrous bed coalescence, Hazlett <sup>53</sup> concluded that doubling the surfactant concentration from 0.5 ppm to 1.0 ppm influenced the coalescence phenomena to a greater extent than a 30 fold change in velocity. The additive did not affect the approach or attachment processes but only affected droplet release. Thus instead of the drops growing into balloon-shaped globules and detaching from the same site by rupture of the neck, they were extended by the force of the continuous phase film into thin fingers, which oscillated normal to the flow and released drops from the tip.

With continuous phase soluble surfactants, a reduction in interfacial tension from  $40 \times 10^{-3}$  to  $10 \times 10^{-3}$  N/m reduces the thermodynamic instability of dispersions and stable emulsions can readily be formed. At values of  $0.1 \times 10^{-3}$  N/m droplets break up spontaneously to form a stable emulsion<sup>60</sup>; such an emulsion cannot be coalesced in a fibrous bed. Even in very low concentrations surfactants affect the interfacial tension. In larger concentrations, however, the drops are completely covered with a 'skin'. For dilute surfactants, the drop surface is not completely covered and size distribution change may occur due to drop interactions. For higher concentrations, the coverage becomes complete and the drops are isolated causing a distribution highly resistant to change. However for primary drops falling through a continuous phase at low Reynolds numbers the surfactant is swept to the rear of the drop by the tangential velocity on the surface forming a 'dust cap'<sup>61</sup>. No comparable work has been published for secondary drops.



### 5.1. INTRODUCTION.

Since both primary and secondary dispersions may co-exist during coalescence in a packed bed and the distinctions between the two types are not well defined, discussion of the mechanisms, whereby their drop sizes are increased will be combined. The coalescence process will be considered in three basic stages, namely capture of dispersed drops, coalescence of the drops and flow of the bulk phase through the packing and finally, release of the coalesced drops. This approach is convenient because most previous workers have defined three stages of capture, flow and release but have disagreed with the mechanism thereof or found them inapplicable to their particular system.

### 5.2. DROP CAPTURE.

Any coalescence device designed to treat flowing secondary dispersions must be able to capture the drops which then maintain close proximity with others. The drops should be retained for a sufficient time to permit drainage of the continuous phase between them thus allowing coalescence to take place. Capture of a drop suspended in a flowing continuous phase is theoretically possible by one or more of the following occurrences,

- (i) Collision with another drop suspended in the dispersion.
- (ii) Collision with an obstruction in the packing structure.
- (iii) Collision with another drop which has been captured and is attached to the packing structure.

The probability associated with the first occurrence is reported to be low by Sareen et al <sup>39</sup> who made photomicrographic studies and observed little or no coalescences between freely moving drops. Although collisions with the packing structure are important, especially during the initial

41

transient operation of a coalescer, the drop collection rate is considerably enhanced by the presence of drops held within the interstices and attached to the packing fibres.

Bitten<sup>62</sup>, in a study of the coalescence rates of water drops on single fibres, observed growth of drops attached to the fibres by coalescence with drops captured from a flowing dispersion. The significant role of retained drops in contributing to capture is also confirmed by the experimental data of Ghosh and Brown<sup>63</sup> and Farley and Valentin<sup>19</sup> who both reported increased drop removal efficiencies in a coalescing bed after several hours operation.

The effect of the dispersed phase saturation in assisting drop capture has been incorporated into models describing drop capture mechanisms. Sherony and Kintner<sup>64</sup> considered the size distribution of retained drops which act as potential collectors and this approach was further modified by Rosenfeld and Wasan<sup>65</sup> by inclusion of an effective fibre diameter. The latter was intended to account for the effect of held drops, but this concept is not consistent with their model which assumes all drops remain discrete and this precludes the existence of a dispersed phase continuum. Spielman and Goren<sup>66</sup> assumed that the dispersed phase exists entirely as discrete, spherical globules and evaluated the capture rate from analysis of the trajectory of a drop approaching a spherical collector. This method permitted independent evaluation of drops captured by packing fibres and those captured by held drops.

Modelling of drop capture processes is difficult due to the complex interfaces which exist between dispersed and continuous phases and the solid phase of the packing structure. Definition of collector geometry and formulation of a mathematical model to describe the hydrodynamic behaviour of

the liquids flowing in a coalescer, where the dispersed phase saturation may exceed 50%<sup>67</sup>, are the chief problems. The first attempts to hypothesize the mechanisms of removal of particles suspended in a flowing fluid were made in studies of aerosol filtration in fibrous beds having porosities greater than 95%. A convenient way of analysing the collection mechanisms is to consider the behaviour of a drop or particle as it approaches a collector. Cylindrical collectors describe the geometry of fibrous beds and spherical collectors characterise granular media.

To describe and compare the possible drop capture mechanisms, the geometrical model illustrated by Fig.5.1. is proposed which represents drops approaching either a cylindrical or spherical collector. Also, initially, the presence of held drops and the effects of interaction with neighbouring collectors will be ignored. The mechanisms which influence drop capture will now be independantly examined to ascertain their relative contributions to the overall capture efficiency.

5.2.1.1. Indirect Interception.

In aerosol filtration and coalescence processes, the diameter of the collector may be comparable to the drop diameter. Under these conditions, the finite size of the drops cannot be neglected and interception between the drop and collector becomes significant. This mechanism is characterised by the value of the Interception number,  $N_R = \frac{d_p}{d_c}$ . The capture efficiency,  $\eta$  is defined as the ratio of the number of drops captured to the number of drops approaching within the projected area of the collector per unit time. Drops are assumed to follow the fluid flow streamlines around the collector and are captured if the distance between the centre of the drop and the periphery of the collector is less than the drop radius.

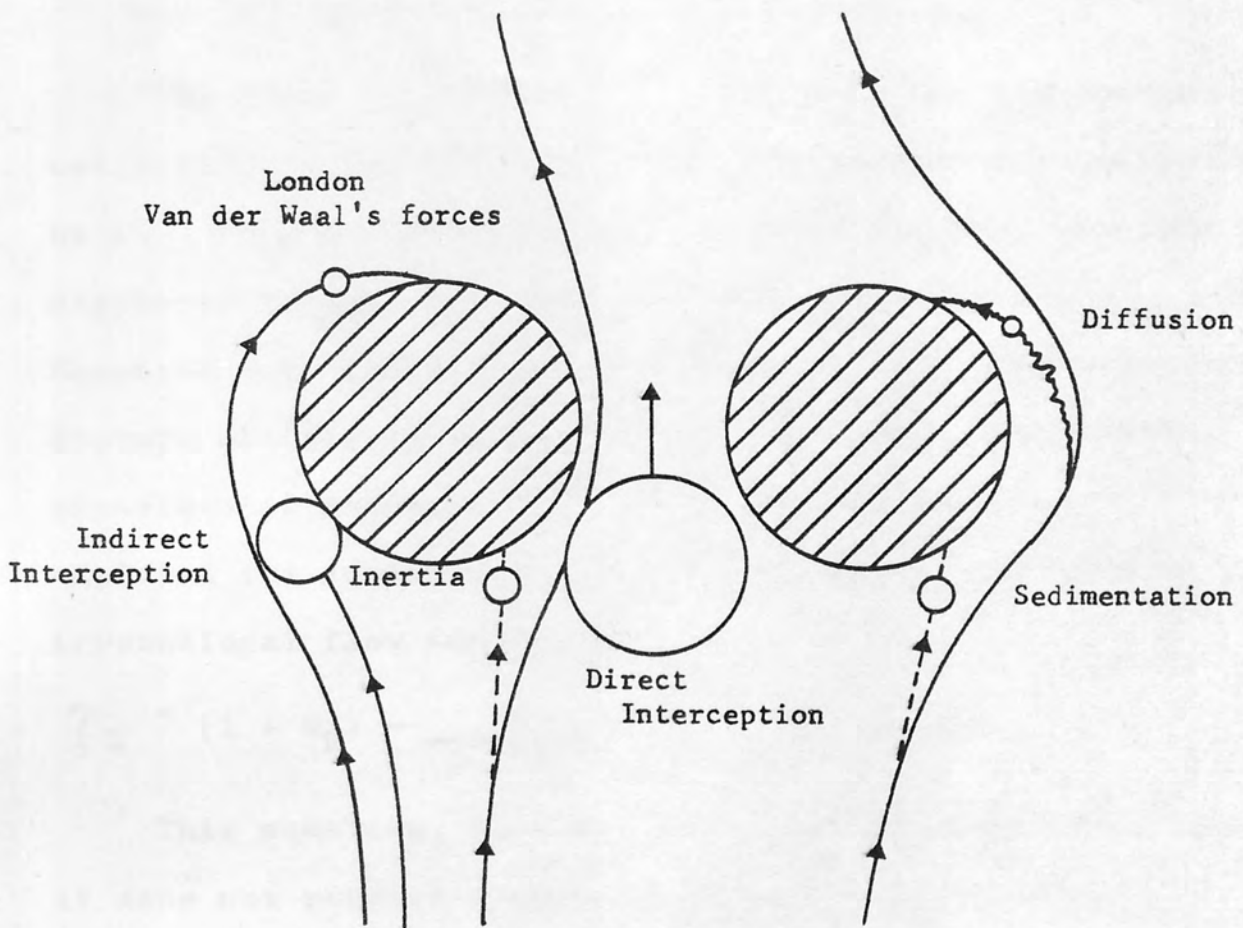


Fig 5.1 Depiction of Drop Capture Mechanisms.

Hazlett <sup>53</sup> proposed the use of an equation developed by Langmuir to evaluate the interception mechanism. This equation determines the capture efficiency of a single cylindrical collector under viscous flow conditions,

$$\eta_I = \frac{1}{2A} \left[ 2(1 + N_R) \ln(1 + N_R) - (1 + N_R) + \frac{1}{(1 + N_R)} \right] \quad 5.1.$$

where the hydrodynamic function,  $A = 2 - \ln N_{Re}$   
and for viscous flow over a cylinder,  $N_{Re} < 1$

The Reynolds' number,  $N_{Re}$ , based on the diameter of the collector, is included since the streamlines are influenced by it. They are affected at a greater distance upstream and displaced further from the collector laterally as  $N_{Re}$  decreases. Equation 5.1. predicts that as the velocity increases, the capture efficiency increases which generally contradicts experimental evidence <sup>19,54,68</sup>. Rosenfeld and Wasan <sup>65</sup> employed the equivalent of the above expression written for irrotational flow conditions,

$$\eta_I = (1 + N_R) - \frac{1}{(1 + N_R)} \quad ; N_{Re} > 1000 \quad 5.2.$$

This equation, however, is no better description since it does not predict a reduced capture efficiency with increasing  $N_{Re}$ . Rosenfeld and Wasan accounted for the effect by empirically fitting their data for velocities greater than an experimentally observed critical value. Further, equation 5.2 is only valid for high Reynolds' numbers which are not encountered in practical coalescers. (See table 5.1)

The decrease in filter coefficient as the superficial velocity increases may not be due to a decrease in drop capture efficiency since Davies and Jeffreys <sup>41</sup> concluded that an optimum velocity exists for a given packing. When the local viscous shear forces exceed the forces of adhesion between the drops and collector, detachment of the drop, or

Investigator	Dimensionless Groups Characterising Mechanisms							Predominant Mechanisms proposed for Drop Capture
	$N_{Re}$	$N_R$	$N_{Rd}$	$N_{Stk}$	$N_G$	$N_{Ad}$	$N_{Pe}^a$	
Ghosh <sup>63</sup>	$10^7$	$10^3$	-	10	$-10^5$	$10^{-9}$	$10^6$	Electrophoresis
Hazlett <sup>43</sup>	1	0.1	-	$10^{-4}$	$10^{-6}$	$10^{-6}$	$10^4$	Interception/Inertial Impaction/Diffusion.
Rajagopalan <sup>69</sup>	10	$10^{-4}$	-	$10^{-6}$	0.1	$10^{-9}$	$10^6$	Interception/London/Diffusion/Sedimentation.
Sareen <sup>39</sup>	1	0.1	-	$10^{-4}$	$-10^{-4}$	$10^{-6}$	$10^5$	Interception/Inertial Impaction/Diffusion
Shalhoub <sup>70</sup>	1	10	-	0.1	$-10^{-2}$	$10^{-6}$	$10^5$	Interception
Sherony <sup>64</sup>	1	1	-	0.1	$10^{-4}$	$10^{-5}$	$10^6$	Interception/Inertial Impaction/Diffusion.
Spielman <sup>66</sup>	0.1	1	-	$10^{-2}$	$\frac{10^7}{-10^4}$	$10^{-2}$	$10^3$	London Forces.
Spielman <sup>67</sup>	10	$10^{-2}$	-	$10^{-2}$	0.	$10^{-6}$	$10^6$	London Forces.
Vinson <sup>54</sup>	$10^{-2}$	0.1	0.1	$10^{-3}$	$-10^{-3}$	-	$10^4$	Interception/Inertial Impaction
This Study	10	0.1	0.1	0.1	$-10^{-2}$	$10^{-5}$	$10^5$	Interception/London/Sedimentation

a. Minimum values of the Peclet number are stated since as  $N_{Pe}$  decreases, the contribution by diffusion to drop capture increases. ; b - See Section 10.2.

Table 5.1. Maximum Values of Dimensionless Groups encountered in Coalescence Studies.

part of the drop, occurs which is manifested as redispersion. Therefore, assuming the validity of the single collector model, the predicted relationship between capture efficiency and velocity may apply to coalescence processes.

#### 5.2.1.2. Hydrodynamic Retardation.

Inspection of equation 5.1 indicates that  $\eta_I$  increases as the parameter,  $N_R$  is increased and although this trend is observed in aerosol filtration, it does not apply to coalescers. The theory of classical interception, which is based on a non-slip continuum model for flow around the collector, becomes invalid when the separation between drop and collector is of the order of the mean free path length of the fluid molecules. For gaseous molecules, this length is approximately  $0.1 \mu\text{m}$  and when the drop/collector separation approaches this value, the hydrodynamic resistance is reduced, thus facilitating capture by interception. For liquids, however, the mean free path is of the order of molecular dimensions and viscous interaction between drop and collector increases as the separation decreases because the rate of drainage of the intervening continuous phase film is reduced.

Hydrodynamic retardation of the interception mechanism has been incorporated into the model of Spielman and Goren<sup>68</sup> which describes the trajectory of a drop in the vicinity of a cylindrical collector. Correction for the increase in drag forces, due to both fluid velocity and motion of the drop, was made using the universal hydrodynamic functions which are described in Appendix M. Unfortunately the only available means to include hydrodynamic retardation effects is to perform a rigorous trajectory analysis. Rajagopalan and Tien<sup>69</sup> theoretically investigated the effect of retardation on deep bed filtration. Their

trajectory analyses, using a single spherical collector model, predicted a monotonic reduction in capture efficiency as  $N_R$  was increased. It was also shown that retardation is significant when the drop/collector separation is less than five drop diameters.

Consequently, for large values of  $N_R$ , hydrodynamic retardation is an important factor, especially when coalescence is induced in low porosity beds. Rajagopalan suggested that, in packed beds, the decrease in capture efficiency is offset by capture of drops by pores whose diameters are less than those of the drops. Although these effects are likely to occur simultaneously, their relative contributions to the drop capture efficiency have not been quantified.

#### 5.2.2. Direct Interception.

Interception by pore catchment occurs when an approaching drop is arrested by a pore through which it cannot pass (see Fig. 5.1 ). Bartle <sup>45</sup> suggested that other drops would then be captured and coalesced with a retained drop. This mechanism predominates in the coalescence of primary dispersions since it is well known that when the drop diameter is less than the equivalent diameter of the packing interstice, the coalescence rate is very low, even when the dispersed phase wets the packing <sup>71</sup> . Direct interception of drops, with subsequent mechanical retention by the packing may be characterised by a second interception number,

$N_{Rd} = \frac{d_p}{d_a}$  . Inspection of  $N_{Rd}$  shows that pore catchment will contribute significantly to the capture rate when either drop diameter increases by coalescence, or when the equivalent diameter of the interstices,  $d_a$  is decreased. The latter occurs when drops captured and retained by the collectors reduce the effective area of the apertures available for

flow of the dispersion. The capture efficiency by direct interception may be mathematically expressed as follows,

$$\left. \begin{array}{l} \eta_{DI} = 1 \quad ; \quad N_{Rd} \geq 1 \\ \eta_{DI} = 0 \quad ; \quad N_{Rd} < 1 \end{array} \right\} \quad 5.3$$

### 5.2.3. Inertial Impaction.

When the density of the drops exceeds that of the continuous phase, the trajectory of the drops as they approach a collector, may not coincide with the fluid streamlines due to inertia of the drop. This mechanism is important in aerosol filtration where the density difference is high and the viscosity of the continuous phase is low.<sup>72</sup> Hazlett<sup>43</sup> and Sherony<sup>64</sup> suggested this mechanism to be relevant to coalescence in fibrous beds and characterised its contribution by the magnitude of the Stokes' number

$$N_{Stk} = \frac{d_p^2 \rho_c u}{9 \mu_c d_c}$$

Impaction becomes significant when  $N_{Stk}$  exceeds a critical value which depends on the Reynolds' number. For viscous flow, values of  $N_{Stk \text{ crit}}$  of between 0.1 and 0.9<sup>73</sup> have been proposed and for potential flow conditions, Langmuir<sup>73</sup> determined  $N_{Stk \text{ crit}}$  to be 0.063. The latter value was used by Sherony<sup>64</sup> for viscous flow conditions which would have overestimated the significance of impaction. Referring to Table 5.1, it appears that the majority of studies in coalescence have been conducted under conditions where  $N_{Stk}$  is less than the critical value. Notable exceptions are the investigations of Sherony<sup>64</sup>, Shalhoub<sup>70</sup> and this study but of these only the work of Sherony involved a situation where the density of the dispersed phase was greater than that of the continuous phase. The other studies were therefore completed under conditions which preclude any contribution to capture by impaction.

An empirical expression relating capture efficiency by inertial impaction to the Stokes' number has been proposed by Landahl<sup>73</sup>,

$$\eta_{II} = \frac{N_{Stk}^3}{N_{Stk}^3 + 0.77 N_{Stk}^2 + 0.22} \quad 5.4$$

$$\text{for } N_{Re} \leq 10 ; N_{Stk} \geq N_{Stk \text{ crit}}$$

#### 5.2.4. Sedimentation.

The density difference between dispersed and continuous phases also causes the drop trajectories to deviate from the fluid streamlines due to buoyancy forces. Their magnitude is characterised by the Gravity number,  $N_G = \frac{d_p^2 (\rho_d - \rho_c) g}{18 \mu_c u}$

which is the ratio of the drop terminal velocity, assuming viscous flow conditions, to the superficial velocity of the dispersion flowing through the bed. Rajagopalan and Tien<sup>69</sup> showed that the capture efficiency is equal to the value of the Gravity number,

$$\eta_G = N_G ; N_G > 10^{-3} \quad 5.5.$$

The condition associated with this equation is not restrictive since the contribution due to sedimentation is negligible for  $N_G < 10^{-3}$ .

With reference to Fig. 5.1, it should be emphasized that gravity forces aid drop capture upstream of the collector but oppose collection on the downstream side. This effect may be taken into account in rigorous determination of efficiency by trajectory analyses

#### 5.2.5. London-Van der Waals' Forces.

Spielman and Goren<sup>65</sup> recognised that the long range attractive forces between a drop and collector may contribute to drop capture. These London or dispersion forces increase rapidly as the drop approaches the collector to overcome the hydrodynamic retardation effects discussed in Section

5.2.1.2 or to offset any double layer interaction described in the following section. Dispersion forces arise due to the polarisation of one molecule caused by fluctuations in the charge distribution within an adjacent molecule and vice-versa. These forces are, however, retarded because a finite time is required for propagation of electromagnetic radiation between the particles.

Hamaker <sup>74</sup> derived an expression from which the London attractive force between a sphere and a plane surface neglecting electromagnetic retardation may be evaluated,

$$F_{Ad} = \frac{2Q}{3a_p (H+2)^2 H^2} \tag{5.6}$$

where  $a_p$  is the sphere radius

H is the dimensionless separation between the sphere and plane surface,  $H = \frac{h}{a_p}$

Q is the Hamaker constant.

Since the London force depends on separation, knowledge of the motion of a drop in the vicinity of a collector is required to determine the capture efficiency. Spielman and Goren <sup>68</sup>, by considering a force balance on a drop, derived an equation to describe the critical trajectory. The capture efficiency may then be deduced since approaching drops, whose paths lie within the flow area associated with the critical trajectory, will contact the collector. The model of Spielman has been applied specifically to values of the operating parameters investigated in this study in Appendix M. The London force term given by equation 5.6 was modified using a more rigorous expression developed by Rosenfeld <sup>75</sup> to describe the attraction between a sphere and cylinder. Correction for electromagnetic retardation is also

included.

The Adhesion number,  $N_{Ad} = \frac{4Q}{9\pi N_R^2} \left[ \frac{1}{\mu_{eud}^2} \right]$  represents a measure of the dispersion forces and Spielman solved the trajectory equation analytically for small Interception numbers and large Adhesion numbers to give the capture efficiency in terms of this dimensionless parameter.

$$\eta_L = \frac{N_R^2}{A} \left( \frac{3\pi A}{2} N_{Ad} \right)^{0.333} \quad 5.7$$

### 5.2.6. Electrical Double Layer Forces.

When two phases are in contact, the phase boundary often carries a net positive or negative charge which may result from the presence of electrons or ions. A negative charge may arise when one phase is a metal and both positive and negative charges occur due to preferential adsorption or dissolution of one ionic species. The ionic double layer then forms by retention of mobile ions adjacent to the phase boundary by electrostatic attraction to the boundary charge. The interaction between the double layers surrounding the drop and collector may be repulsive or attractive depending on whether their respective charges are like or opposite.

Spielman and Fitzpatrick<sup>76</sup> give the following expression for the double layer force between a drop and collector,

$$F_{DL} = \epsilon \zeta_p \zeta_c N_{DL} \left[ \frac{e^{-N_{DL} H}}{1 + e^{-N_{DL} H}} \right] \quad 5.8$$

where  $\epsilon$  is the dielectric constant of the continuous phase;  $\zeta_p$ ,  $\zeta_c$  are the zeta potentials of the drop and collector respectively.

The Double Layer group,  $N_{DL} = \frac{Kd_p}{2}$ , where K is the

reciprocal Debye length indicates the relative thickness of the double layer.

When the Electrokinetic group,  $N_{E2} = \frac{2\zeta_c \zeta_p}{(\zeta_c^2 + \zeta_p^2)}$  is

positive, the force given by equation 5.8 is repulsive and when the converse is true, the force is attractive.

For low electrolyte concentrations in the continuous phase, double layer forces only become significant when the distance between drop and collector is less than to an order of 20 nm<sup>77</sup>. As London forces also become important for separations of this magnitude, the relative numerical values of these forces determine whether the surface interactions are favourable to promote drop capture.

Spielman<sup>76</sup> developed a criterion to neglect double layer forces in trajectory analysis which was based on the requirement that,

$$F_{DL} \ll F_{Ad} \quad \text{at} \quad H = H^* \quad 5.9$$

where  $H^*$  is the dimensionless separation at the rear stagnation point of the critical trajectory (see Appendix M ).

Rajagopalan and Tien<sup>69</sup> established that the resultant force, calculated as the sum of the double layer interaction and the retarded London attraction, indicated no barrier against drop-collector contact for parameters relevant to coalescence processes. They concluded that these surface interactions, when considered as transport mechanisms, are unimportant providing that their net effect is attractive in the vicinity of the collector.

An expedient way considering the case of unfavourable surface interaction is to regard the collection efficiency under these conditions to be a fraction of that under favourable interaction. This fraction could be related to

the parameter,  $\beta$  introduced by Sherony<sup>64</sup> to account for the ratio of the number of coalescence events to the collision frequency.

### 5.2.7. Diffusion.

Drops of submicron size possess a random transverse motion which causes them to depart from the flow streamlines. This Brownian motion, due to bombardment of suspended drops by continuous phase molecules may contribute to the capture efficiency. Inclusion of the random force that induces Brownian motion into equations describing drop trajectories, considerably complicates their solution, but Prieve and Ruckenstein<sup>78</sup> have demonstrated that separate treatment of this mechanism is adequate.

The Peclet number,  $N_{Pe} = \frac{d_c u}{D}$ , is often introduced to characterise diffusion and is a measure of the ratio of transport by convective forces to transport by molecular diffusion. Many workers investigating diffusion for low Reynolds' numbers and small particle sizes employ the Sherwood number,  $N_{Sh} = \frac{I}{\pi d_c D C}$  as a measure of the mass transfer or deposition rate. This approach is useful for correlation of results for different collector geometries. For a cylindrical collector, the Sherwood number is related to capture efficiency by the following,

$$N_{Sh} = \eta_D N_{Pe} \quad 5.10$$

The equations developed through several investigations of transport by diffusion have been rearranged using equation 5.10 and presented in Table 5.2. Examination of these modified forms shows a common relationship between capture efficiency and Peclet number, with slightly differing dependency on Reynolds' number. The efficiencies, calculated for values of these groups typically encountered in coalescence processes, exhibit close agreement. From

Investigator	Proposed Transport Equation	Diffusion Capture Efficiency (Modified form)	Calculated Value x10 <sup>-5</sup>
Langmuir <sup>43</sup>	$\mathcal{Q}_D = 2.16 (2A)^{-1/3} N_{Pe}^{-2/3}$	$2.16(2A)^{-1/3} N_{Pe}^{-2/3}$	1.04
Natanson <sup>73</sup>	$N_{Sh} = 1.17 \pi (2A)^{-1/3} N_{Pe}^{1/3}$	$3.68(2A)^{-1/3} N_{Pe}^{-2/3}$	1.77
Friedlander <sup>79</sup>	$N_{Sh} = 1.035 \pi (2A)^{-1/3} N_{Pe}^{1/3}$	$3.25(2A)^{-1/3} N_{Pe}^{-2/3}$	1.57
Ranz <sup>73</sup>	$\mathcal{Q}_D = \frac{\pi}{N_{Pe}} \left\{ \frac{1}{\pi} + 0.55 N_{Sc}^{1/3} N_{Pe}^{1/2} \right\}$	$N_{Pe}^{-1} + 1.727 N_{Re}^{1/6} N_{Pe}^{-2/3}$	1.32
Emi <sup>80</sup>	$\mathcal{Q}_D = 6 N_{Re}^{1/6} N_{Pe}^{-2/3}$	$6 N_{Re}^{1/6} N_{Pe}^{-2/3}$	4.57
Rajagopalan <sup>69</sup>	$\mathcal{Q}_D = 4.04 N_{Pe}^{-2/3}$	$4.04 N_{Pe}^{-2/3}$	3.22
Prieve <sup>78</sup>	$N_{Sh} = 0.995 N_{Pe}^{1/3}$	$3.98 N_{Pe}^{-2/3}$	3.17
Spielman <sup>66</sup>	$\mathcal{Q}_D = 2.3 (2A)^{-1/3} N_{Pe}^{-2/3}$	$2.3(2A)^{-1/3} N_{Pe}^{-2/3}$	1.35

a - Calculations performed for  $A = 2 - \ln N_{Re}$ ,  $N_{Re} = 0.763$ ,  $N_{Pe} = 4.44 \times 10^7$

Table 5.2. Comparison of Equations describing Drop Capture by Diffusion.

this comparison, it may be concluded that, although the proposed equations assume apparently different forms, they are basically similar when examined closely. Therefore, any of the equations may be applied without incurring significant errors especially since the capture efficiency due to diffusion alone is relatively small.

In addition to capture of drops by a stationary collector, coalescence between pairs of drops moving in the interstices of the packing is feasible by the mechanism of turbulent coagulation. However, Sherony<sup>64</sup> and Shalhoub<sup>70</sup> evaluated a theoretical collision frequency due to coagulation using the hydraulic diameter of the interstices as a first estimate for the size of large scale turbulence. Their calculations indicate a negligible contribution by this mechanism which is supported by experimental observations as discussed in Section 5.2.

This section concludes the description of drop capture mechanisms known to feature in secondary dispersion coalescence; their relative contributions to the overall capture efficiency are further investigated quantitatively in Section 10.2.

### 5.3. COALESCENCE PROCESSES.

#### 5.3.1. Coalescence Sites.

After capture, by either held drops or packing fibres, drops will continue to coalesce until hydrodynamic forces cause detachment from the coalescence site. Fig. 5.2 shows the different forms of drop behaviour that may occur, resulting in coalescence. When the drops are small compared with the collector and aperture diameters, coalescence may take place between adjacent drops located on the collector surface (Fig. 5.2a). Bitten<sup>62</sup> observed that this is a slow process for the coalescence of drops on single fibres

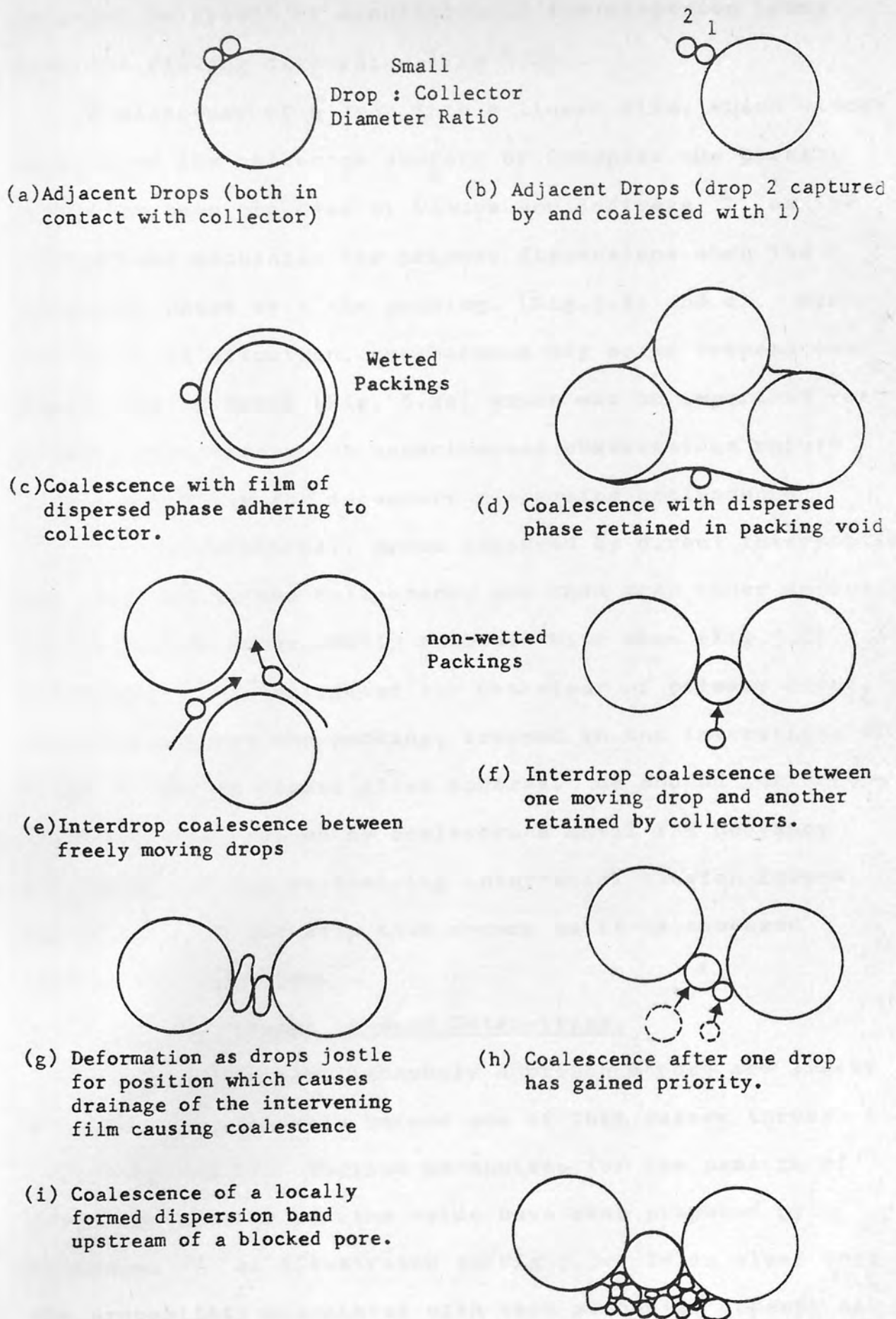


Fig 5.2 Coalescence Mechanisms in a Packed Bed.

compared to growth by acquisition of the dispersed phase from the flowing dispersion (Fig 5.2b).

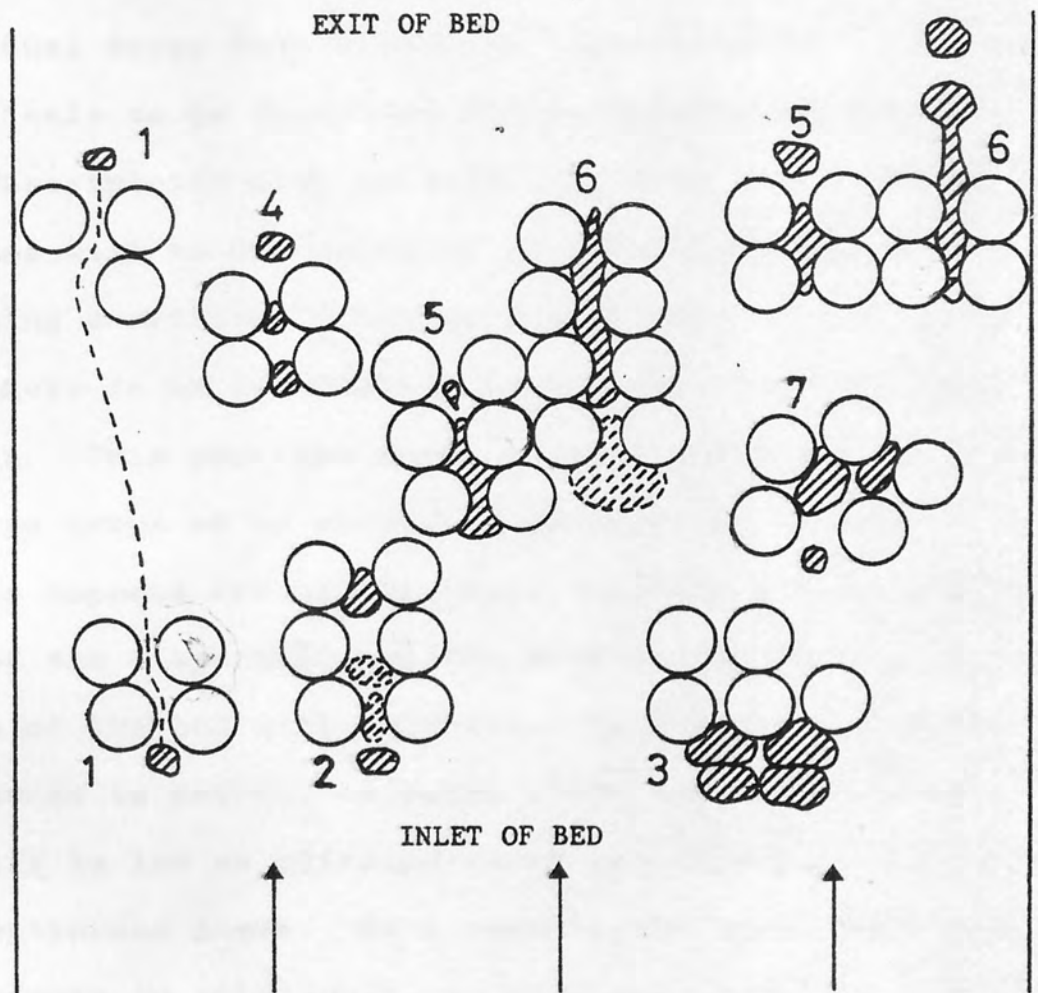
Coalescence of a drop into a liquid film, which either adheres to the collector surface or occupies the packing void, has been proposed by Davies and Jeffreys<sup>41</sup> as the predominant mechanism for primary dispersions when the dispersed phase wets the packing. (Fig.5.2c and d). For the converse situation, coalescence may occur between two freely moving drops (Fig. 5.2e) which may be important for primary dispersions but experimental observations refute this possibility for secondary dispersion coalescence<sup>64</sup>

<sup>39</sup>. Alternatively, drops captured by direct interception and retained by the collectors, may then trap other approaching drops and subsequently coalesce with them (Fig 5.2f). Wilkinson<sup>81</sup> investigated the behaviour of primary drops, that did not wet the packing, trapped in the interstices of a bed of random packed glass spheres. He showed that drops increase their volume by coalescence until the buoyancy forces exceed the restraining interfacial tension forces; deformation of the drop then occurs as it is squeezed through the aperture.

### 5.3.2. Drop Passage through Interstices.

Drops which simultaneously approach a pore are likely to jostle for priority before one of them passes through it. (Fig 5.2g and h). Various mechanisms for the passage of drops through the packing voids have been proposed by Wilkinson<sup>81</sup> as illustrated in Fig 5.3. It is clear that the probability associated with each mechanism depends on the value of the direct interception number  $N_{Rd}$  (See Section 5.2.2.).

However, important differences exist between the conditions under which secondary and primary coalescers



- 1 Unrestricted drop passage.
- 2 Restricted drop passage (penetration due to kinetic forces)
- 3 Inlet drop restriction
- 4 Retention-Impact-release
- 5 Unrestricted drop release
- 6 Restricted drop release
- 7 Preferential flow-path

Fig 5.3 Proposed Droplet Hydrodynamics in a Non-wetted Packing of equal-sized spheres.

operate. Firstly, secondary drops possess more surface energy per unit mass due to their size and also buoyancy forces are usually negligible as shown by the magnitude of the gravity number in Table 5.1. Therefore drop deformation and drainage of the intervening continuous phase film prior to coalescence is less easily accomplished. For this reason, the retention-impact-release mechanism, whereby small individual drops deform to pass through micron sized pores, is unlikely to be important for secondary dispersions.

Unrestricted drop passage, may also be insignificant since as will be demonstrated in the following section, drops attaining a critical diameter for release from a collector are likely to be immediately recaptured by direct interception. This provides evidence that pores may become blocked by large drops or by simultaneous approach of smaller ones. If this happens frequently fewer channels are available for flow of the dispersion and the pressure gradient per unit length of the bed will increase. Captured drops will then be induced to retreat to sites where the interstitial velocity is low so offering least resistance to the flow of the continuous phase. As a result, the drops will tend to concentrate in relatively few channels where they queue in a localised 'dispersion band' type formation until coalescence occurs with adjacent drops and the drop which blocks the pore. As more flow paths become blocked, eventually the increasing pressure gradient will be sufficient to force coalesced drops through the pores. This proposed mechanism, illustrated in Fig 5.2i, is also consistent with observations of thread formation by restricted drop release (see Fig 5.3) as coalesced pools of dispersed phase are squeezed through the apertures of the packing.

This discussion has been confined to cases where the

dispersed phase is non-wetting but it is suggested that this mechanism could equally apply to wetting situations. An experimental study of collision and coalescence of drops on single fibres <sup>62</sup> showed that capture efficiency is unlikely to be affected by whether or not the fibre is wetted. But the passage of drops through the pores will meet with less resistance, due to capillary action, as they coalesce directly with a flowing continuum of the dispersed phase. This behaviour would imply a relatively lower pressure drop for beds where the dispersed phase wets the packing. Lower pressure gradients, due to easier drop removal from the coalescence site, may, however, alleviate deformation of drops in the local 'dispersion bands' with a possible lowering of coalescence efficiency.

#### 5.4. DISPERSED PHASE FLOW REGIME.

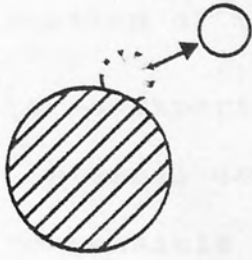
Drops, which have been collected by the packing fibres and reside in the packing interstices until they are coalesced, act as potential collectors for other drops entering the bed. Therefore, both the number and distribution of drops within the packing are important factors governing capture rate and pressure drop under steady state conditions.

##### 5.4.1. Drop Redispersion.

After coalescence by one of the mechanisms described in the previous section, movement of the coalesced dispersed phase may occur by release of the drop from the fibre when the drag forces exceed adhesive and London attractive forces as shown in Fig 5. 4(a).

Adhesive failure causes release of the whole drop, but when adhesion is strong and interfacial tension low, Vinson <sup>54</sup> states that cohesive failure results when only part of the drop is detached. The cohesion mechanism

Adhesive Failure



Cohesive Failure

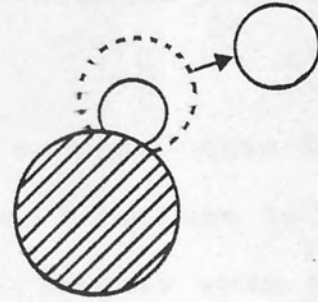


Fig 5.4 (a) Internal Drop Release Mechanisms.

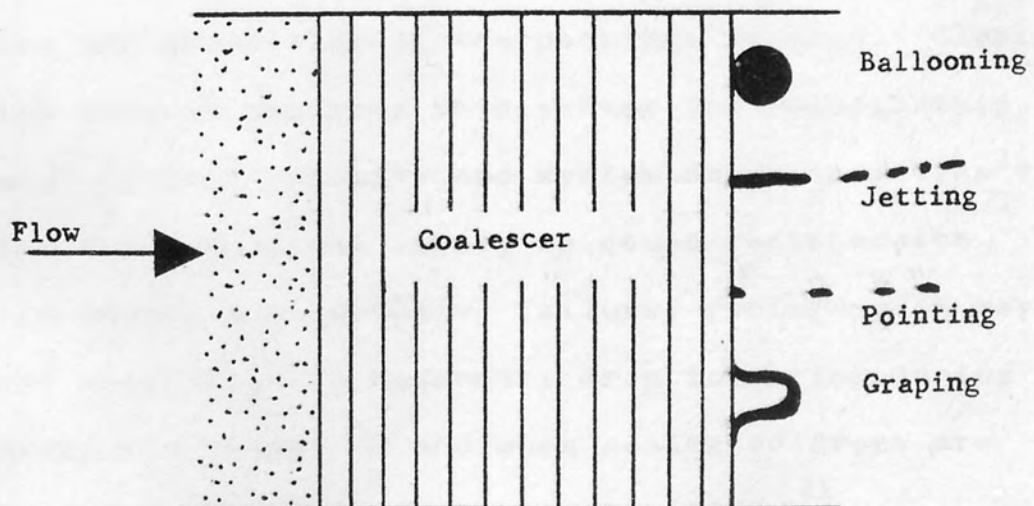


Fig 5.4(b) Exit Drop Release Mechanisms.

involves formation of threads which subsequently break up into smaller drops which are then redispersed into the flowing continuous phase. The size of these drops depends on attenuation of the liquid threads which is suggested to be a function of the viscosity ratio ,  $\frac{\mu_d}{\mu_c}$ <sup>54</sup> although there is no experimental evidence to support this hypothesis. Internal drop release by cohesive failure is thought to be responsible for low filter coefficients when the dispersed phase exhibits a high wetting affinity for the packing material<sup>19</sup>. Also the existence of a critical velocity, above which redispersion considerably reduces efficiency, has been reported by many workers but the value of this velocity varies over two orders of magnitude<sup>70</sup>. Therefore, these values are of little use in practical coalescer design because they are specific to the liquid systems and properties of the packings studied. Clearly, further work is required to discover the relationship between critical velocity and system characteristics to predict the conditions likely to cause redispersion.

In addition to cohesive failure, redispersion may also be attributed to secondary drop formation during the coalescence process<sup>82</sup> and when coalesced drops are squeezed through pores at high velocities<sup>81</sup>.

#### 5.4.2. The Travelling Drop Hypothesis.

Sherony and Kintner<sup>64</sup> and Rosenfeld and Wasan<sup>65</sup>, among others have proposed that drop release is by adhesive failure, after which the large drops travel through the pores of the medium, eventually being released at the downstream face. Their models, presented in Section 10.1 describe coalescence of secondary dispersions in high porosity beds and are based on this travelling drop hypothesis.

They assume that a pendular saturation regime prevails within the bed which precludes the existence of a dispersed phase continuum. Rosenfeld<sup>75</sup> claims that the assumption is justified when the dispersed phase is dilute and because channels should not be present in beds with porosities greater than 0.9. However, Brown<sup>83</sup> showed that the dispersed phase passed through the intermediate portion of a bed using the same channels repeatedly. The threads were observed to pulse and they varied in diameter and flowrate with time. In many cases, the threads were discontinuous, but when flow restarted, the same channels were utilised. Similar behaviour was reported by Hazlett<sup>43</sup> when threads of water were observed in a fibrous bed during the coalescence of a water in fuel dispersion. This experimental evidence suggests that a funicular saturation regime would better represent the dispersed phase distribution.

The saturation in a coalescer, defined as the fraction of pore space occupied by the dispersed phase, cannot be a unique function of the phase ratio of the inlet dispersion. It must also depend on interaction between the packing fibres and the two liquid phases and the superficial velocity. Shalhoub<sup>70</sup>, using a conductivity technique, in high porosity beds showed that saturation was independent of phase ratio. Saturations in the region of 20% are typical for high porosity beds<sup>84</sup> but if the coalesced dispersed phase flows in a small number of preferential channels, then a low saturation does not necessarily imply the absence of a continuum.

#### 5.4.3. Critical Drop Diameter.

The travelling drop models also assume that when drops are detached from fibres, their passage through the bed to the exit face remains unimpeded. Their diameters should

described visual observations of coalescence of water drops in jet fuel on individual fibres of glass, Teflon, Dacron and Nylon. Individual fibres were reported to retain drops having diameters many times those of the fibres without re-entrainment for velocities up to  $2 \times 10^{-2}$  m/s. Glass fibres of 5-6  $\mu\text{m}$  diameter could retain 400-500  $\mu\text{m}$  drops before release but the polymeric fibres, having diameters in the 11-17  $\mu\text{m}$  range, were less retentive as drops were detached when their diameters exceeded 65-75  $\mu\text{m}$ . It may be concluded that characteristic interfibre spacings of 2 or 3 fibre diameters will not permit progressive travel of drops which are 90 or even 5 fibre diameters.

Rosenfeld<sup>75</sup> developed an equation to calculate the critical drop diameter for release but claims that unrealistically large values are predicted by it. There is no evidence to support this; and application of the equation to the data of Bitten<sup>62</sup>, shown in Appendix B considerably underestimates the critical diameter. Calculations performed in this appendix for both high and low porosity beds using maximum values of saturation and superficial velocity yield minimum critical diameters which are several times larger than the pore sizes. However, the results do indicate that redispersion is possible for low porosity beds at velocities greater than  $5 \times 10^{-2}$  m/s.

#### 5.4.4. Dispersed Phase Continuum Model.

Despite the low accuracy of such calculations, the evidence presented in the preceding discussion generally refutes the travelling drop hypothesis in favour of the model proposed by Spielman and Goren<sup>84</sup>.

They assumed that two readily distinguishable regimes of the dispersed phase exist within the packing. One

regime consists of drops that are suspended in the continuous phase; the other is coalesced dispersed phase that is held up in the pores and assumed to form a network of channels which are sufficiently well connected to sustain viscous flow of the dispersed phase by capillary conduction. This model implies that captured drops are immediately coalesced into the continuum which is contrary to observations since coalescence time is large for drops of secondary dimensions.

Spielman and Su<sup>67</sup> recently proposed an additional regime corresponding to an intermediary coalescing dispersed phase, which is a better physical description of the process. This phase consists of a distribution of drop sizes varying from newly-captured drops, which continuously coalesce, to drops which then participate in channel flow. Spielman and Su<sup>67</sup> assumed that the intermediary phase constituted the majority of the total dispersed phase saturation with only a negligible proportion being comprised of newly captured drops and the capillary-conducted phase. Although feasible, this assumption cannot be universally applied, because, if the diameter of the captured drops are comparable to the mean pore diameter, then the proportion of the intermediary phase would be considerably less.

In conclusion, the dispersed phase flow regime proposed by Spielman and Su is probably the most accurate description and is, in most respects, consistent with experimental observations especially for low porosity packings.

#### 5.5. SATURATION PROFILES.

The distribution and quantity of dispersed phase held up in a packed bed depends on the capture, coalescence and internal drop release processes. Therefore, the nature of the saturation profile over the bed depth is closely

related to the dispersed phase flow regime.

Without exception, those workers who postulated the travelling drop hypothesis assumed that the saturation is low and independant of axial position in the bed. An increase in saturation decreases the effective void fraction of the packing and so decreases the continuous phase permeability. Sherony and Kintner<sup>64</sup> and later Shalhoub<sup>70</sup> showed that the Blake-Kozeny equation accurately described single phase flow in packed beds (see Chapter 9). By substituting experimental values of two phase pressure drop into this equation, the effective voidage,  $e_2$  may be calculated. The average saturation in the bed is then determined using,

$$\bar{S} = 1 - \frac{e_2}{e_1} \quad 5.11$$

Rosenfeld<sup>75</sup> used this method to investigate the variation of bed saturation with velocity and produced the following empirical equation,

$$\bar{S} = 2.92 \frac{(1-e_1)u^{-0.2}}{e_1} \quad 5.12$$

The use of an average saturation is however of limited value since experimental evidence has conclusively proved that saturation varies considerably through the length of the bed. Bitten and Fochtman<sup>85</sup> measured the distribution of water in a fibrous bed where a hydrocarbon fuel was the continuous phase. They determined the saturation profile by dismantling the bed after operation and analysing the quantity of water retained in different sections of the bed after extraction using anhydrous methanol. The maximum saturation occurred at the influent face of the bed which rapidly decreased to a fairly constant value for the remaining two thirds of the bed length. Fluctuations about

this constant saturation were observed in the end part of the bed which were attributed to local changes in interstitial velocity caused by perforated plates separating the bed sections.

An increase in superficial velocity always increased the saturation in the forepart of the bed and decreased the saturation in the middle. High velocities also produced a dampening of the internal fluctuations. Low porosity beds possessed much higher saturation values than high porosity packings and the phase ratio of the inlet dispersion did not significantly affect the saturation. These observations indicate that the majority of capture and coalescence predominates in a relatively narrow section in the forepart of the bed and Bitten and Fochtman<sup>85</sup> showed that increasing the length of a bed did not increase the coalescence efficiency or total hold up of dispersed phase.

Shalhoub<sup>70</sup> qualitatively investigated the hold up profile by measurement of electrical conductivity between copper meshes embedded in a fibreglass packing, whilst coalescing a toluene in water dispersion. His measurements confirmed the results of Bitten and Fochtman<sup>85</sup> but the saturation was found to increase significantly near the exit face for which no explanation was given.

The inherent problem of determining saturation profiles, especially for thin, low porosity beds, is selection of a technique to measure the local hold up without disturbing the coalescence process. Spielman and Su<sup>67</sup> surmounted this difficulty by investigating saturation profiles in beds of glass ballotini having depths in excess of 200mm. They were able to determine hold up using an X-ray absorption technique and also by calculation of permeability from pressure drop measurements taken over increments



of the bed length. The results from these techniques exhibited close agreement and the shapes of the saturation profiles were very similar to those obtained by Bitten and Fochtman. Also, samples of the dispersion were taken from corresponding positions in the bed and the rate of coalescence of the dispersion showed a first order dependence on the dispersed phase saturation.

Experimental data indicates, for both high and low porosity beds, that saturation decreases from a high value near the inlet face to a constant value over the remainder of the bed. Drop capture and coalescence processes predominate where the saturation is high and flow of the coalesced phase, probably in discrete channels, is associated with a constant hold up.

The saturation profiles determined by previous experimental studies are examined in greater detail in Section 10.4 as they form the basis for a mathematical model which attempts to describe the variation of saturation with bed depth.

#### 5.6. EXIT DROP RELEASE.

Various observed drop release patterns are illustrated in Fig. 5.4(b),

##### a) Ballooning.

In an ideal situation, one thread feeds a drop at the downstream face of the bed. The balloon-shaped drop then grows until the hydrodynamic buoyancy forces exceed the interfacial tension forces. Rupture occurs at the neck of the drop whose size, when released, depends on the flow velocity and interfacial tension. Hazlett<sup>86</sup> stated that adhesion forces may be significant when the dispersed phase wets the packing material. For the non-wetting situation, Hazlett<sup>53</sup> derived an expression to predict the size of

released drops,

$$d_{pe} = \frac{0.55 d_a^{0.71} \gamma^{0.71}}{\Delta u \rho_c^{0.29} \mu_c^{0.43}} \tag{5.13}$$

for  $d_a < 0.1 d_{pe}$

and  $0.3 < N_{Re}' < 1000$

$$\text{where } N_{Re}' = \frac{d_p \rho_c u}{\mu_c}$$

To apply this equation, it is necessary to experimentally determine the flowrate of dispersed phase in the supply channels so that the difference between drop and continuous phase velocities,  $\Delta u$  may be evaluated.

b) Jetting.

When surfactants are present in the liquid system, an extended thread or jet of the dispersed phase ruptures by Rayleigh instability to form a series of small drops of uniform diameter. Many correlations, reviewed by Wilkinson<sup>81</sup> are available for prediction of drop sizes by jetting and other mechanisms but they only apply when the continuous phase is stationary. Inclusion of a term to account for hydrodynamic forces caused by the flowing continuous phase would considerably enhance the scope of such equations and this aspect is worthy of further study.

c) Pointing.

Another type of release mechanism is pointing, in which 'fingers' of collected drops project beyond the exit face. These 'fingers' taper to a point, vibrate and kick small drops from the tip.

d) Graping.

Langdon<sup>56</sup> and Lindenhofen<sup>59</sup> reported a graping release pattern which is encouraged when the phase ratio is high or when the dispersed phase wets the packing. This

170

mechanism produces bubbles of the continuous phase enclosed by a film of the dispersed phase. After release, the bubbles frequently agglomerate in clusters and may eventually burst to produce a large number of very small drops.

Attarzadeh <sup>87</sup> has recently observed that drop formation takes place by a combination of all the mechanisms described above when the bed consisted of random fibres. However formation by ballooning or the drip-point mechanism is desirable since it produces large drops that require short residence times in a settler.

The first step in the design of a continuous process is the selection of the raw materials and the determination of the quantities of each. This is done by a study of the chemical reaction and the physical properties of the materials. The next step is the selection of the equipment and the determination of the size and the number of units. This is done by a study of the reaction rate and the heat and mass transfer requirements. The final step is the design of the control system and the determination of the operating conditions. This is done by a study of the process dynamics and the control requirements.

CHAPTER 6.

EXPERIMENTAL WORK.

The experimental work is carried out in a laboratory or a pilot plant. The first step is the selection of the equipment and the determination of the size and the number of units. This is done by a study of the reaction rate and the heat and mass transfer requirements. The next step is the design of the control system and the determination of the operating conditions. This is done by a study of the process dynamics and the control requirements. The final step is the carrying out of the experiments and the recording of the data. This is done by a study of the process dynamics and the control requirements.

Charts showing of the continuous process.

## 6.1. EQUIPMENT DESIGN.

The function of the ancillary equipment used was to supply a secondary dispersion of known drop size and dispersed phase concentration at a specified flowrate to a coalescence section. Lines and apparatus were incorporated to facilitate recycling of the liquid during single phase pressure drop measurements, and for irrigation of the mesh beds with the dispersed phase during coalescence operations. The coalescer design was modified several times during this study and will be described in the following section.

The flow diagram of the apparatus is shown in Fig 6.1 and the general arrangement presented in Fig 6.2. The continuous phase was produced by distillation of tap water using an electrically heated boiler with a capacity of  $8 \text{ dm}^3/\text{h}$ . Water leaving the still at  $330 \text{ K}$  was allowed to cool to ambient temperature in a  $350 \text{ dm}^3$  capacity tank of stainless steel construction as shown in Fig C.1. The baffles and turbine agitator were included in this design to permit investigation of coalescence when the continuous phase contains dissolved or dispersed solids. The maximum liquid level inside the tank was automatically controlled using a pressure sensor which is connected to the boiler power supply. It was essential to cover the storage tank because the partially de-aerated water would otherwise absorb air during cooling and be evolved at many points throughout the equipment. The large number of potential nucleation sites and a relatively rapid fall in pressure then caused considerable air evolution within the coalescer producing apparently high pressure drops and erratic drop release during operation.

Course adjustment of the continuous phase temperature

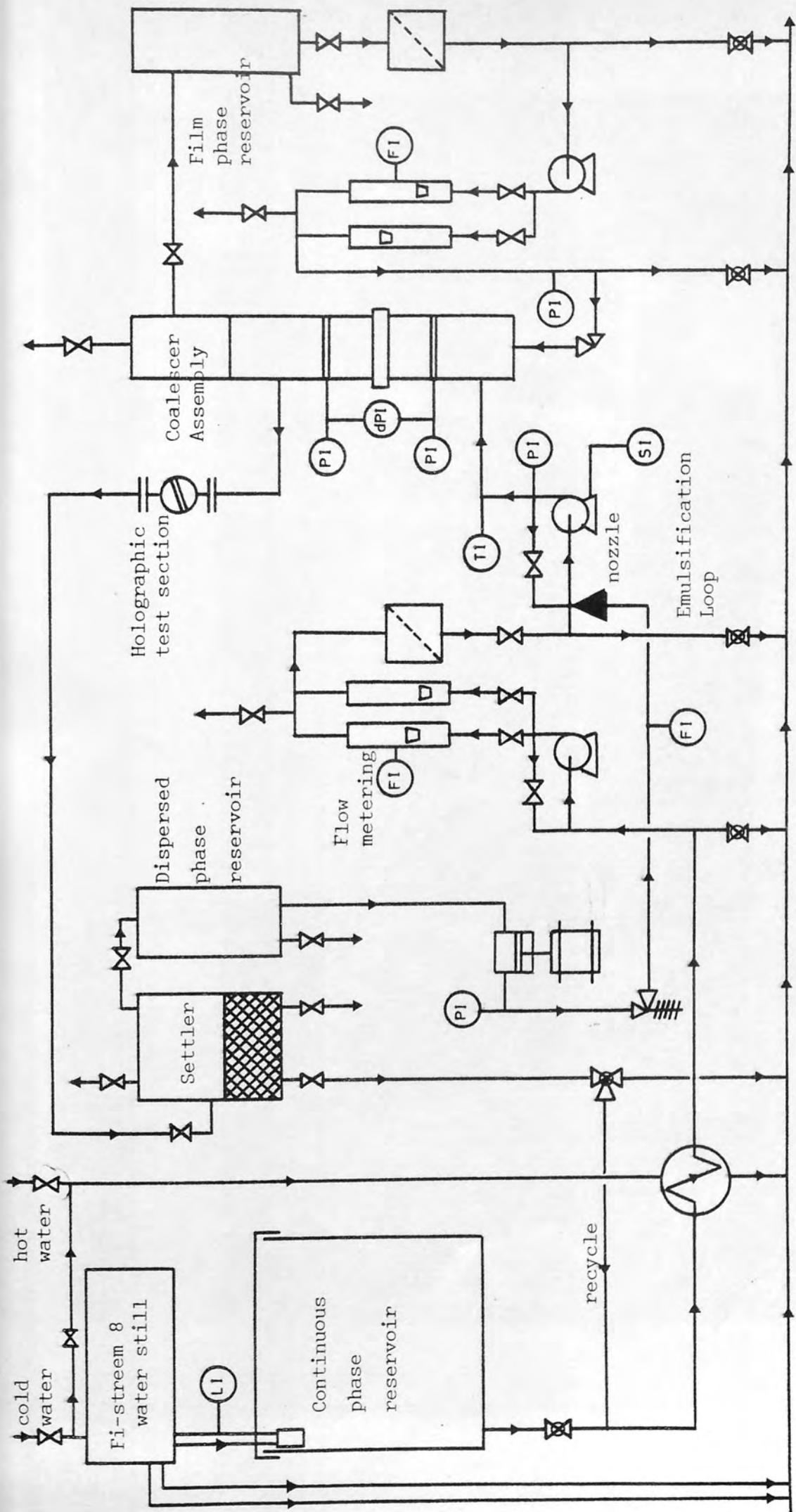
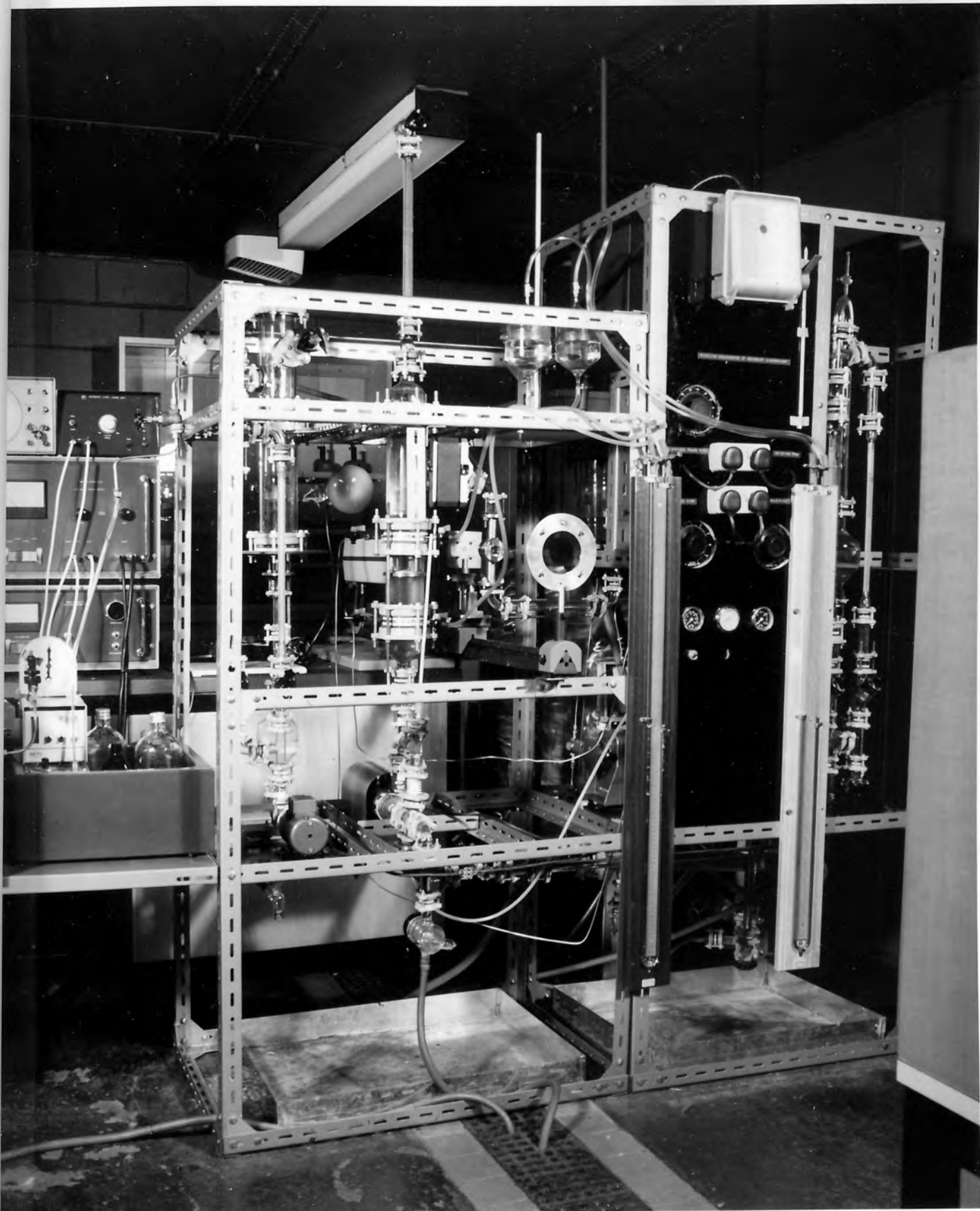


Fig. 6.1. Flow Diagram of Equipment



was accomplished using a water cooled heat exchanger. A gravity-fed stainless steel centrifugal pump with Viton seals was used to transfer the water through the flow metering equipment, coalescence device, and via a gravity settling vessel to drain. Accurate flow control was maintained using a combination of a rheostat installed on the pump power supply, control valve on the delivery line and a control valve on a loop line between the delivery and suction sides of the pump. Flowrates were monitored using two glass rotameters with stainless steel floats which provided a range of superficial velocity from 0 to  $7 \times 10^{-2}$  m/s within the coalescer. Preparation of the continuous phase was completed by filtration through a sintered glass disc of  $110 \mu\text{m}$  mean pore size. Glass pipelines of 18 mm bore, connected using P.T.F.E. gasket rings were used throughout the construction to permit visual detection of possible air ingress, whilst facilitating easy cleaning and avoiding contamination of the liquid systems. Stainless steel was employed in the fabrication of non-standard components such as reducing flanges and vessel covers.

The low concentration (1000 p.p.m.) of the dispersion necessitated a maximum flowrate of  $0.230 \text{ dm}^3/\text{h}$  of the dispersed phase. From a storage vessel, the dispersed phase was gravity fed through 3 mm bore stainless steel tubing to a metering pump operating at 100 strokes/minute. Using a pressure relief valve, the delivery pressure was maintained at approximately 3 bar which ensured efficient operation of the non return valves in the pump head during the suction stroke and prevented excess flow due to the head of the liquid in the storage vessel during delivery. A variable area flowmeter, containing a stainless steel

ball float, placed downstream of the pressure relief valve confirmed that the pump delivered the desired flowrates consistently and accurately. However, due to the reciprocating action of the pump, fluctuations were observed in the delivery pressure and to a lesser extent in the measured flowrate.

The mixing and emulsification techniques available for production of a secondary dispersion are described in Chapter 2. A centrifugal pump with a recycle loop was selected for its inexpensive, simple construction and ease of operation and control. Previous work<sup>17,70</sup> showed that for a given throughput and pump design, the angular velocity of the impellor determined the mean drop size produced. This has been confirmed and the results are discussed in Chapter 8. The pump speed was monitored using an electronic tachometer and maintained at a constant value of 67 rev/s using a rheostat. The dispersed phase was injected through a 1 mm bore stainless steel tube into the suction line of the pump causing immediate break up of the organic phase forming a secondary dispersion. Separation of the dispersion within the recycle loop was not observed even after considerable operating periods and the oscillations caused by the metering pump delivery were effectively damped for all throughputs.

Both transfer of the continuous phase and the emulsification process using centrifugal pumps caused variable and significant increases in the liquid temperature thus preventing isothermal operation over long periods. The liquid temperature was measured upstream of the coalescer using a thermometer inserted in the recycle loop.

After passing through the coalescer, the primary dispersion is recovered in a section of pipe above the

bed and the effluent flows through the holographic test section, whose design is discussed in Section 7.6.2, to a 152 mm. diameter settler. The lower section of the glass settler accommodated a woven stainless steel mesh pad to avoid contamination of the effluent by the highly flammable liquids used as the dispersed phase. The latter could be recycled using the line from the top of the settler to the dispersed phase reservoir.

For irrigation purposes equipment was installed for introduction of a primary dispersion upstream of the coalescer. The irrigating liquid, which may or may not be identical to the dispersed phase, is stored in a reservoir supplied by the coalesced primary dispersion and recycled irrigating liquid. After filtration through a sintered glass disc, the liquid is pumped using a stainless steel centrifugal pump through rotameters to a stainless steel nozzle located just downstream of the emulsification section. The primary dispersion formed at this nozzle may then flow co-currently with the secondary dispersion to the coalescing bed.

## 6.2. COALESCER DESIGN.

Probably the chief disadvantage of a coalescer is its poor performance and reduced operating life when fluids containing particulate material are treated. Irrigation of woven mesh media during gas filtration has been found to increase both the efficiency and life of the filters

88

at the expense of increased pressure drop. A water film falling down the mesh crossflow to the dust laden gas stream increased the particle collection rate by 'shutter' action as the liquid temporarily blocked the apertures of the mesh; the majority of the collected particles were then entrained in the liquid film and not

retained by the fibres. The range of superficial velocities investigated was similar to that relevant to coalescence of secondary dispersions in packed beds and the feasibility of coalescer irrigation was investigated. Also, theoretically, the presence of a liquid film should reduce the effective aperture of the mesh but the increased pressure drop should be compensated by the use of a mesh with a larger aperture size. The selection of the media for coalescence is discussed in the following section.

The initial coalescer design is shown in Fig. 6.3 in which the meshes are clamped to the stainless steel base assembly using a plate secured by two studs, spacers and nuts. A square (40 mm x 40 mm) flow cross section was employed to encourage even distribution of the irrigating fluid over the coalescer surface. The liquid distributor, screwed directly beneath the flow area, consisted of a small header with 1 mm diameter holes drilled along its length. One face of the header was inclined so that liquid emerging from the holes would contact the mesh. The outer grooves of the assembly were designed to accommodate a 76.2 mm bore glass pipe section, thus enclosing the entire coalescer within the liquid system. Although clamping the assembly at a pipe joint would be easier, this method was rejected because it impaired visual observations of the coalescence process and prevented presoaking of the bed. The metal assembly was bonded to the ground glass faces of the pipe using a fluorocarbon based adhesive/sealant, Silastic 733RTV as supplied by Dow Corning which performed adequately in terms of mechanical strength and solvent resistance throughout the work. The coalescer is shown under typical operating conditions by Fig 6.4 in a vertical arrangement and in the absence of an irrigating liquid.

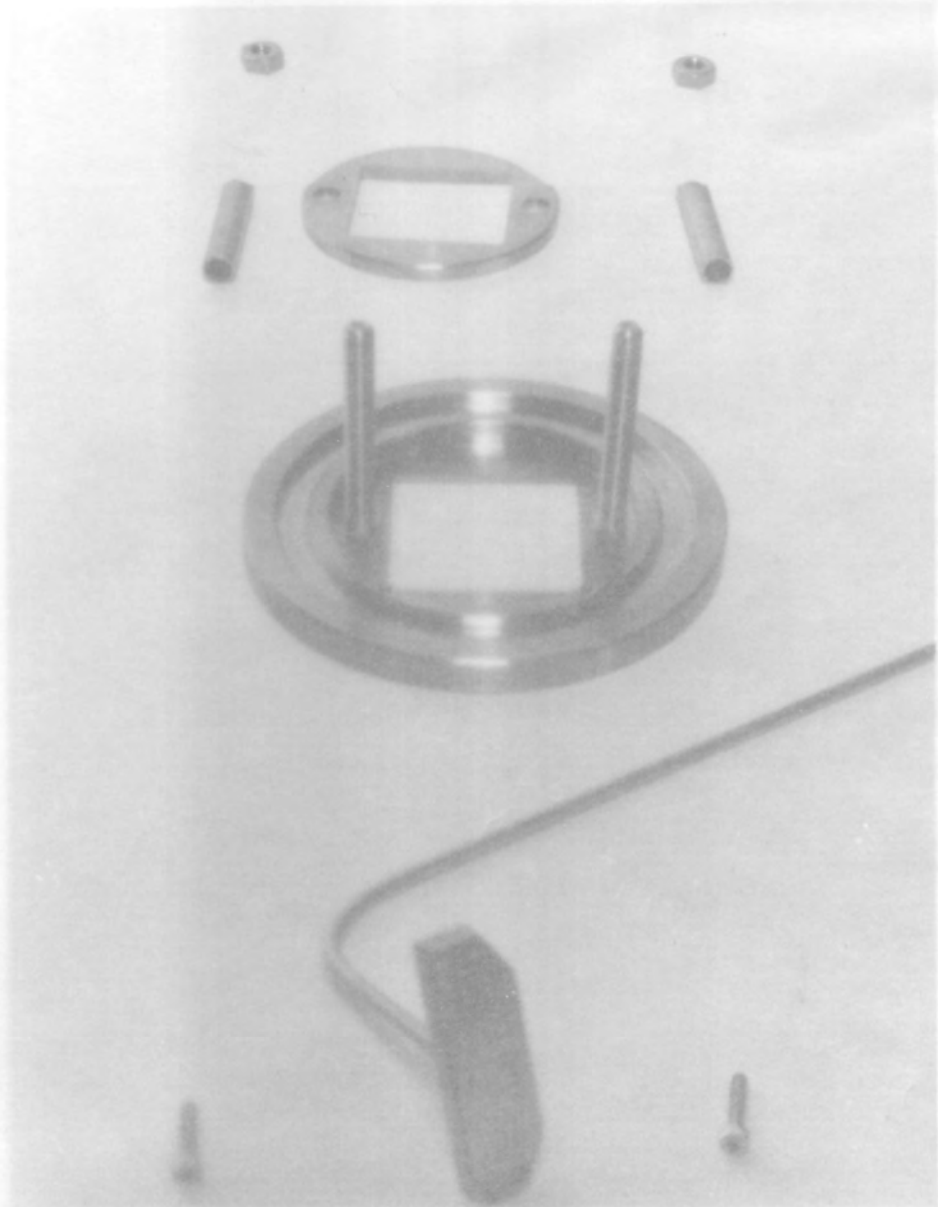
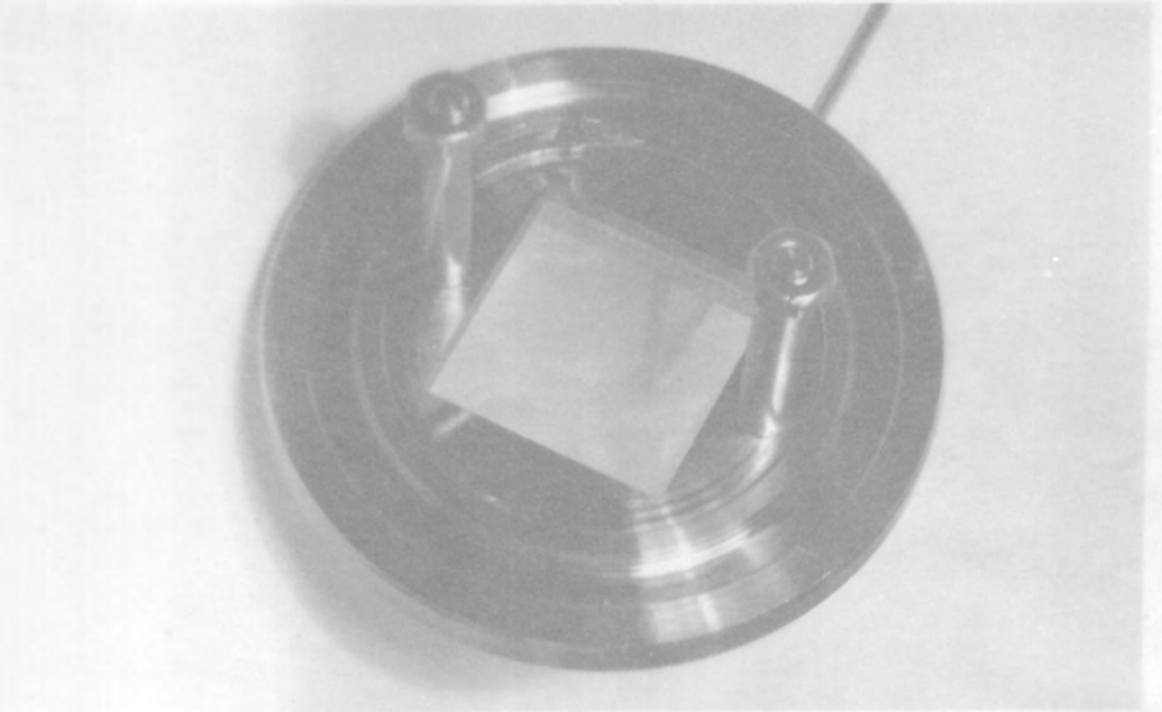
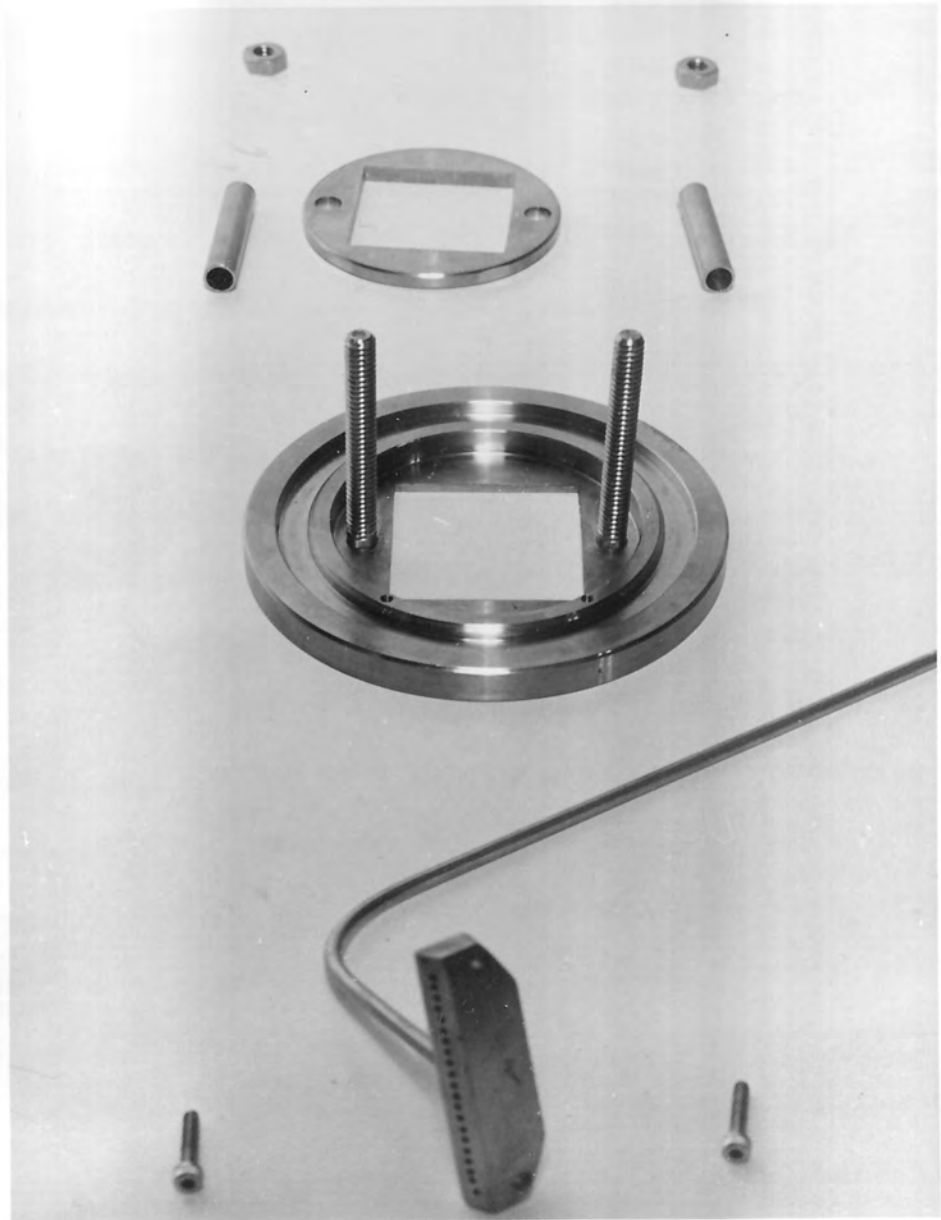
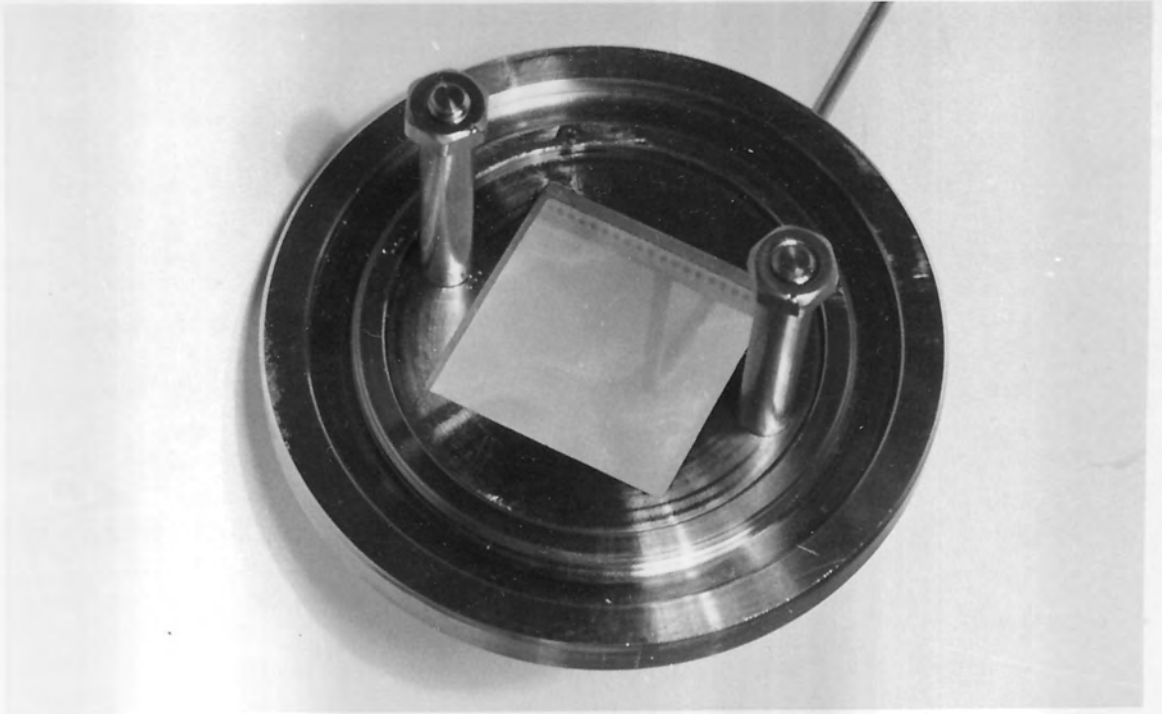


Fig. 6.3. Initial Coalescer Design



Preliminary commissioning tests of this coalescer for use with an irrigating liquid were not successful. The flow of the dispersion was horizontal and the drops of the irrigating liquid, toluene, were formed at the nozzles but released before contact with the mesh was established. By covering the holes to leave a small slit between the distributor and meshes the liquid was induced to contact the latter but surface forces quickly ruptured the film and the toluene flowed upwards as discrete drops clinging to the mesh surface.

The reluctance of the irrigating liquid to form a film on the mesh surface was attributed to poor initial contact between the liquid and the mesh and also to unfavourable properties of the liquid. The toluene /water system has a relatively high interfacial tension and density difference, the former being responsible for the reduction of interfacial area by formation of large drops and the latter contributing to rapid rupture of the film by increased buoyancy forces. As a better alternative, diethyl carbonate was selected for its low interfacial tension and density difference.

Also, the system employed to retain the coalescing media in the assembly was not satisfactory as insertion of the meshes over the studs was practically difficult and their removal was too slow for saturation measurements to be made and severely damaged the fibres. During coalescence operations, the studs and nuts became covered with primary drops, that were observed to grow to approximately 10 mm by coalescence after which they became detached. Drop size measurements would not accurately characterise drop release from the exit surface of the coalescer under these circumstances.

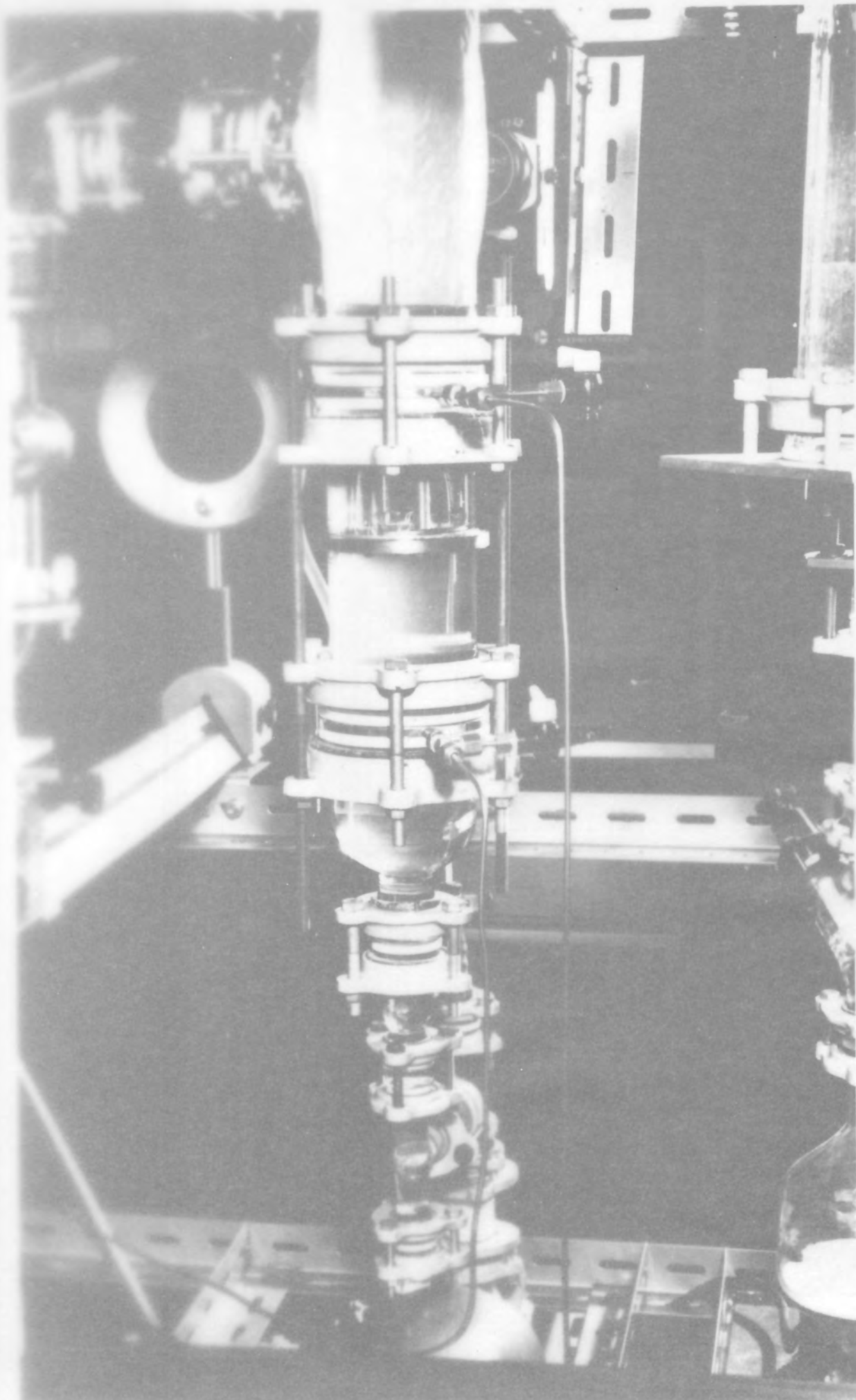
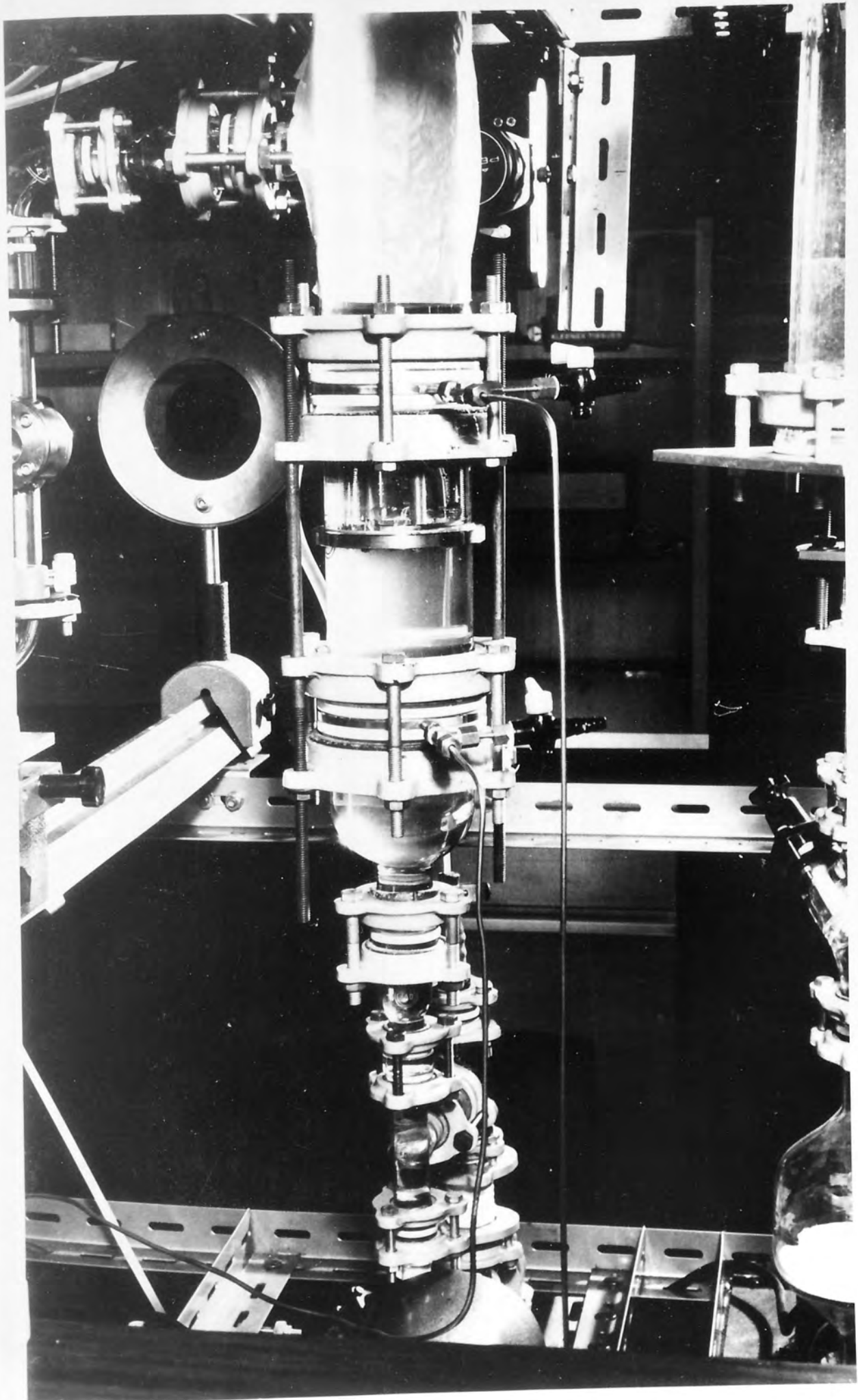


Fig. 6.4. Initial coalescer design  
installed in vertical arrangement



The second coalescer design is illustrated in Fig.6.

5.(a). Here, the mesh is immersed in the irrigating liquid as it is pumped through a slit equal in width to the thickness of the mesh. Provision for removal of the liquid, after flowing over the mesh, was incorporated into the design and pressure tappings were an integral part of the assembly. The two halves of the coalescer, separated by a P.T.F.E. gasket of identical thickness to the mesh, were clamped externally by four screws. Fig 6.5.(b) shows this coalescer assembled and installed horizontally. However, this design and the change in liquid system produced only marginal improvement with persistent drop formation of the irrigating liquid and detachment of these drops from the mesh when the superficial velocity of the dispersion was as low as  $0.1 \times 10^{-2}$  m/s.

Irrigation of the coalescer using the above methods was found to be impractical and an alternative technique devised whereby a primary dispersion of the irrigating liquid could be injected upstream of the coalescer and then flow cocurrently through the packed bed, with the coalescing secondary dispersion, to be removed and recycled downstream.

This method permitted a vertical arrangement of the coalescer, which could be simply designed and fabricated as shown in Fig.6.6(a) and (b), facilitating rapid mesh insertion, with presoaking in either phase as required, and mesh removal for saturation measurements. Bolts were employed to externally clamp the meshes between the stainless steel sections and a P.T.F.E. 'O' ring provided a sliding liquid seal effective for all bed depths. A circular cross sectional flow area was preferable for this coalescer because it could be installed in a 38.1 mm bore glass pipe thus minimising stagnant areas at the periphery

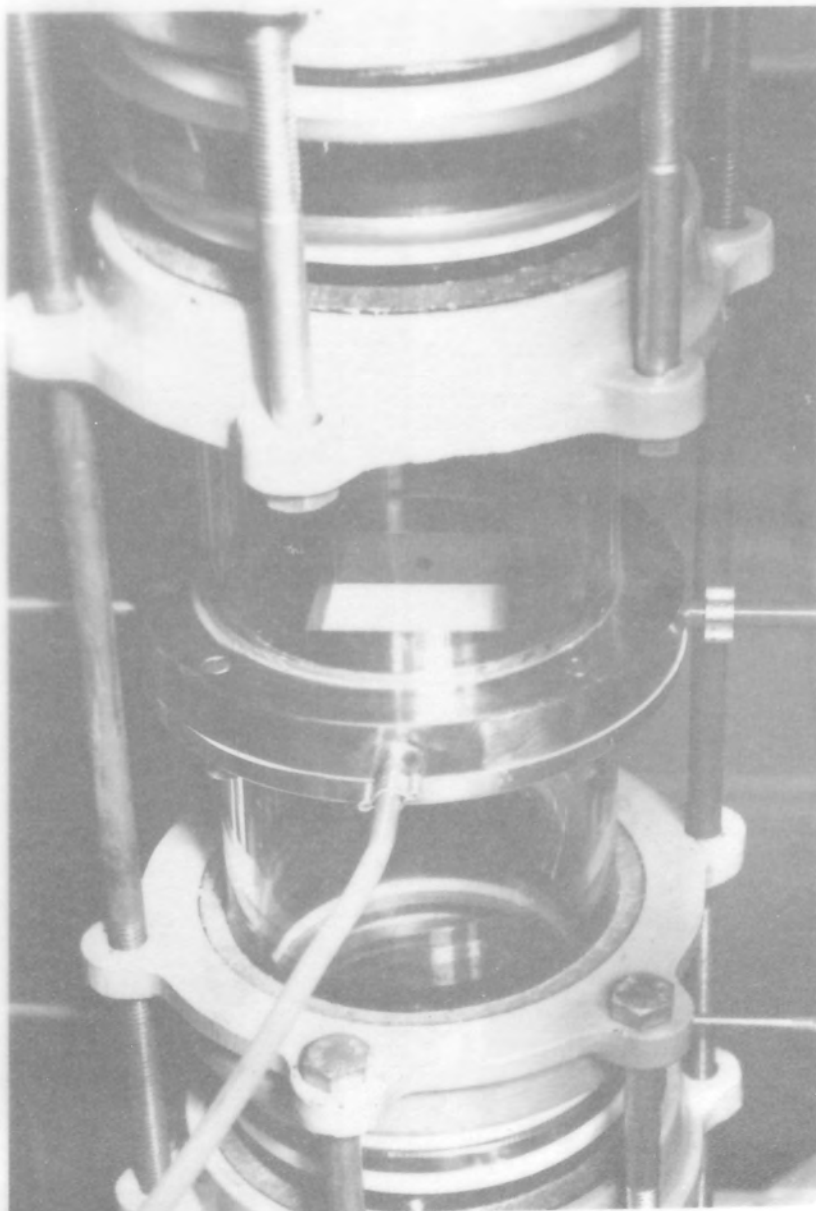
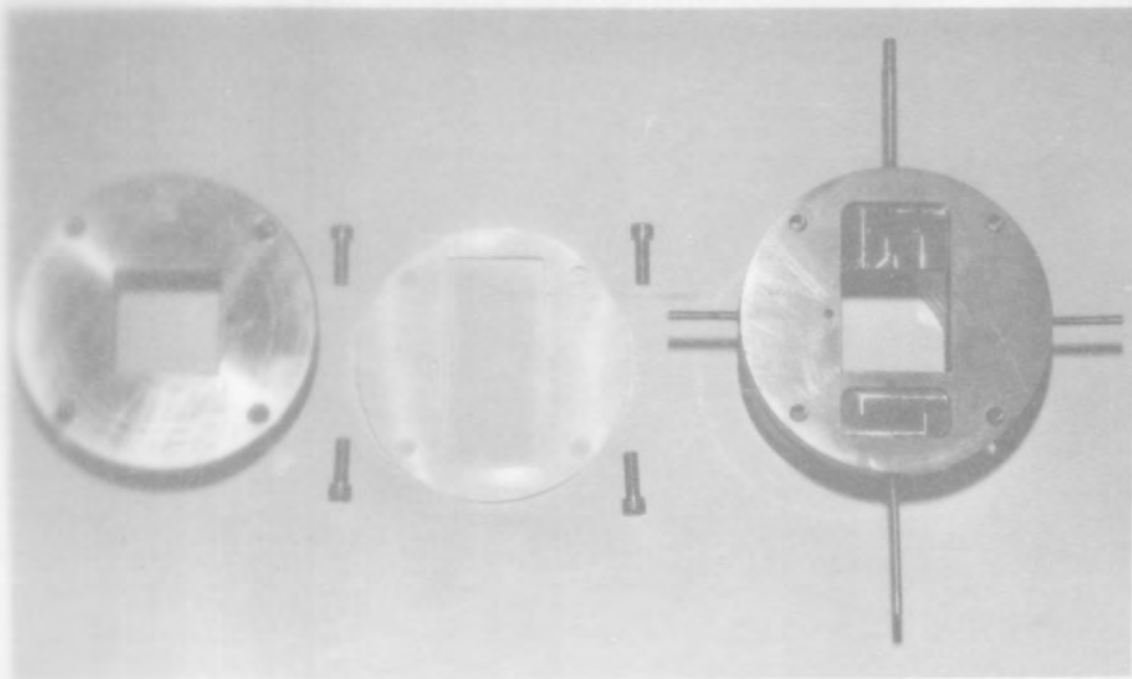
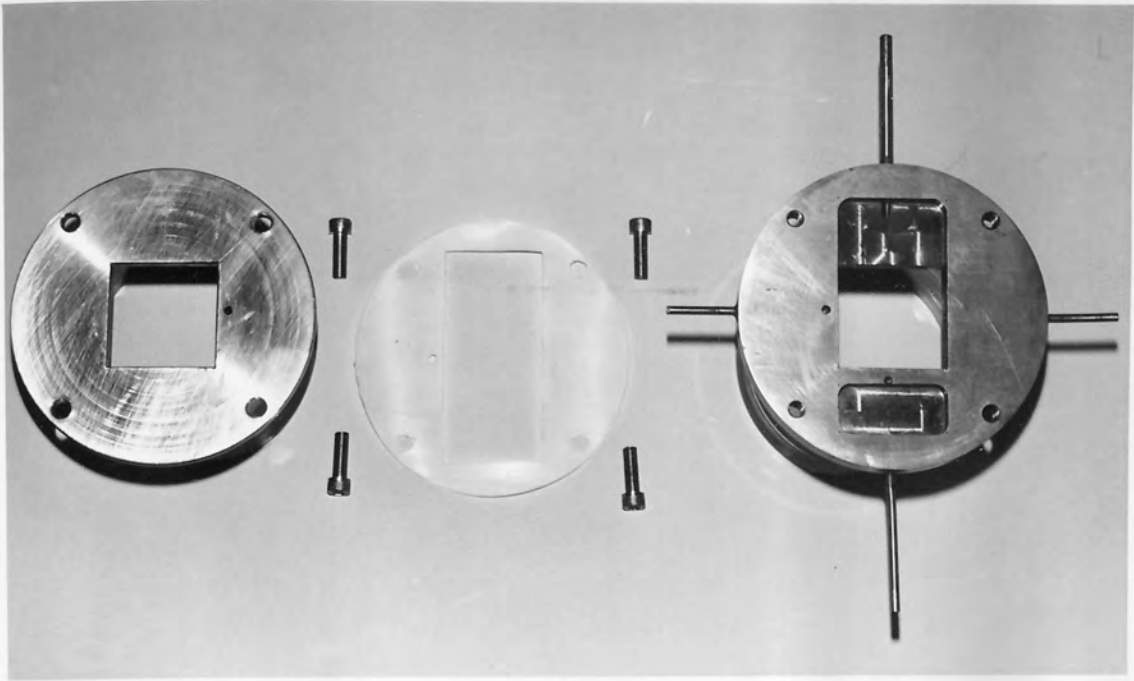


Fig. 6.5. Second coalescer design



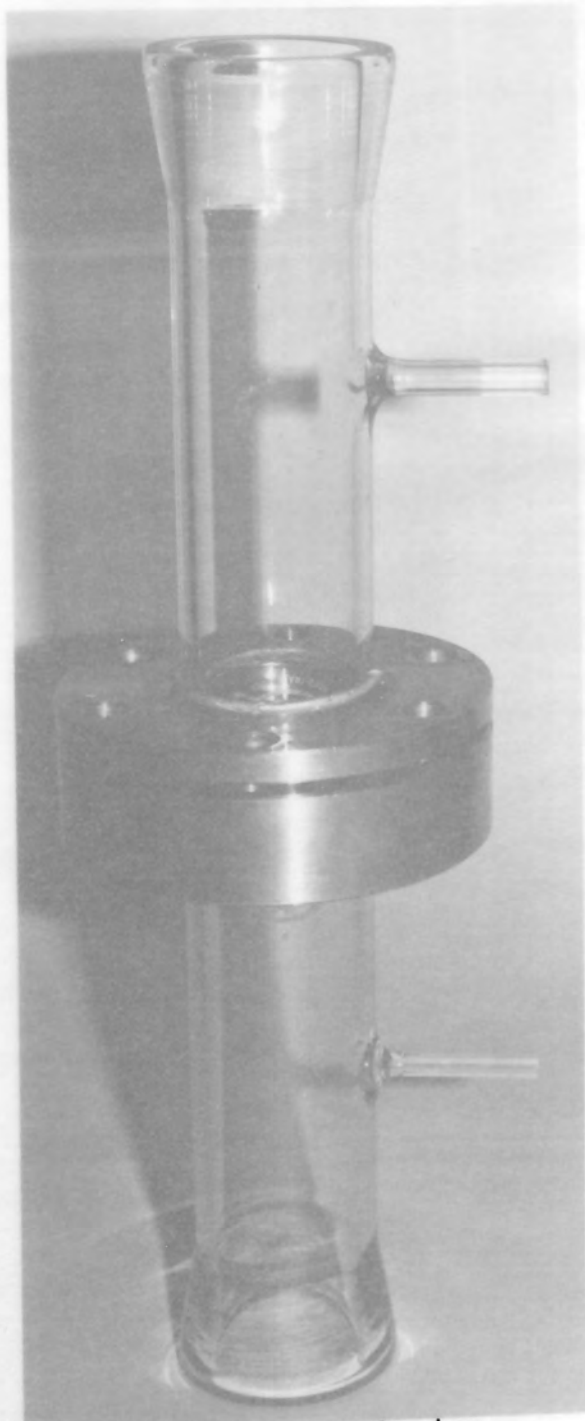
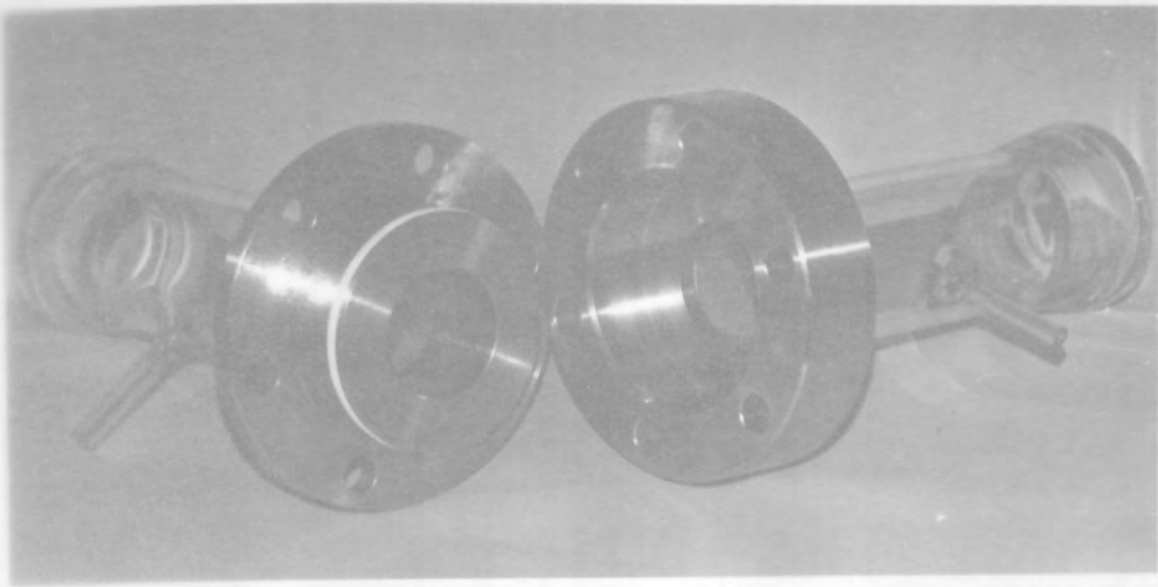
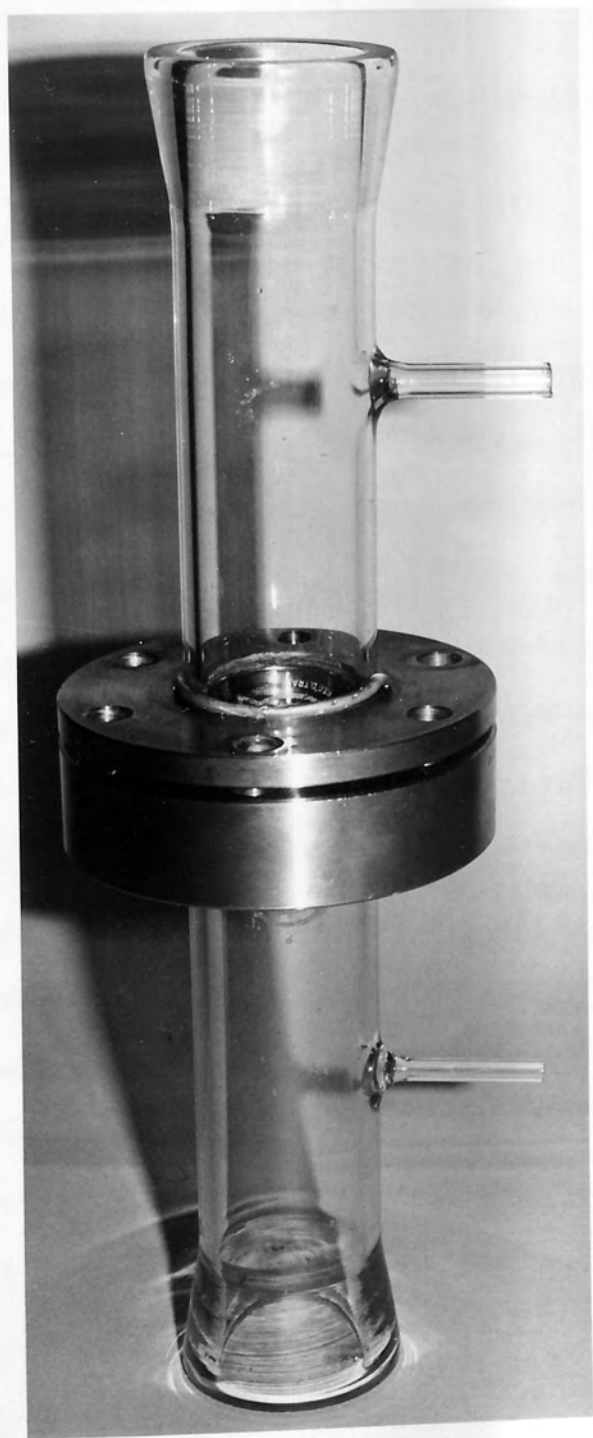
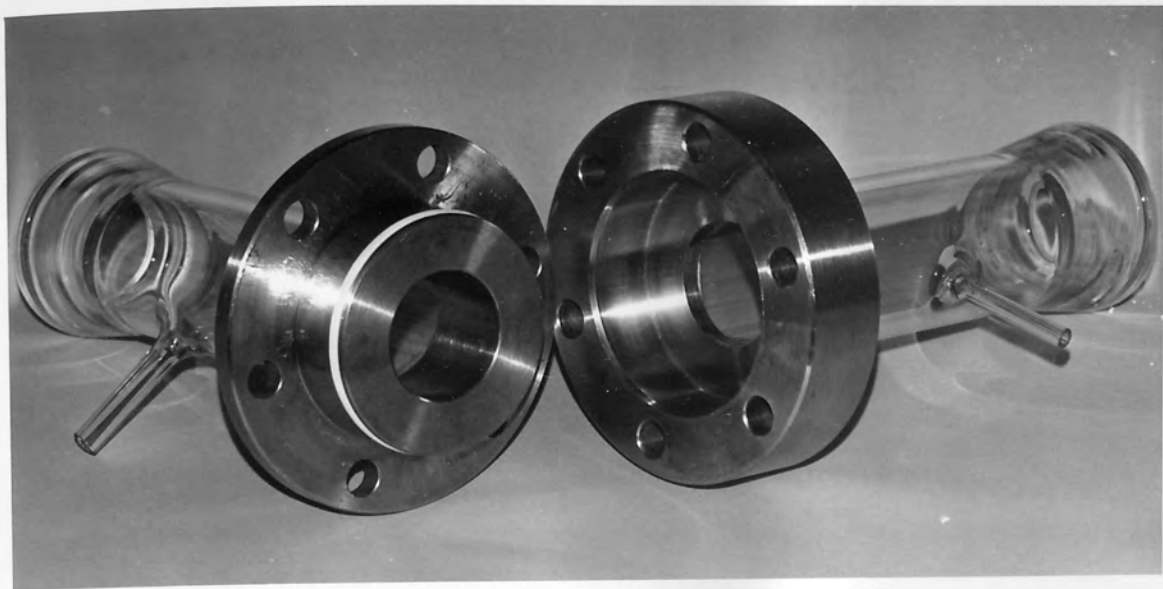


Fig. 6.6. Final coalescer design



of the meshes. The dimensions of this coalescer, which was employed for the majority of the experiments, is illustrated in Fig.C.2.

### 6.3. PACKING SELECTION AND PREPARATION.

Many recent investigations into the coalescence of secondary dispersions in packed beds have employed randomly arranged matrices usually consisting of glass fibres<sup>65,66,70,42</sup> Glass as a raw material is favoured because it is relatively inexpensive, is resistant to the extreme thermal and chemical environments commonly used in cleaning procedures and its wetting properties may be modified by the attachment of silicone groups to the surface of the fibres<sup>89</sup>.

Simple compression of a quantity of fibrous material to the required voidage fraction produces an acceptable structure but a more uniform arrangement results when a slurry of the fibres is filtered and dried. Frequently, the glass fibres used have a distribution of diameters and the above packing techniques produce a bed with a pore size distribution and where the fibre orientations are unknown. Although coalescers fabricated in this way may be very efficient, the lack of an accurate geometrical description of the bed necessitates the use of assumptions during mathematical modelling of the process. A coalescer, consisting of layers of fine woven meshes, does not possess the inherent disadvantages of a glass fibre bed. The fibre diameter and mesh apertures are constant and the fibre orientation is known. For a specified weave type, the thickness of each layer, voidage fraction and surface area per unit volume can be expressed mathematically in terms of the fibre and aperture diameters. 'Becosyn' mono-filament meshes and fine mesh gauze, as supplied by

Begg Cousland Ltd., were selected since the effect of fibre and aperture diameter on coalescer performance could be independantly investigated for fibres of different composition, i.e. surface energy of the material.

The mesh types used in the experimental work are summarised in Table 6.1 and the properties of the fibre

Material	Code	Fibre Diameter $d_c$ ( $\mu\text{m}$ )	Aperture Diameter $d_a$ ( $\mu\text{m}$ )	Weave <sup>a</sup> type	Mesh Count $\text{m}^{-1} \times 10^3$
Stainless Steel	S300	30.5	53	PS	11.98
Nylon	N70/45	35	70	PS	9.52
	N70/29	60	70	PS	7.69
	N69/38	43	69	PS	8.93
	N53/36	35	53	PS	11.36
	N50/35	35	50	PS	11.76
	N25/21	30	25	FT	18.18
	N25/18	35	25	FT	16.67
	N20/16	30	20	FT	20.00
Polyester	PE53/33	40	53	PS	10.75

a - PS = Plain Square ; FT = Full Twill.

Table 6.1 Geometric Details of Meshes.

material presented in Appendix D.

Microscopic examination of the meshes confirmed that the relevant dimensions were both consistant and accurate to the manufacturers specifications. Inspection of the nature of the fibre surfaces using stereoscan photography for several mesh types, as shown in Figs. 6.7 to 6.11, revealed the smoothness and regular arrangement of the fibres for all materials and a quantitative assessment of surface roughness was not attempted.

Investigation of possible chemical reactions between the liquids used and the meshes revealed that Nylon 66

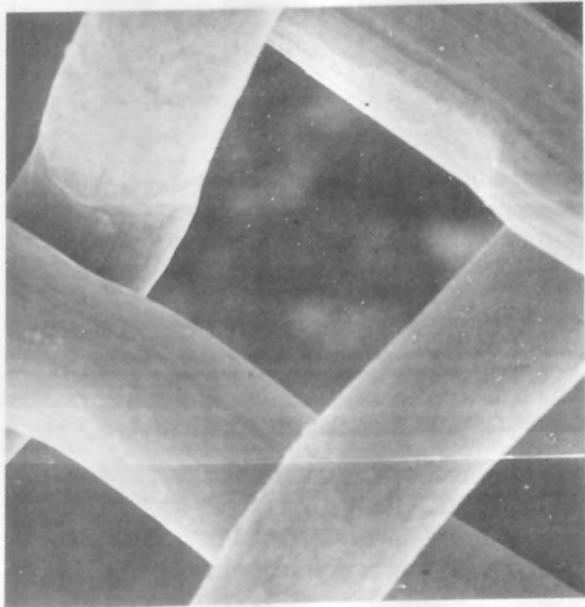


Fig. 6.7. Stainless Steel  
S300 (x750)

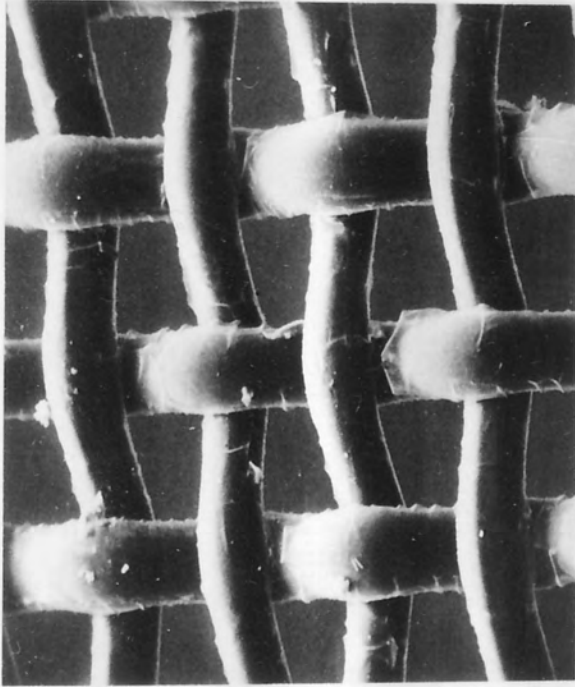


Fig. 6.8. Nylon  
N70/45 (x350)

Stereoscan photographs of meshes

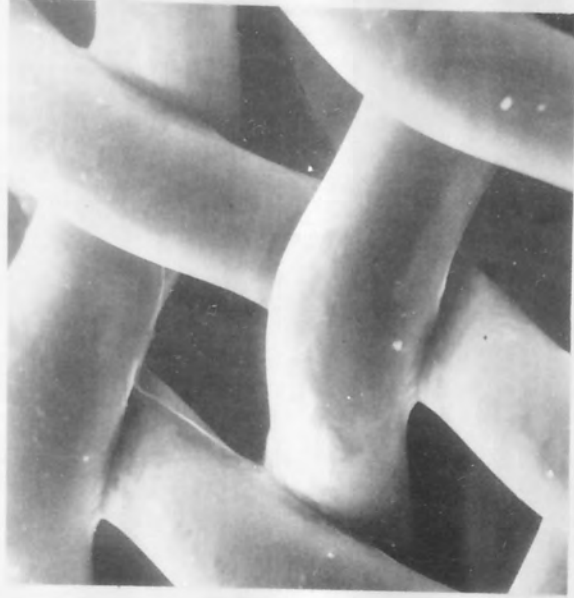


Fig. 6.9. Polyester  
PE53/33 (x400)



Fig. 6.10. Nylon  
Full Twill weave N25/18  
(x500)



Fig. 6.11. Nylon fibre  
illustrating degree of fibre  
roughness (x500)

Stereoscan photographs of meshes

fibres are susceptible to swelling in aqueous environments<sup>90</sup> Immersion of a nylon mesh sample in water at ambient temperature did not produce any detectable swelling when the fibres were examined microscopically over a period of 100 h. However, a bed consisting of 20 layers of a full twill weave mesh, N20/16, operating intermittently for different superficial velocities of the continuous phase, exhibited an increasing pressure drop as the immersion time increased. The data, presented in Appendix D, when examined using the equation fitted to single phase flow through nylon meshes, suggested that the fibre diameter may have swelled by 5% after 90 h immersion with no further change up to a period of 200 h. A decrease in surface tension of the water and a 5% increase in viscosity after 90h may be explained by leaching of material from the fibres. The presence of foreign matter accumulated after 200h operation is shown by the photomicrograph in Appendix D together with the viscosity increase, may also contribute to the decreased permeability of the bed. These effects were not considered to be significantly important as to invalidate the data acquired for the nylon meshes, since the total immersion time was four hours, at most.

The polyester and stainless steel meshes did not exhibit any detectable interaction with the liquids used and the latter was used as the coalescing medium for most of the experiments.

Circular pieces of mesh 63.5 mm in diameter, were prepared from the supplied sheets using a specially designed punch which was manufactured from high carbon steel. As shown in Fig.6.12, meshes for all coalescence devices could be prepared by this method, the small punch being used to cut the holes for the mesh clamping studs

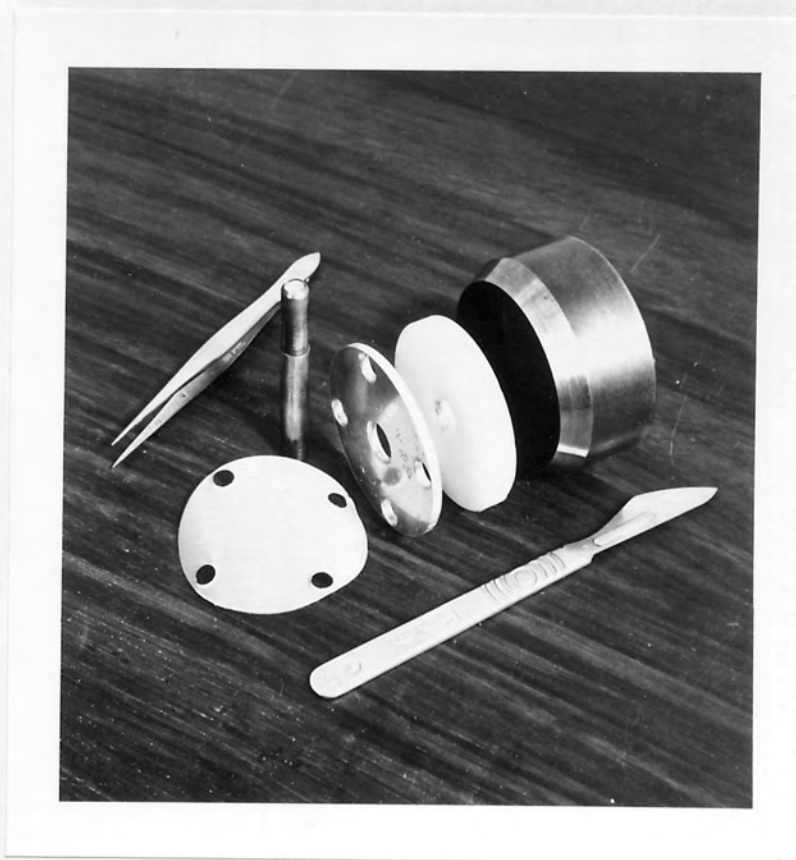


Fig. 6.12. Punch assembly used in mesh preparation

illustrated in Fig.6.3. After cutting, the meshes were washed for 5 minutes in isopropyl alcohol before packing in the coalescence device. The pieces were manipulated using tweezers to prevent contamination of the surface by grease marks.

If the coalescer was assembled under dry conditions, complete removal of air using displacement by the continuous phase was impossible and therefore it was necessary to pack the meshes together whilst submerged in liquid. Consequently the bed was used after presoaking in either the continuous or dispersed phase.

Due to the accumulation of small quantities of foreign material after long operating periods, new meshes were employed for each run. Removal of these surface impurities from stainless steel meshes was achieved by immersion in hot, concentrated hydrochloric acid solution, followed by rinsing in distilled water. No measurable enhancement or deterioration of performance occurred after this treatment.

#### 6.4. LIQUID SYSTEM DESCRIPTION.

The equipment was designed for coalescence of an organic liquid dispersed in distilled water. Toluene was selected as a relatively non-toxic, non-corrosive and inexpensive solvent. G.P.R. grade toluene was distilled to within  $\pm 1$  K of its boiling point and stored in clean, dark glass bottles to prevent exposure to sunlight which has been reported to cause degradation <sup>91</sup>.

Any effects due to the mutual solubility of toluene and water were minimised by allowing the two phases to attain mutual saturation by contact for over 24 hours before use. Mass transfer effects could not be completely eliminated due to the temperature coefficients of solubilities. Since accurate temperature was impractical,

due to heat generation by pumping and emulsification, the physical properties of the system were determined as a function of temperature and presented in Appendix E. The high sensitivity of both continuous and dispersed phase viscosities, and hence pressure drop to temperature changes emphasizes the need for temperature monitoring during single and two phase flow experiments. The continuous phase rotameters were calibrated experimentally at 20 deg.C and the effect of temperature fluctuations was evaluated theoretically from the calibration handbook<sup>92</sup>. An 8 deg.C change in temperature was found to cause a 5% maximum error in flowrate. Instruments of this type possess inherent errors, due to random flow disturbances, and accuracies of better than 3 or 4% would not be realised in practice. Temperature correction of the calibration curves was therefore unwarranted.

#### 6.5. PRESSURE DROP MEASUREMENT.

Two differential 'U-tube' manometers were used to indicate the pressure drop across the coalescer. A mercury manometer was used to measure pressure drops greater than 100 mm Hg. and one containing carbon tetrachloride used for the lower range of values. The manometers were connected in parallel to pressure tappings upstream and downstream of the coalescer by tubes containing distilled water. Location of the interface between the carbon tetrachloride and water was improved by colouring the organic phase using the dye, 'oil-soluble yellow'. Since the ambient temperature varied, the density of the carbon tetrachloride was determined gravimetrically and was found to be  $1604 \text{ kg/m}^3$ ; it varied by less than 0.4% over the temperature range 10-30 deg.C.

During experiments for single phase flow through the

coalescer, it was discovered that a different value of pressure drop was obtained for the same superficial velocity depending on whether the flowrate was progressively increased or decreased. Modification of the manometer system as described by Fig 6.13 eliminated this hysteresis effect which was only detectable using the carbon tetrachloride manometer. This phenomenon, which has been observed previously in low pressure drop measurements<sup>93</sup> may be attributed to an advancing and receding interfacial contact angle as the pressure drop rises and falls. The liquid levels in the water reservoirs were equalised before the measurements were taken from either manometer.

#### 6.6. OPERATING PROCEDURE.

Following assembly, the equipment was filled with a 2%  $\frac{1}{4}$  solution of Decon 90 and allowed to stand for 24 hours. After thorough rinsing by tap water, followed by distilled water, the rig was filled with distilled water. Further contact with surface active agents was avoided to prevent contamination of the liquid system since minute quantities of surfactants which may be absorbed onto glass surfaces are extremely detrimental to the coalescence process.

After preparation of the coalescer by packing the required number of layers of mesh in the submerged condition and assembly of the components, the equipment was operated in the recycle mode when only flow of the continuous phase was permitted. The temperature and pressure drop were recorded for a range of superficial velocities from 0 to  $7 \times 10^{-2}$  m/s. This procedure provided sufficient data for single phase flow analysis and ensured correct assembly of the coalescer through pressure drop checks.

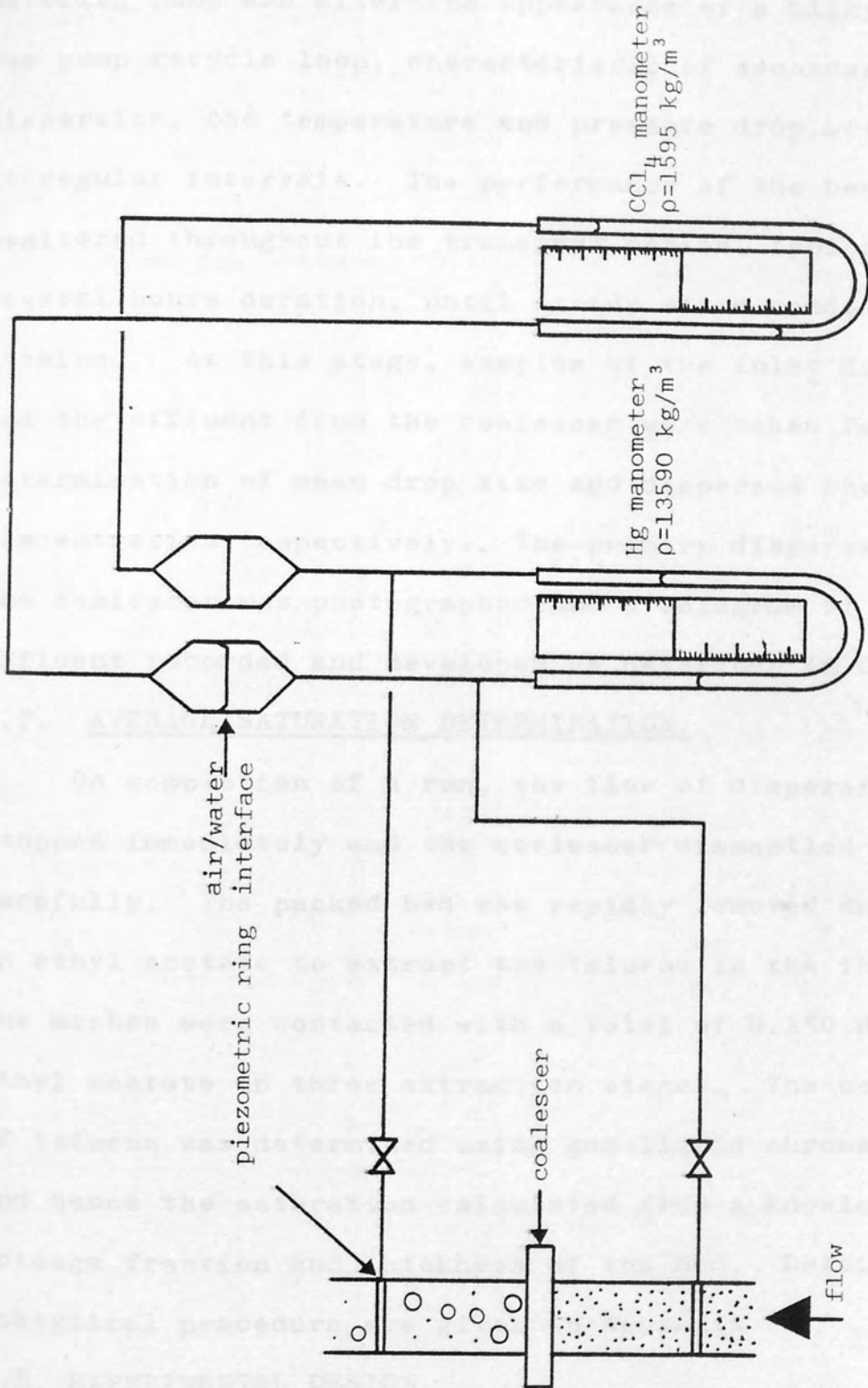


Fig. 6.13 Schematic arrangement of manometry system

The isolation valves were then adjusted to alter the operating mode from recycle to a 'once through' condition and the flow regulated to the desired value. The emulsification pump was started, followed by the dispersed phase metering pump and after the appearance of a milky haze in the pump recycle loop, characteristic of secondary dispersion, the temperature and pressure drop were recorded at regular intervals. The performance of the bed was monitored throughout the transient period, typically of several hours duration, until steady state conditions were attained. At this stage, samples of the inlet dispersion and the effluent from the coalescer were taken for determination of mean drop size and dispersed phase concentration respectively. The primary dispersion leaving the coalescer was photographed and a hologram of the effluent recorded and developed as described in Chapter 7.

#### 6.7. AVERAGE SATURATION DETERMINATION.

On completion of a run, the flow of dispersion was stopped immediately and the coalescer dismantled very carefully. The packed bed was rapidly removed and immersed in ethyl acetate to extract the toluene in the interstices. The meshes were contacted with a total of  $0.150 \text{ dm}^3$  of ethyl acetate in three extraction stages. The concentration of toluene was determined using gas-liquid chromatography and hence the saturation calculated from a knowledge of the voidage fraction and thickness of the bed. Details of the analytical procedure are given in Appendix F.

#### 6.8. EXPERIMENTAL DESIGN.

The factors which affect the coalescence process may be categorised as those parameters relevant to the liquid system, those pertaining to the media employed and those determined by the operating conditions. Contamination of

the liquid system by particulate matter, dissolved solids and surfactants also influence coalescence efficiency. In view of the complex interactions between these variables shown by Fig 6.14, it is necessary to design experiments carefully. The scope of this research was restricted to investigation of coalescence of a single, pure liquid system so that the effects of bed properties and operating conditions could be determined in greater detail.

6.8.1. Mesh Properties.

The meshes were selected so that the effects of fibre diameter, aperture diameter and fibre material could be independently assessed. Nylon meshes were employed for comparison of packing dimensions because of their availability in a wide range of sizes. The design, presented in Table 6.2, was adopted for the experimental work. A lower limit was imposed on the level of these variables by availability of meshes in woven form and the upper limit determined by the ability of the meshes to coalesce the inlet dispersion.

Aperture Diameter, $d_a$ ( $\mu\text{m}$ )	Fibre Diameter, $d_c$ ( $\mu\text{m}$ )		
	35	43	60
25	N25/18	-	-
53	N53/36	-	-
70	N70/45	N69/38	N70/29

Table 6.2. Experimental Design for Mesh Dimensions.

A comparison was made to determine the effect of wettability of the packing material by the dispersed phase. The three meshes, given in Table 6.3, are of similar dimensions and qualitative microscopic examination revealed no significant differences between surface roughness.

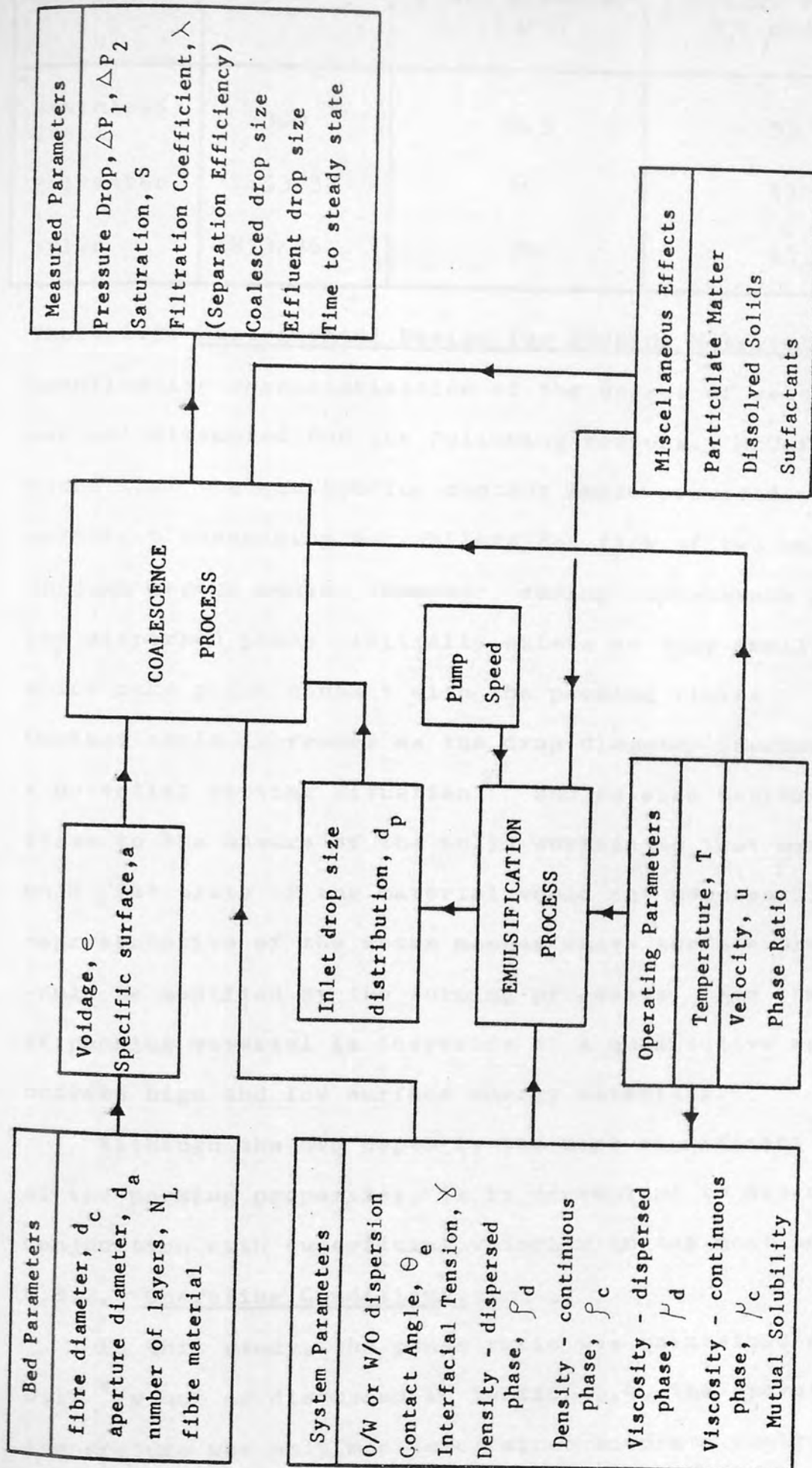


Fig 6.14. Interaction between Variables in Secondary Dispersion Coalescence Studies.

Material	Mesh	Fibre Diameter $d_c$ ( $\mu\text{m}$ )	Aperture Diameter $d_a$ ( $\mu\text{m}$ )
Stainless Steel	S300	30.5	53
Polyester	PE53/33	40	53
Nylon	N53/36	35	53

Table 6.3. Experimental Design for Packing Material.

Quantitative characterisation of the degree of wettability was not attempted for the following reasons. McCaffery<sup>94</sup> found that the equilibrium contact angle provided a useful criterion describing wettability for flow of two bulk phases through porous media. However, during coalescence processes, the dispersed phase initially exists as very small spheres which make point contact with the packing fibres<sup>86</sup>.

Contact angle increases as the drop diameter increases for a potential wetting situation<sup>95</sup> and is also extremely sensitive to the nature of the solid surface so that measurements on a flat plate of the material would not necessarily be representative of the woven meshes whose surface properties would be modified by the forming processes. The comparison of packing material is therefore of a qualitative nature between high and low surface energy materials.

Although the bed depth is the most significant variable of the packing properties, it is convenient to discuss it in conjunction with superficial velocity in the next section.

#### 6.8.2. Operating Conditions.

In this study, the phase ratio was maintained at 0.1%  $v/v$  but as discussed in Section 6.4, the operating temperature was only monitored since accurate control was impossible.

Both bed depth and superficial velocity were investigated simultaneously because an analysis of variance of preliminary pressure drop results as a response to variation of these factors revealed that the effect of the interaction of these variables was more significant than their individual contributions. Therefore, a factorial design is essential and the experimental work was completed according to the scheme represented by Table 6.4.

The initial range of variables selected was extended so that the mathematical model described in Chapter 10 could be verified over a greater range of applicability. The highest level of bed depth was determined by the capacity of the coalescer assembly and the maximum velocity depended on the storage capacity of the continuous phase reservoir.

Velocity, $u$ ( $\times 10^{-2}$ m/s)	Bed Depth (layers)					
	10	20	30	60	90	120
0.5	X	X	X	X	X	
1.5	X	X	X	X	X	X
2.5	X		X	X	X	
3.5	X		X	X	X	
7.0	X		X	X	X	X

Table 6.4. Complete Experimental Design for Investigation of Bed Depth and Velocity for Stainless Steel Mesh Beds.

(Inner block represents initial design)

The effect of presoaking the bed was investigated by duplicating the experiments within the inner block of Table 6.4.



### 7.1. INTRODUCTION.

The method used to prepare a secondary haze in this study produces a polydispersion which is a desirable feature of the technique since very few dispersions encountered in industrial processes are monodisperse. A knowledge of the drop size distributions, in addition to the mean drop size is necessary in order to characterise a dispersion. Furthermore, the capture efficiency of drops flowing through a packed bed depends on their diameters and as the mechanisms of coalescence are being investigated, the sole use of a mean diameter could be misleading.

The dispersion produced by the centrifugal pump was analysed at regular intervals during an experiment to ascertain the drop size distribution and to check that the feed to the coalescer was consistent. Outlet dispersions from the unit were also monitored to measure coalescence efficiency. Preliminary experiments revealed that operation at high velocities caused breakthrough of the secondary dispersion which flowed from the exit face of the bed cocurrently with the primary dispersion produced by coalescence. Simultaneous analysis of these drops was impossible due to their different sizes and not desirable since combination into a binodal distribution curve obscures information about capture and drop release mechanisms.

### 7.2. ANALYSIS OF THE EFFLUENT PRIMARY DISPERSION.

Despite the inherent tedious nature of drop size distribution analysis using manual counting methods, photography was selected because of its simplicity and reliability. Photographs of the drops leaving the coalescer were obtained using an Asahi Pentax camera with a  $f$  2.8, 35mm Tessar lens on Kodak TriX-Pan 35mm, 400 A.S.A. film. Shutter speeds of less than  $4 \times 10^{-3}$  s were employed to

eliminate image distortion caused by drop movement.

Illumination of the dispersion from the rear was provided by a 250W Photoflood bulb through a diffuser.

The circular pipe section, which retained the flowing dispersion, did not cause detectable distortion or magnification of the drops thus eliminating the need for special optical arrangements. Enlargement of the prints to approximately 5 x magnification was found to be satisfactory with respect to size and contrast for the counting procedure. A metric scale placed on the outer tube wall for calibration purposes is shown by Fig.7.1, a typical photograph of the coalesced dispersion.

Manual counting of the drops recorded on the photographs was accomplished by a Zeiss T63 Particle Counter to identify and record linear drop dimensions. The data acquired was then processed in a computer program to output mean diameter and standard deviation of the distribution. Typical results are shown in Fig.7.2.

### 7.3. CHARACTERISATION OF THE INLET DISPERSION.

Various methods of drop size determination are available for secondary dispersions including microscopy, light reflectance and light scattering. Of these techniques, only microscopy is suitable for polydisperse systems since the above alternatives can only produce a mean drop size of a dispersion with a narrow size distribution.

In microscopy, a sample of the dispersion is diluted, placed in a well of a glass slide and examined under the microscope. The resolving power of the microscope imposes a lower limit of resolution of approximately  $0.25 \mu\text{m}$  and an upper limit of  $20 \mu\text{m}$  is determined by the diameter of the drop in relation to the depth of field of the optical system. Further inaccuracies result from the long periods

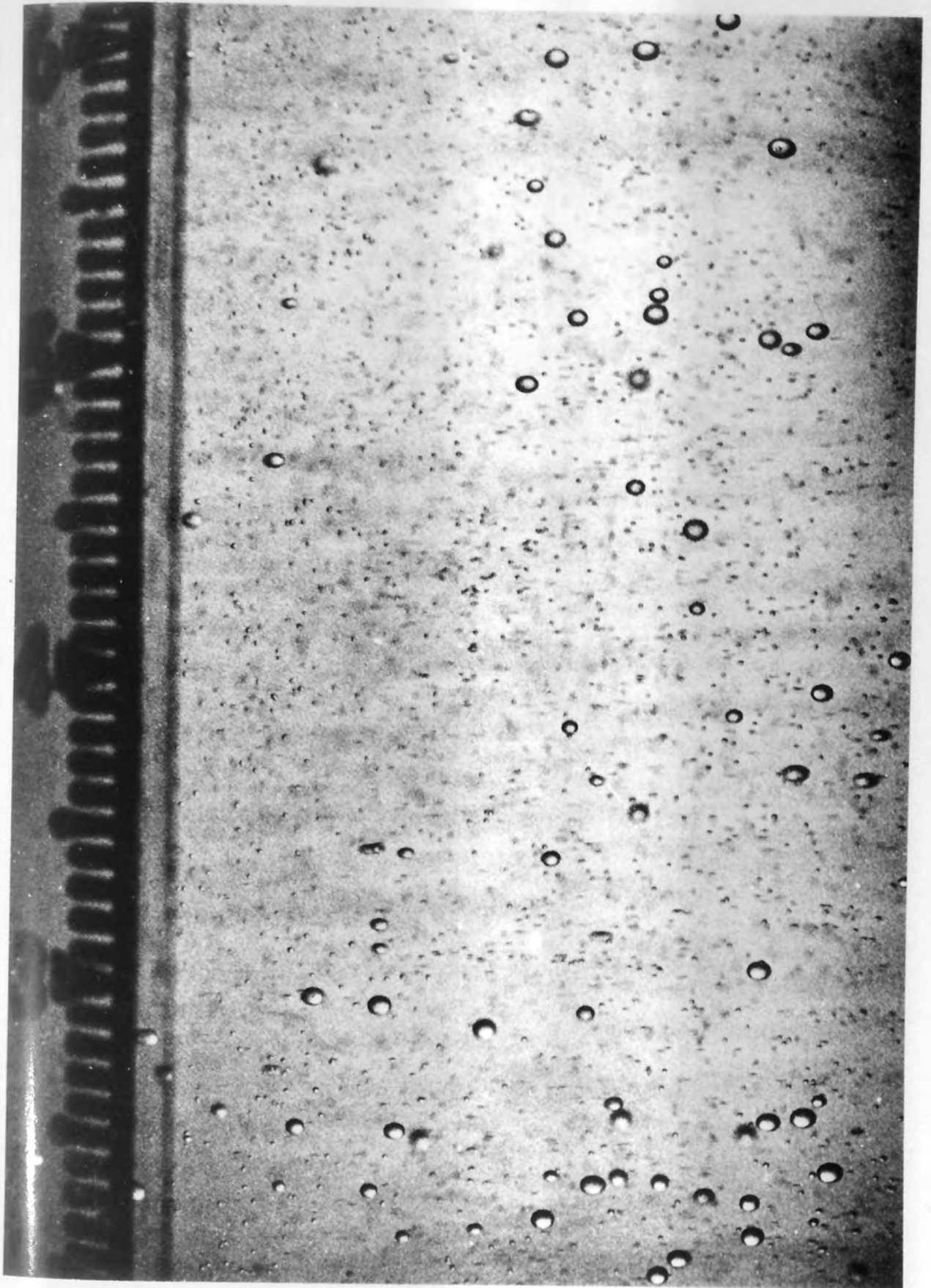


Fig. 7.1, Typical photograph of condensed dispersion

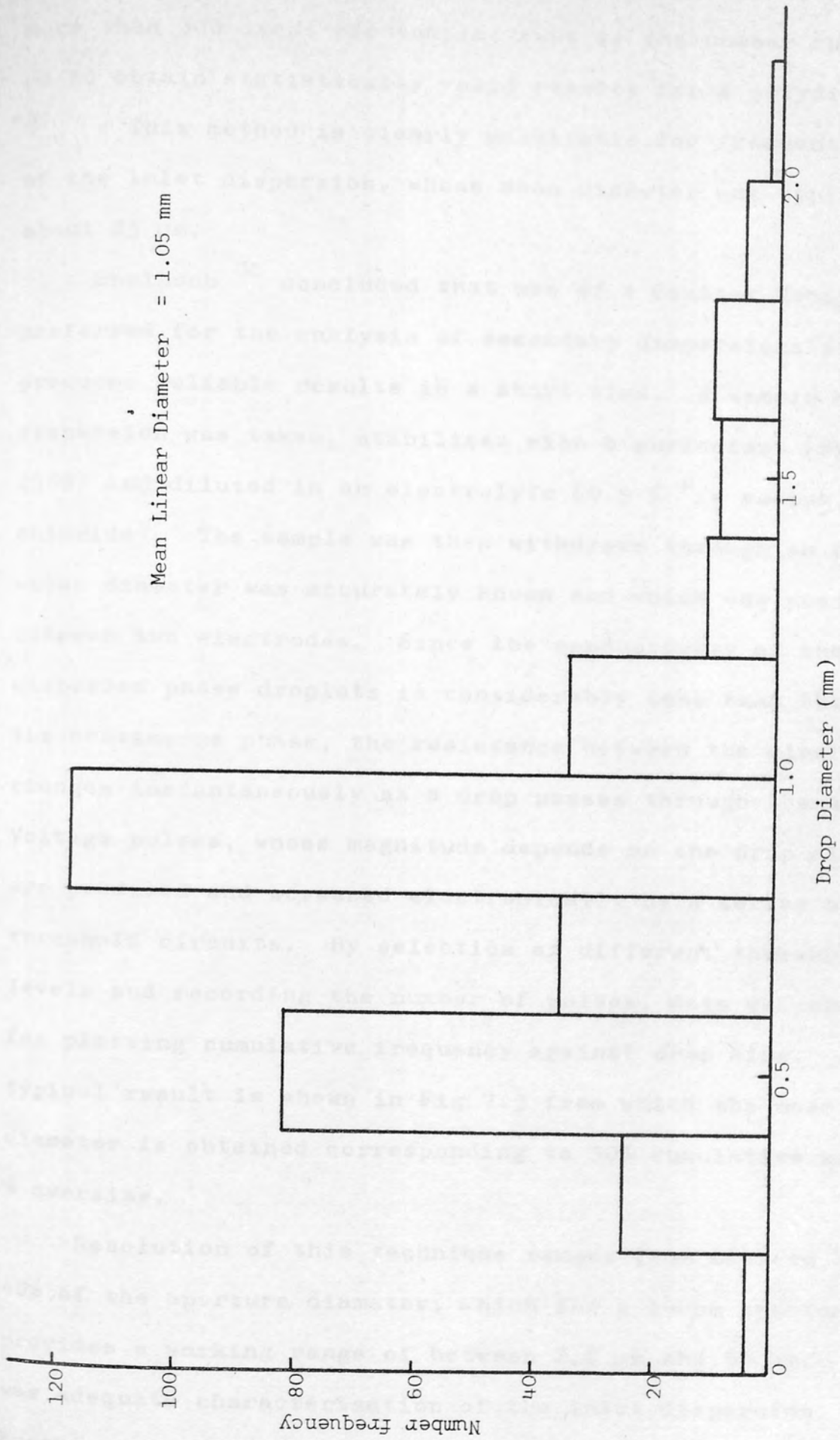


Fig. 7.2. Typical size distribution of coalesced drops leaving exit face

during which drops may settle and it is necessary to count more than 300 drops per sample; that is the number recommended to obtain statistically valid results for a polydispersion<sup>96</sup>. This method is clearly unsuitable for frequent sampling of the inlet dispersion, whose mean diameter was typically about 25  $\mu\text{m}$ .

Shalhoub<sup>70</sup> concluded that use of a Coulter Counter is preferred for the analysis of secondary dispersions since it produces reliable results in a short time. A sample of the dispersion was taken, stabilised with a surfactant (Hyamine 2389) and diluted in an electrolyte (0.9 % w/v sodium chloride). The sample was then withdrawn through an aperture whose diameter was accurately known and which was positioned between two electrodes. Since the conductivity of the dispersed phase droplets is considerably less than that of the continuous phase, the resistance between the electrodes changes instantaneously as a drop passes through the aperture. Voltage pulses, whose magnitude depends on the drop diameter, are produced and screened electronically by a series of threshold circuits. By selection of different threshold levels and recording the number of pulses, data was obtained for plotting cumulative frequency against drop size. A typical result is shown in Fig 7.3 from which the mean diameter is obtained corresponding to 50% cumulative weight % oversize.

Resolution of this technique ranges from between 2% to 40% of the aperture diameter, which for a 140 $\mu\text{m}$  aperture tube provides a working range of between 2.8  $\mu\text{m}$  and 56  $\mu\text{m}$ . This was adequate characterisation of the inlet dispersion. Further details of this technique are to be found in Shalhoub's dissertation.

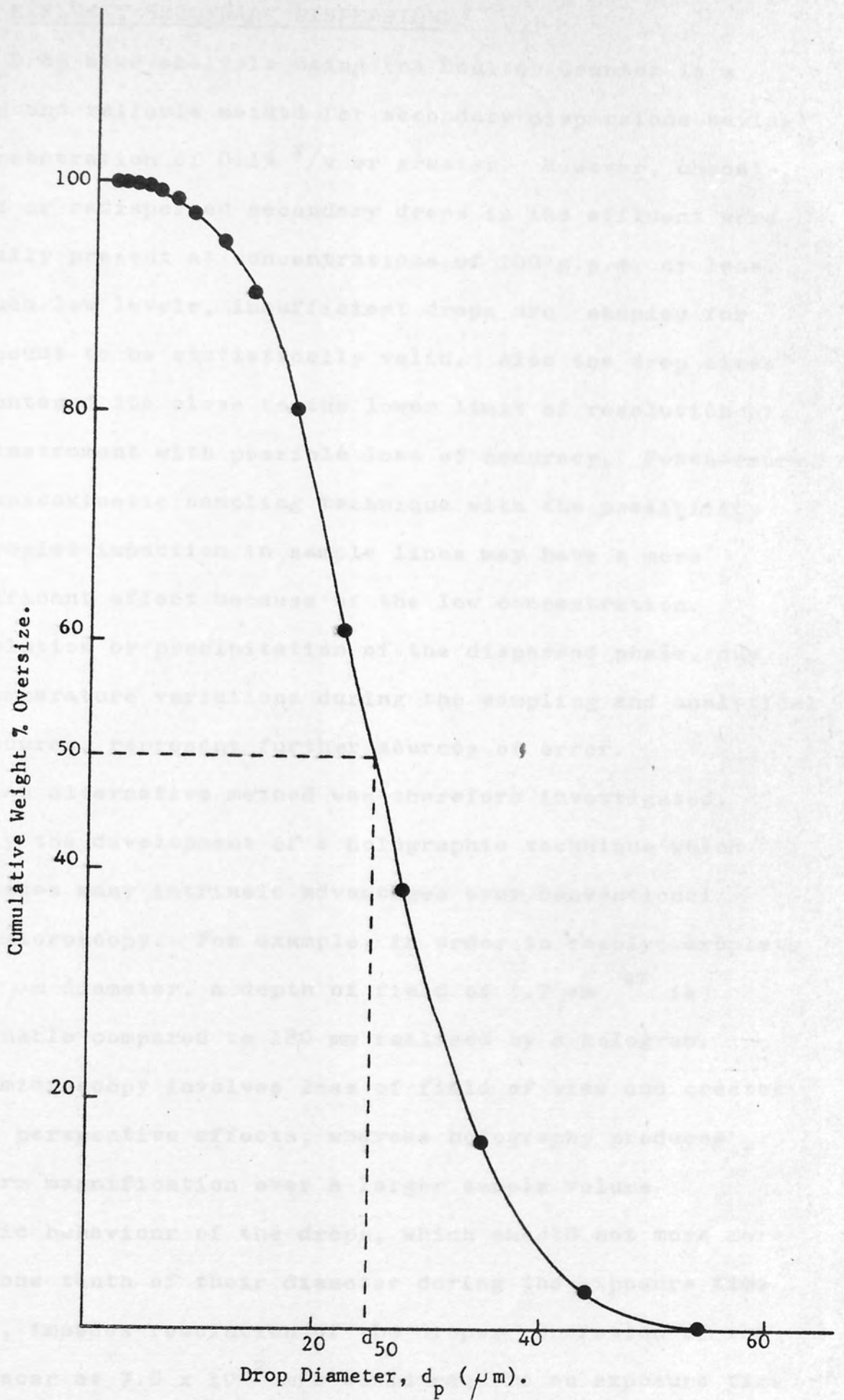


Fig 7.3. Typical Size Distribution of Inlet Dispersion.

#### 7.4. EFFLUENT SECONDARY DISPERSION.

Drop size analysis using the Coulter Counter is a rapid and reliable method for secondary dispersions having a concentration of 0.1% v/v or greater. However, uncoalesced or redispersed secondary drops in the effluent were normally present at concentrations of 100 p.p.m. or less. At such low levels, insufficient drops are sampled for the count to be statistically valid. Also the drop sizes encountered lie close to the lower limit of resolution of the instrument with possible loss of accuracy. Furthermore, the anisokinetic sampling technique with the possibility of droplet impaction in sample lines may have a more significant effect because of the low concentration. Dissolution or precipitation of the dispersed phase, due to temperature variations during the sampling and analytical procedures, represent further sources of error.

An alternative method was therefore investigated, namely the development of a holographic technique which possesses many intrinsic advantages over conventional photomicroscopy. For example, in order to resolve droplets of 50  $\mu\text{m}$  diameter, a depth of field of 1.7  $\mu\text{m}$ <sup>97</sup> is obtainable compared to 180 mm realised by a hologram. Photomicroscopy involves loss of field of view and creates image perspective effects, whereas holography produces uniform magnification over a larger sample volume. Dynamic behaviour of the drops, which should not move more than one tenth of their diameter during the exposure time<sup>98</sup>, impedes resolution of the drops. Operation of the coalescer at  $7.0 \times 10^{-2}$  m/s would require an exposure time of less than  $0.3 \times 10^{-6}$  s to resolve a 50  $\mu\text{m}$  droplet which is prohibitive for conventional shutter arrangements.

The requirements of a reasonable depth of field,

alleviation of droplet impaction and recording of large numbers of drops, with high magnification and short exposure time, led to development of the holographic technique.

#### 7.5. THE HOLOGRAPHIC TECHNIQUE.

Holography is a method of recording an image of an object using the entire content of the light reflected or transmitted by that object. The light source used must be coherent, when the electromagnetic waves incident upon the object are in phase, and lasers are employed to provide a source of monochromatic, coherent light to satisfy this requirement.

Phase variations are caused by placing an object in the path of a coherent light beam (signal beam). When combined with a similar undistorted beam (reference beam) on a photographic plate, the phase variation on the signal beam is transferred into an intensity variation by the formation of a complex interference pattern. The intensity variation acts as a diffraction grating which, on illumination with coherent light, superimposes the original phase distribution onto the illuminating beam causing an image of the object to appear in its original position and form. Not only does the photographic plate act as a diffraction grating but each part of the plate is, in itself, a grating so that the image consists of a large number of separate images each with a different perspective. This gives the image a three dimensional appearance and parallax may be observed.

##### 7.5.1. 'Off-axis' Holography.

The two basic types of holography system, 'in-line' and 'off-axis', differ according to the relative paths of the signal and reference beam before they coincide at the

recording plane. An 'off-axis' hologram is recorded by dividing the laser beam using a beam splitter, allowing one portion to pass through the sample volume and the reference beam to pass directly to the photographic plate as shown in Fig 7.4(a). Spatial and temporal coherence of the beams is the chief limitation and the optical system must be carefully arranged to match the path length of the two beams. This holography system is particularly suitable for reflection holograms when the object is opaque, or for transmission holograms, when the concentrations of droplets in the sample volume is high.

7.5.2. 'In-line' Holography.

'In-line' holograms are produced when the portion of the beam, which passes through the sample volume without interaction with droplets, constitutes the reference beam. Typically about 80% of the incident light must pass through the field without modulation to produce a good 'in-line' hologram <sup>99</sup>. The first holograms made by Gabor <sup>100</sup> were also 'in-line' but resulted from an interference between the Fresnel pattern of the object and an 'in-line' background. With reference to Fig. 7.4(b), if the distance between the drops and the recording plane, Z is such that  $Z > \frac{d^2}{\lambda}$  where d is the drop diameter and  $\lambda$  is the wavelength of the incident illumination, the interference field produced by diffraction from the drops and the reference beam is a Fraunhofer pattern. <sup>101</sup>

Fraunhofer or far field holograms consist of a series of concentric circular fringes, with a central maximum, associated with each drop. Unlike other holograms, far field patterns may be readily interpreted by direct analysis of the fringes.

Fraunhofer holography was originally developed as a

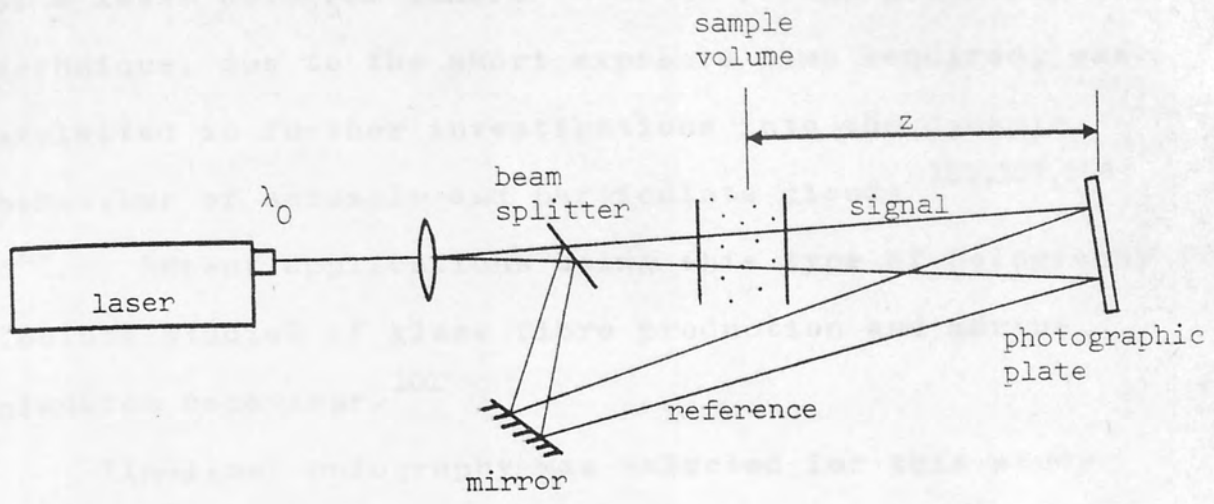


Fig. 7.4(a) 'Off-axis' holography

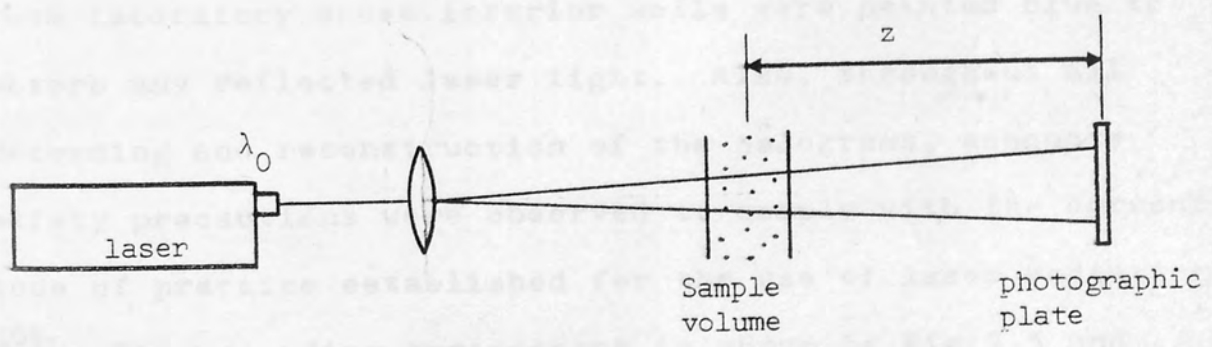


Fig. 7.4(b) 'In-line' holography

technique to monitor the size distribution of naturally occurring fog droplets <sup>98,104</sup> which led to the design of a laser hologram camera <sup>105,106</sup>. The potential of the technique, due to the short exposure time required, was exploited in further investigations into the dynamic behaviour of aerosols and particulate clouds <sup>103,107,108</sup> <sup>109</sup>. Recent applications using this type of holography include studies of glass fibre production and marine plankton behaviour. <sup>101</sup>

'In-line' holography was selected for this study because relatively few optical components and low space requirements permitted modification of the technique for in situ analysis of a secondary dispersion during operation of the coalescence process.

7.6. HOLOGRAM RECORDING.

The recording process requires the complete absence of light from extraneous sources and the whole of the equipment used in this investigation was housed in a dark-room laboratory whose interior walls were painted blue to absorb any reflected laser light. Also, throughout all recording and reconstruction of the holograms, adequate safety precautions were observed to comply with the current code of practice established for the use of laser radiation <sup>102</sup>. The recording arrangement is shown by Fig 7.5 and its position relative to the coalescence equipment is illustrated in Fig 7.6.

7.6.1. The Light Source.

The coherent light source was provided by a Barr and Stroud LU6 pulsed ruby laser. The components consist of a ruby rod as the active element which is activated by a flashtube within a water cooled cavity. Operation in the Q-switched mode was achieved using a spinning prism Q-switch

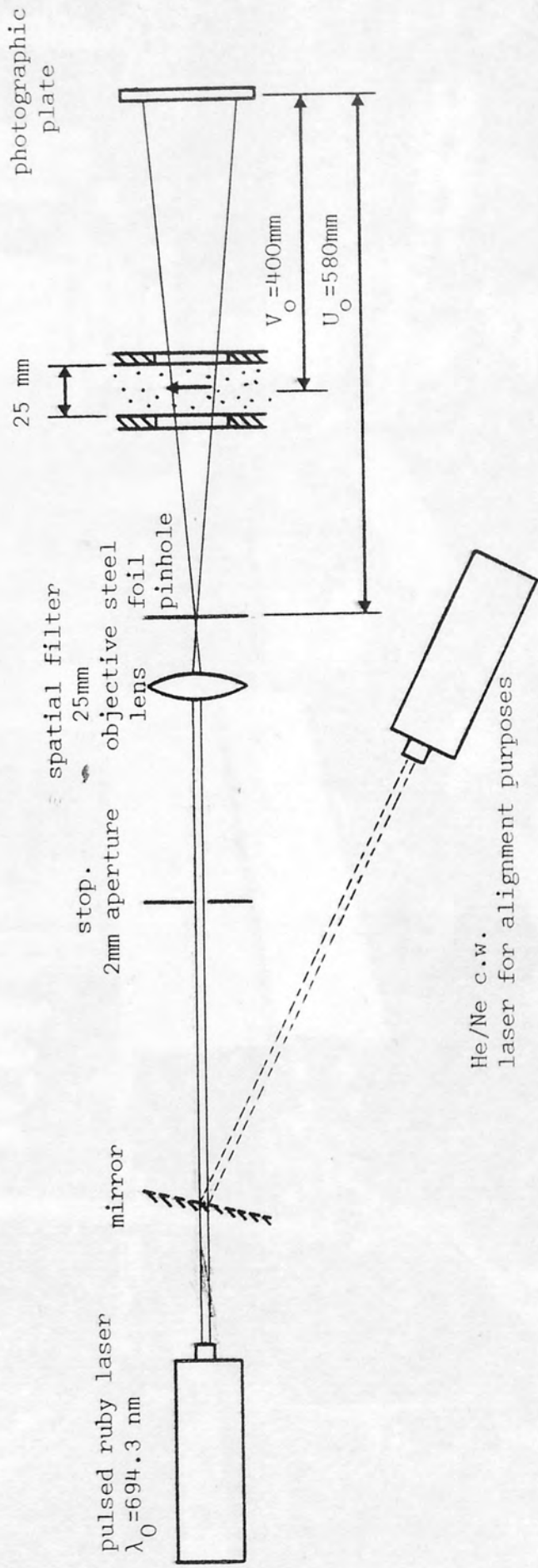


Fig. 7.5. Hologram recording configuration (Fourier 'in-line' system)

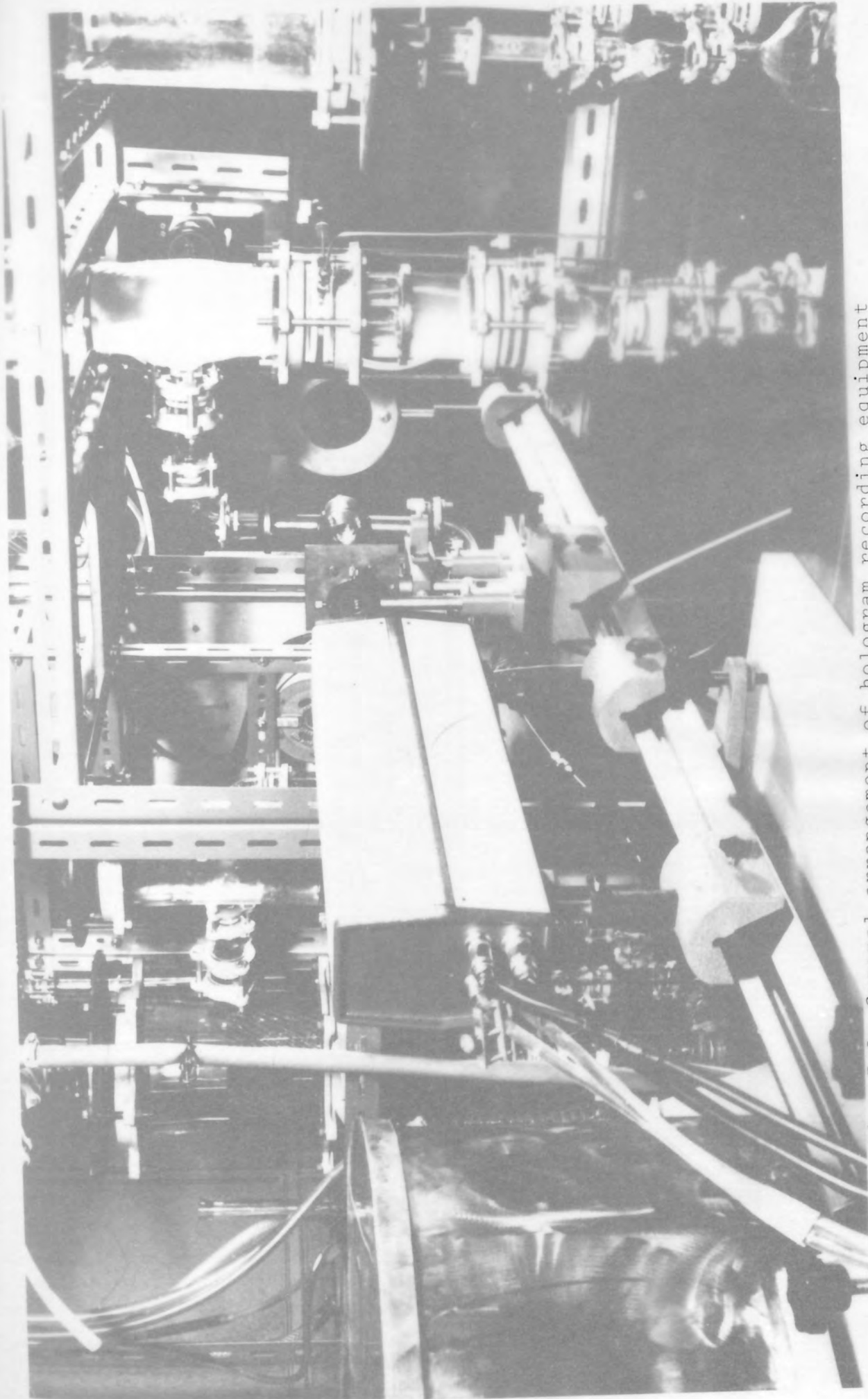


Fig. 7.6. General arrangement of hologram recording equipment

located in the rear of the unit with a resonant reflector at the head. The laser produced a pulse of approximately 20 ns. duration with an output wavelength of 694.3 nm.

Applying the criterion that Thompson suggested, the short exposure time implies a theoretical lower limit of resolution due to drop motion of  $< 0.03 \mu\text{m}$  which is better than the overall resolution of the system as discussed in Section 7.6.3.

The laser beam was then passed through a 2 mm diameter aperture, which eliminates background illumination from the flash tube, to a spatial filter assembly whose function is to produce a diverging spherical wavefront of undistorted light. The filter, shown in Fig 7.7 consisted of a microscope objective lens of 25 mm focal length which focusses the parallel beam onto a steel foil of 0.5 mm thickness. The foil was clamped between two brass plates for stability and the assembly mounted on two transverse slides for alignment purposes. After alignment of the lens with the pulsed laser beam using a continuous He/Ne laser (see Fig 7.5), the steel foil was positioned at the focal point of the lens using a collimator. When the pulsed laser was subsequently triggered, the focussed beam vapourised the steel which formed a pinhole of approximately  $80 \mu\text{m}$  diameter after a few pulses.

Thompson<sup>98</sup> has estimated that approximately 1% of the laser output energy is effectively employed in forming the hologram which is due to various effects throughout the optical system. Webster<sup>103</sup> discovered that focussing the beam of a pulsed ruby laser, of the type used in this study, causes breakdown of the air forming a plasma which is optically opaque. The problem was surmounted by placing the spatial filter in an evacuated glass envelope but such

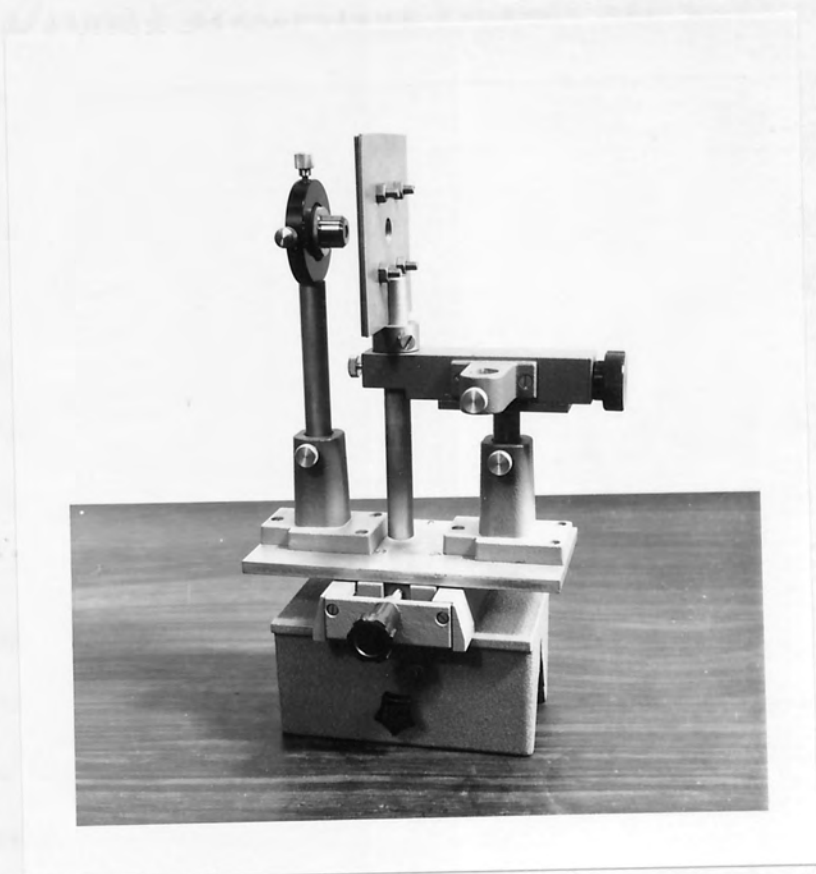


Fig. 7.7. Spatial filter assembly

complex practical measures were found to be unnecessary in this case.

### 7.6.2. Test Section Design.

The chief difference between previous work and this development of Fraunhofer holography for analysis of liquid/liquid dispersions is that the beam must traverse through the continuous phase and two glass windows which retain the dispersion. Preliminary experiments with the dispersion flowing through a sight glass produced holograms which were considerably under exposed and this was attributed to energy losses by reflection of the laser beam at the four additional interfaces created by the glass and continuous phase.

A sight glass, illustrated in Fig.7.8, was specially designed to accommodate two optically flat, coated windows. The windows were 25 mm diameter and 5 mm thick with both sides flat to ( $\lambda/4$  at 694.3 nm) and parallel to 30 seconds of arc. An anti-reflection coating specific to light of this wavelength was also applied to the windows. They were then sealed into the sight glass using a fluoro-carbon sealant, Silastic 733 RTV and held in position with stainless steel rings between P.T.F.E. gaskets. The stainless steel assembly was carefully designed to minimise dead space between the window so avoiding the formation of turbulent eddies within the sample volume. This would have caused drop entrainment within the eddies with possible impaction onto the window surfaces causing detrimental effects on image quality. Thompson<sup>98</sup> has experimentally determined the maximum practical depth for recording and reconstructing particles by holography, thus the maximum sample depth =  $49(d^2/\lambda)$ , which for drops of 20  $\mu\text{m}$  diameter, corresponds to a depth of 28.2 mm. A sample depth

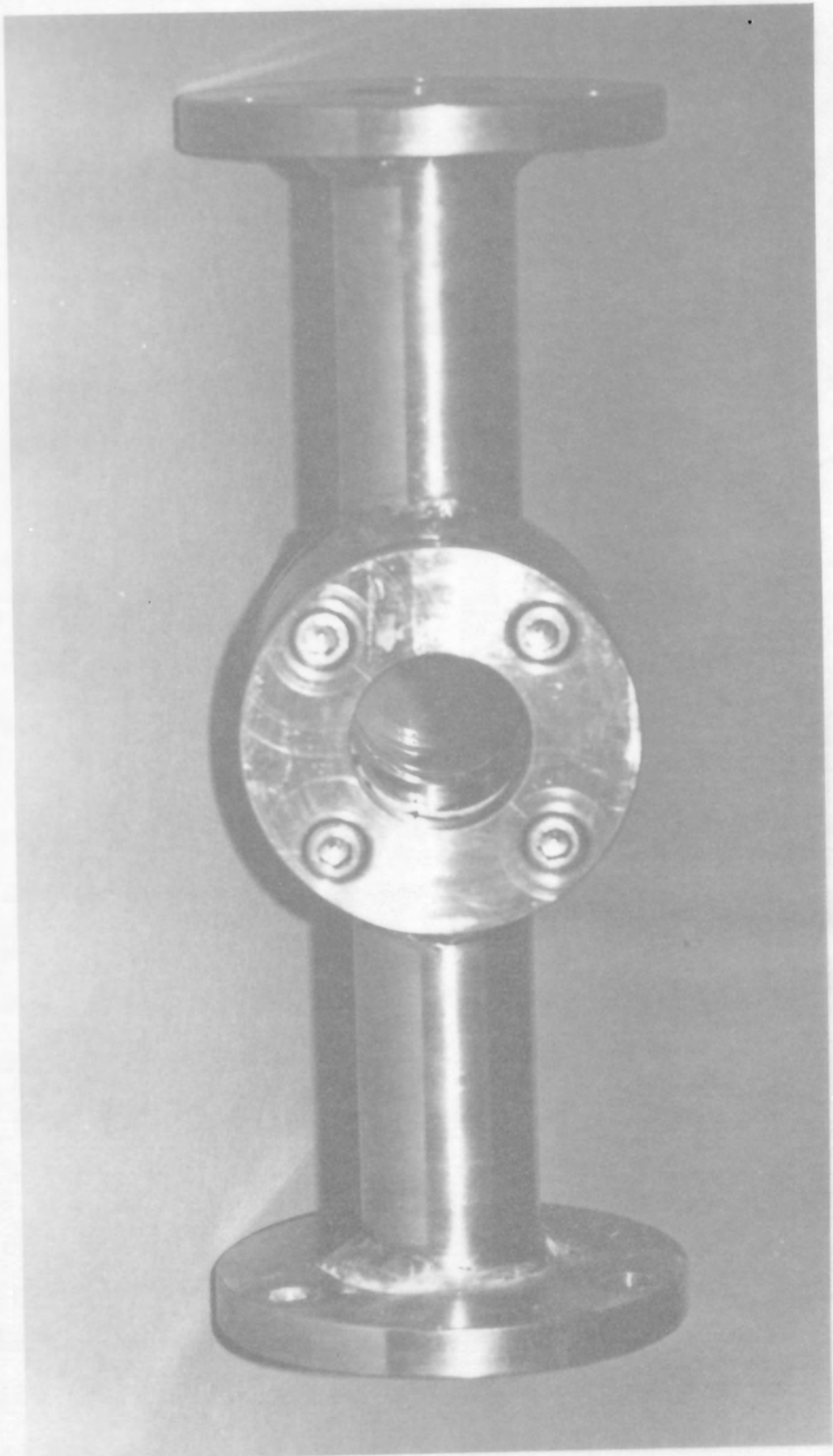


Fig. 7.8. Holographic test section design

of 25.4 mm was thus employed which also accommodated the other preferred features of the design.

The final design of the test section proved to be entirely satisfactory as no drop impaction occurred within the sample volume and energy losses were sufficiently reduced to produce holograms of acceptable quality. The longitudinal position of the sight glass along the axis of the recording system was selected so that the diverging incident beam just filled the circular face of the windows.

The distance between the sight glass and the recording plane was determined by considerations of hologram quality and the desired magnification. Firstly the minimum distance should be greater than one far field distance ( $d^2/\lambda$ ) of the drops to produce Fraunhofer holograms. This also ensures that the virtual image contribution to the hologram is negligible.<sup>98</sup> The far field distance for 20  $\mu\text{m}$  drops is 0.58 mm and therefore this condition was easily achieved. As the recording distance increases, consistent with the far field condition, high magnification results but also the required temporal coherence of the beam increases<sup>101</sup> A distance of 400 mm (approximately 700 far field distances) was found to be an acceptable compromise between these conflicting requirements for which the spectral bandwidth of the laser, 0.001 nm, was satisfactory.

### 7.6.3. Selection of Photographic Recording Material.

The photographic plate was retained in a stainless steel holder as shown in Fig 7.9. Prior to exposure, the plate was inserted in the holder and remained there during exposure and processing to avoid handling and to promote intimate contact between the film and the processing solutions.



Fig. 7.9. Photographic plate holder

of this furnace is described in reference (10) which  
and receives a 2.2  $\mu$  drop. Slightly higher resolution is  
achieved with the 5875 type emission but at the expense of  
lower sensitivity and the 5875 was employed in the present  
plate form in the recording of the holograms.

### 7.1. DEVELOPMENT OF HOLOGRAMS

In a hologram, a three-dimensional surface  
constituted of small silver grains forms the image. Therefore  
and it is necessary to retain the image formed by the  
size of each grain geometrically in perspective so that  
it is therefore essential to use developing solutions which  
do not significantly alter the relative positions of grains  
by subsequent shrinkage, expansion or other processes.

The hologram itself is often the poorest quality, optical element in the system because the emulsion adds phase and amplitude noise to the recording and reconstruction process<sup>99</sup>. The dimensions of the structure of the interference pattern to be recorded are of the order of magnitude of the wavelength of light used for exposure and a very high resolving power is essential. A high speed is also necessary to cope with the short exposure. High resolution and high speed are somewhat incompatible properties necessitating the development of emulsions specific to the wavelength of light used<sup>110</sup> Schultze<sup>111</sup> has described the properties of emulsions sensitised to red light of which three types are suitable for use with 694.3 nm wavelength illumination.

Zinky<sup>112</sup> derived an expression relating the minimum diameter of an object that can be resolved to the sensitivity of the recording material,  $d = 2\lambda/l_{\max}$  and application of this formula to Scientia emulsion 10E75 which has a resolution ( $l_{\max}$ ) of 2800 lines/mm shows that this film will resolve a 2.2  $\mu\text{m}$  drop. Slightly higher resolution is achieved with the 8E75 type emulsion but at the expense of lower sensitivity and the 10E75 was employed in photographic plate form in the recording of the holograms.

#### 7.7. DEVELOPMENT OF HOLOGRAMS.

In a hologram, a three-dimensionally arranged constellation of small silver grains forms the image structure and it is necessary to retain the image contributing qualities of each grain geometrically in perspective to each other. It is therefore essential to use developing techniques which do not significantly alter the relative positions of grains by subsequent shrinkage, expansion or other unsymmetric effects.

Perspective stability of elementary grains is achieved by hardening the film immediately after exposure. After development of the photographic plate, an amplitude hologram is formed. Observation of the virtual image during the reconstruction process is possible with this type of hologram but quantitative analysis of the real image was prevented since the He/Ne laser was not able to transmit sufficient illumination through the high density interference pattern. Therefore, a subsequent bleaching process was employed to transform the holographic silver image to a transparent silver salt. The resulting phase hologram produces bright, low noise images on reconstruction with little loss in contrast; the hologram also remains stable for long periods if the bleaching process adopted is specific to the emulsion used<sup>110</sup>. The process used in this work was a modification, developed by Phillips<sup>113</sup>, of the emulsion manufacturers procedure to give slightly higher (>40%) diffraction efficiency, which is the percentage of incident light diffracted into the first order. The composition of the solutions and the procedure for complete processing of the holograms are given in Appendix G.

Diffraction efficiencies up to 70% have been attained using bromine vapour as a bleaching agent<sup>114</sup> but this technique was rejected since processing time is markedly increased and also bromine is deleterious both to the skin and respiratory tract.

#### 7.8. HOLOGRAM RECONSTRUCTION.

The reconstruction system, shown in Fig 7.10 and 7.11 is similar in design to that proposed by Thompson<sup>98</sup>. The coherent light source was provided by a Spectra Physics Model 132M Multimode 3.5 mW He/Ne laser. The

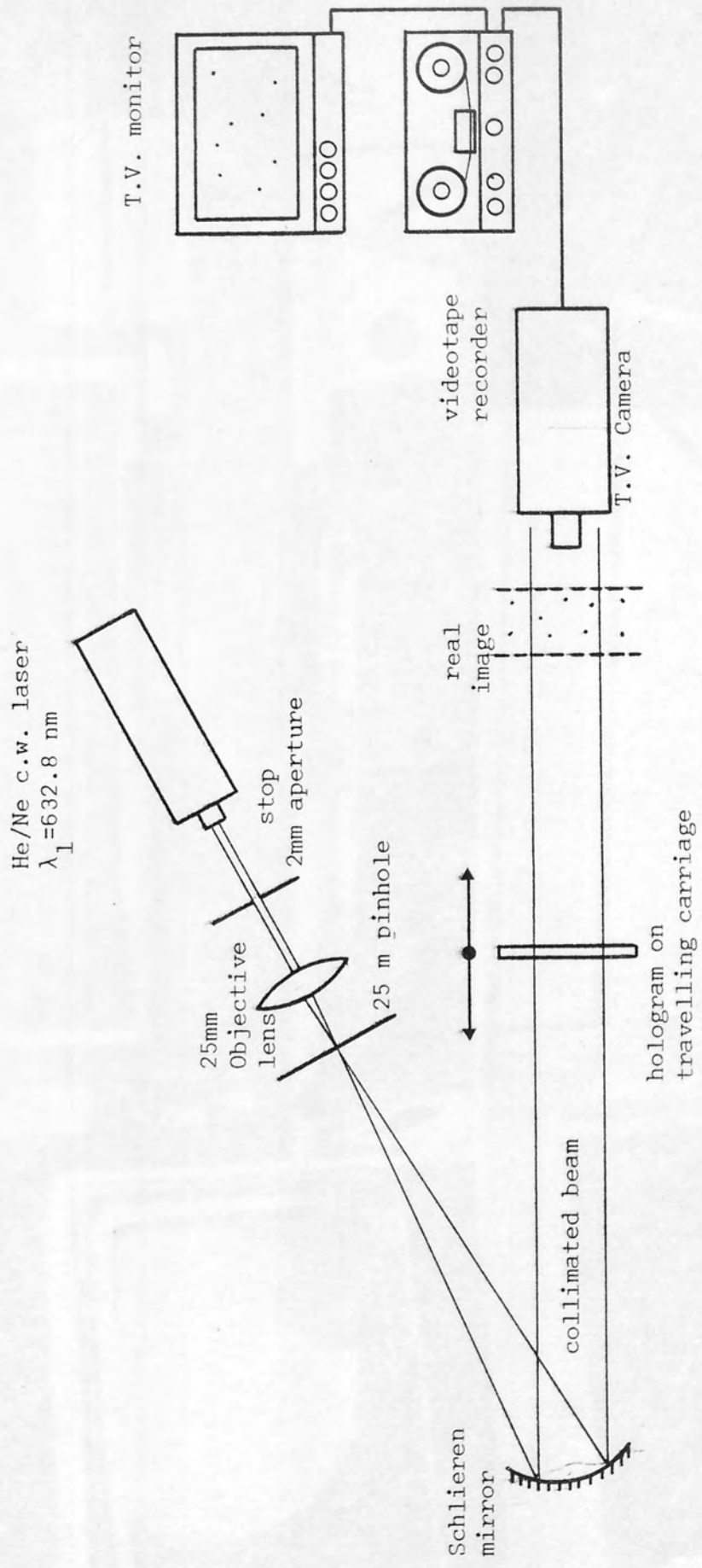


Fig. 7.10 Hologram reconstruction configuration

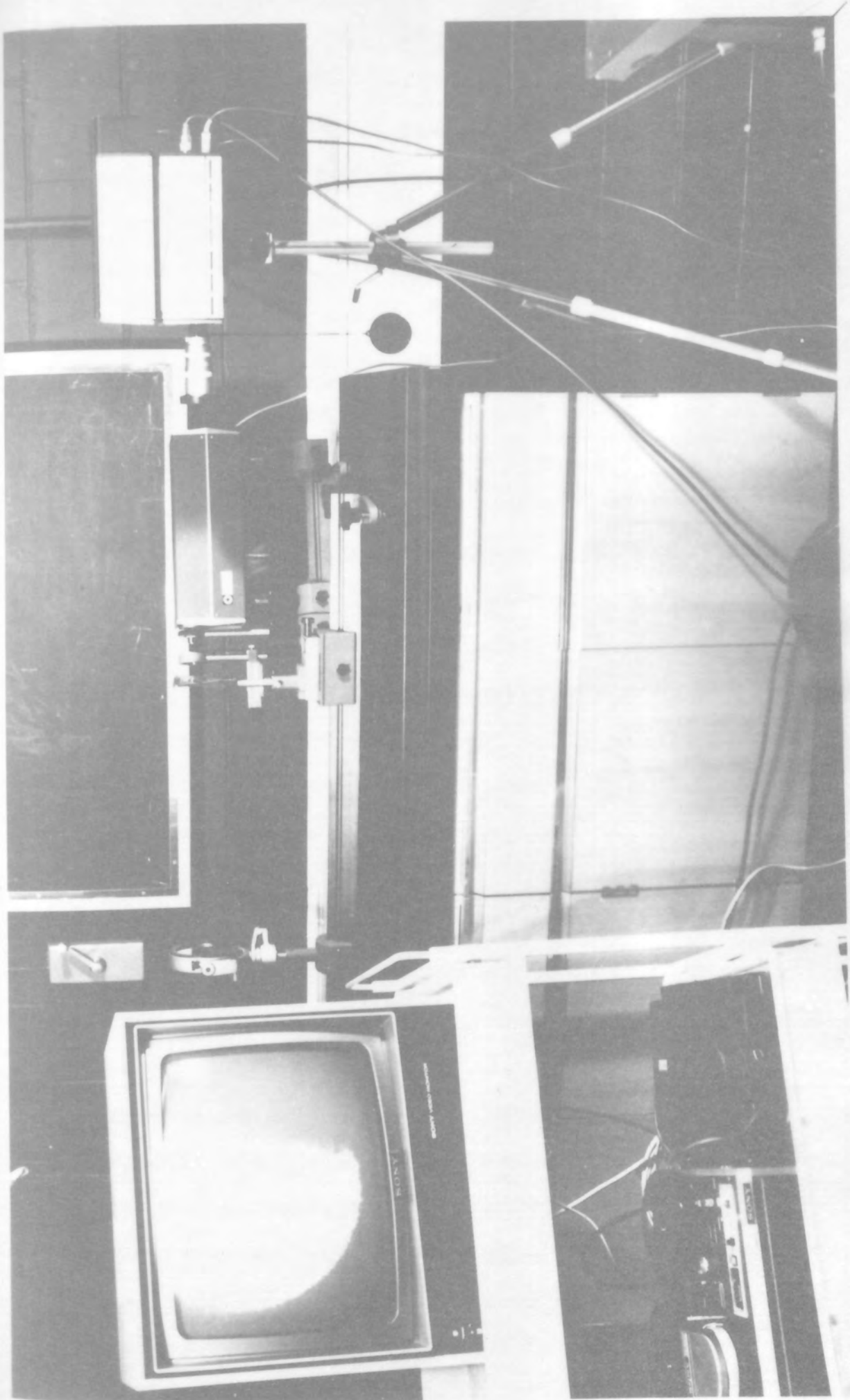


Fig. 7.11. General arrangement of hologram reconstruction equipment

multimode type was selected since the output beam has a more uniform intensity distribution than the conventional type of gas laser where the distribution is Gaussian. Consequently, the beam is more suitable for holographic viewing. From the laser, the beam is focussed using a microscope objective of 25 mm focal length onto a 25  $\mu$ m diameter pinhole. The diverging beam was then collimated using a front silvered Schlieren mirror of 152 mm diameter placed at a distance equal to its focal length after the pinhole. The plane wave illumination then passed through the hologram, carried on a moving optical mounting, to reconstruct the real image of the sample volume.

Movement of the hologram enabled the drop images at different planes within the sample volume to be focussed and recorded using a still camera or a closed circuit television system. The latter method has several advantages,

1. High image magnification; up to 30X was attained using a Sony closed circuit system.
2. Increased image brightness.
3. Adjustable contrast to ensure that only 'in focus' drops are displayed on the monitor.
4. Facility to record the information contained in the hologram in a series of two dimensional planes using a videotape recorder.

The images could then be subsequently retrieved and analysed by an automatic scanning device such as a Quantimet. This technique was recently applied to the analysis of a primary dispersion from shadowgraphs by Wilkinson<sup>81</sup> However development of automatic analysis of the hologram images was prevented in this study due to the incompatible scanning systems of the closed circuit television equipment and the available Quantimet instrument. This problem

has been eliminated by the recent introduction of an integrated hologram reconstruction and image analysis system described by Bexon<sup>108</sup> which finds application in aerosol sizing. This instrument however, does have the disadvantages of extremely high cost.

### 7.9. DATA ACQUISITION.

Despite the high magnification associated with video equipment, manual sizing of the focussed images from the television monitor is subject to considerable eye strain caused by close proximity to the scanning lines of the monitor. An alternative approach was therefore adopted whereby the sequence of images from the hologram were recorded in a series of photographs which were processed using the method described in Section 7.2. A typical series of photographs obtained in this way are shown in Fig 7.12 illustrating how the drop images move in and out of focus thus confirming the three dimensional properties of the hologram.

'In-line' holograms possess the additional advantage that the object magnification may be computed directly from the optical geometries and the wavelength of the illumination used in recording and reconstruction using the nomenclature described in Fig.7.5,

Magnification of recording configuration,  $m_o = \frac{u_o}{u_o - v_o}$  and for  $u_o = 580$  mm. and  $u_o = 400$  mm,  $m_o = 3.22X$ .

Hologram reconstruction using a collimated beam does not affect the magnification but a small change is caused by the use of coherent light of different wavelengths for the recording and reconstruction stages, thus,  $m_1 = \frac{\lambda_1}{\lambda_0}$ .

With  $\lambda_1 = 632.8$  nm and  $\lambda_0 = 694.3$  nm,  $m_1 = 0.911$  and

therefore overall magnification,  $M = m_o m_1 = 2.93$ .

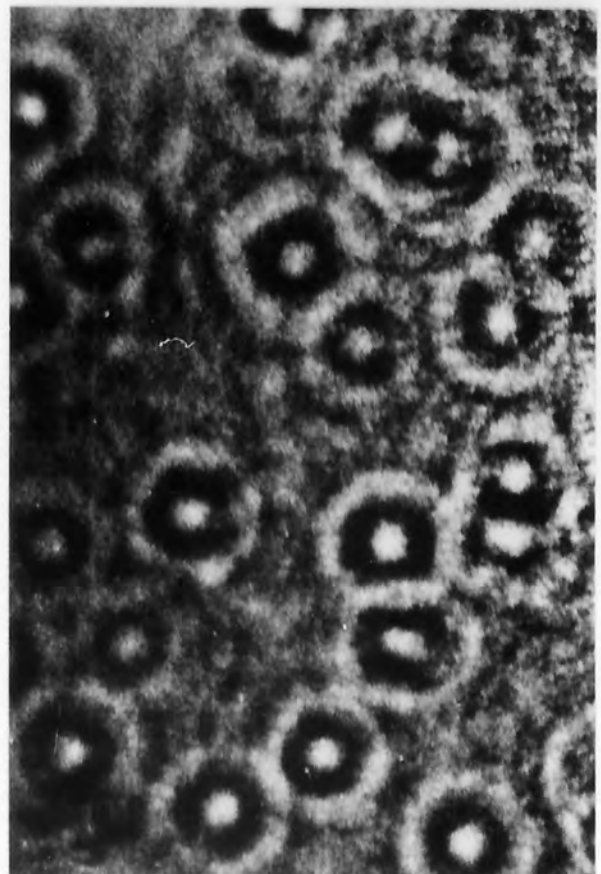
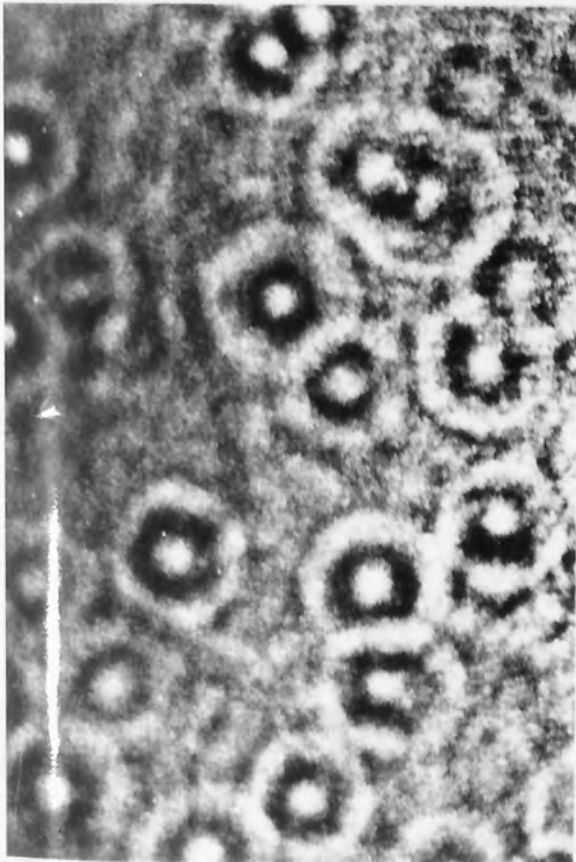
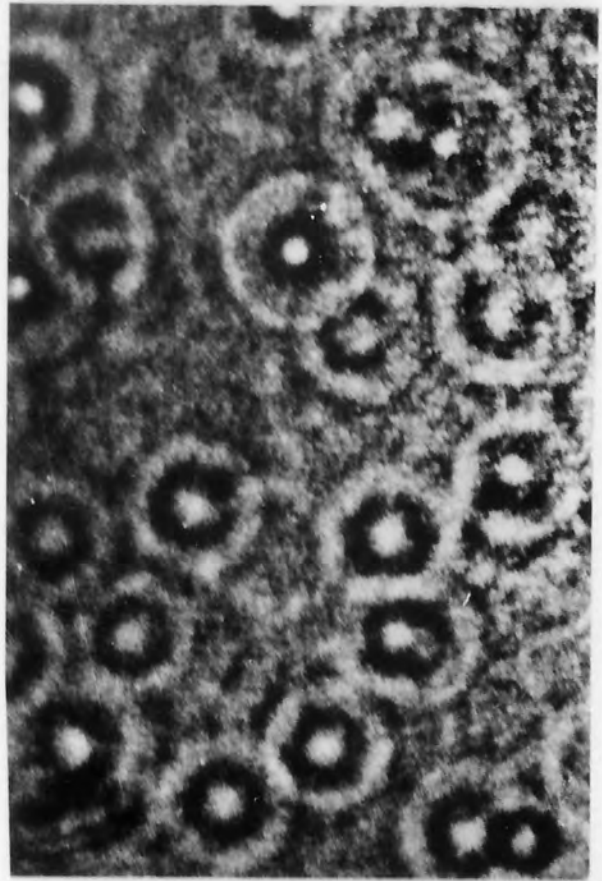
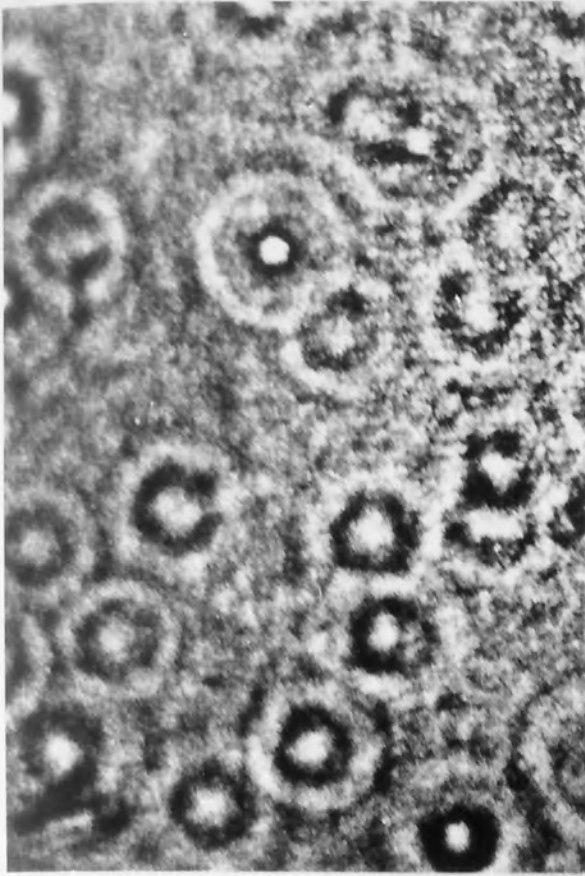


Fig. 7.12 Photographs of a reconstructed hologram illustrating focussing of droplet images

This calibration of the system was checked by taking a hologram of essentially monosize particles dispersed in water within the sample volume. Results obtained by measurement of the diameters of the images formed by the hologram reconstruction using the video system are presented in Table 7.1. The magnification of the video equipment was maintained at 29.7, giving an overall theoretical magnification of 87X which represents good agreement with the experimentally determined values. The increasing discrepancy observed for the smaller particle sizes was attributed to difficulty in visually resolving between the perimeter of a focussed image and the surrounding fringe pattern.

Sample	Diameter ( $\mu\text{m}$ )	Measured <sup>a</sup> Diameter(mm)	Magnification
Lycopodium powder	26.4	2.49	94.5
Pecan pollen	41.6	3.77	90.8
Corn pollen	79.0	7.07	89.6

a - mean of a minimum of 90 measurements

Table 7.1 Calibration of Holographic System

... the mean size of collected drops, determined by ...  
 ... was linear diameter, was found to decrease with an increase ...  
 ... in superficial velocity as shown in Fig. 8.2. This is in ...  
 ... agreement with other workers ...  
 ... degree of collection decreased with increasing velocity ...  
 ... For each initially free from disturbance phase, the rate of ...  
 ... decrease is reduced to approximately 10% at a velocity of ...  
 ... corresponds to the values indicated in Fig. 8.2. ...  
 ... by previous workers ...  
 ... subjected with disturbance ...  
 ... phenomenon did not ...  
 ... (Fig. 8.2) ...  
 ... of the ...

### CHAPTER 8

### EXPERIMENTAL RESULTS

8.2. COLLECTED DROP SIZE

8.2.1. Stainless Steel Meshes

The mean size of collected drops, determined by ...  
 ... was linear diameter, was found to decrease with an increase ...  
 ... in superficial velocity as shown in Fig. 8.2. This is in ...  
 ... agreement with other workers ...  
 ... degree of collection decreased with increasing velocity ...  
 ... For each initially free from disturbance phase, the rate of ...  
 ... decrease is reduced to approximately 10% at a velocity of ...  
 ... corresponds to the values indicated in Fig. 8.2. ...  
 ... by previous workers ...  
 ... subjected with disturbance ...  
 ... phenomenon did not ...  
 ... (Fig. 8.2) ...  
 ... of the ...

### 8.1. INLET DROP SIZE.

For a given liquid system, the mean drop size of a secondary dispersion produced by a centrifugal pump in a bi-pass loop depends on the pump speed<sup>17,70</sup>. A recent study<sup>115</sup> showed that the level of turbulence in the vicinity of the pump impellor far exceeds that inside the loop so that drop break-up by viscous shear is the most likely mechanism. As the emulsification pump was operated at constant speed, the dispersion was analysed for each velocity since when the latter increases, the residence time of the dispersion in the loop is reduced. The results, presented in Fig 8.1, indicate that mean drop size is independent of superficial velocity above  $2.5 \times 10^{-2}$  m/s but decreases significantly at lower flowrates. The reproducibility of the technique was estimated to be approximately  $\pm 5 \mu\text{m}$ .

### 8.2. COALESCED DROP SIZE.

#### 8.2.1. Stainless Steel Meshes.

The mean size of coalesced drops, determined as the mean linear diameter, was found to decrease with an increase in superficial velocity as shown in Fig 8.2. This is in agreement with other workers<sup>39,116,117</sup>, who found that the degree of coalescence decreased with increasing velocity. For beds initially free from dispersed phase, the rate of decrease is reduced at approximately  $1.5 \times 10^{-2}$  m/s which corresponds to the 'critical separating velocity' defined by previous workers<sup>41,75</sup>. This velocity is usually associated with breakthrough of the secondary haze but this phenomenon did not occur until the superficial velocity exceeded about  $3.5 \times 10^{-2}$  m/s. (see Fig 8.7). However, despite breakthrough, operation up to  $7.0 \times 10^{-2}$  m/s still

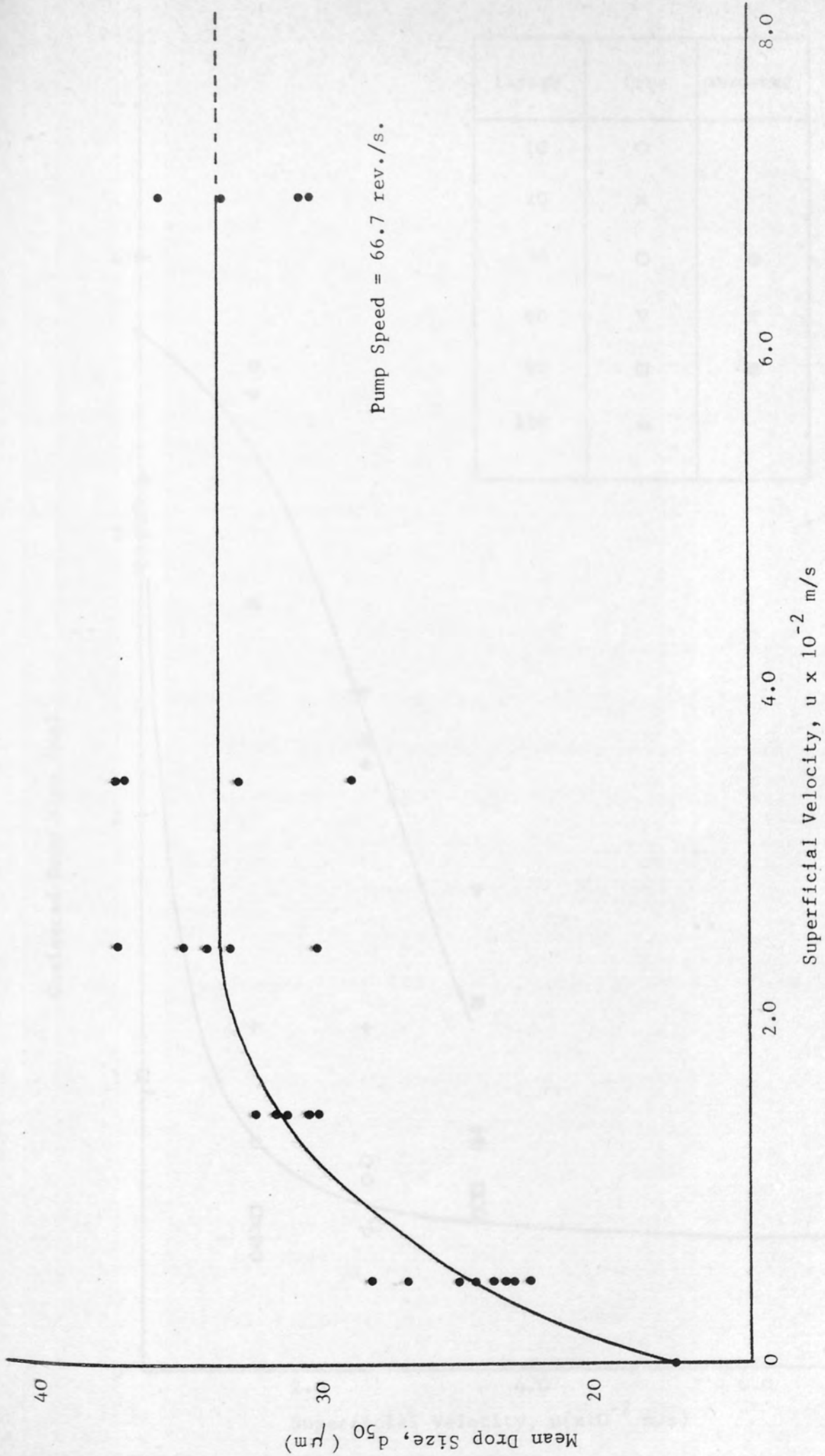


Fig.8.1. Variation of Inlet Drop Size with Velocity for Toluene/Water System.

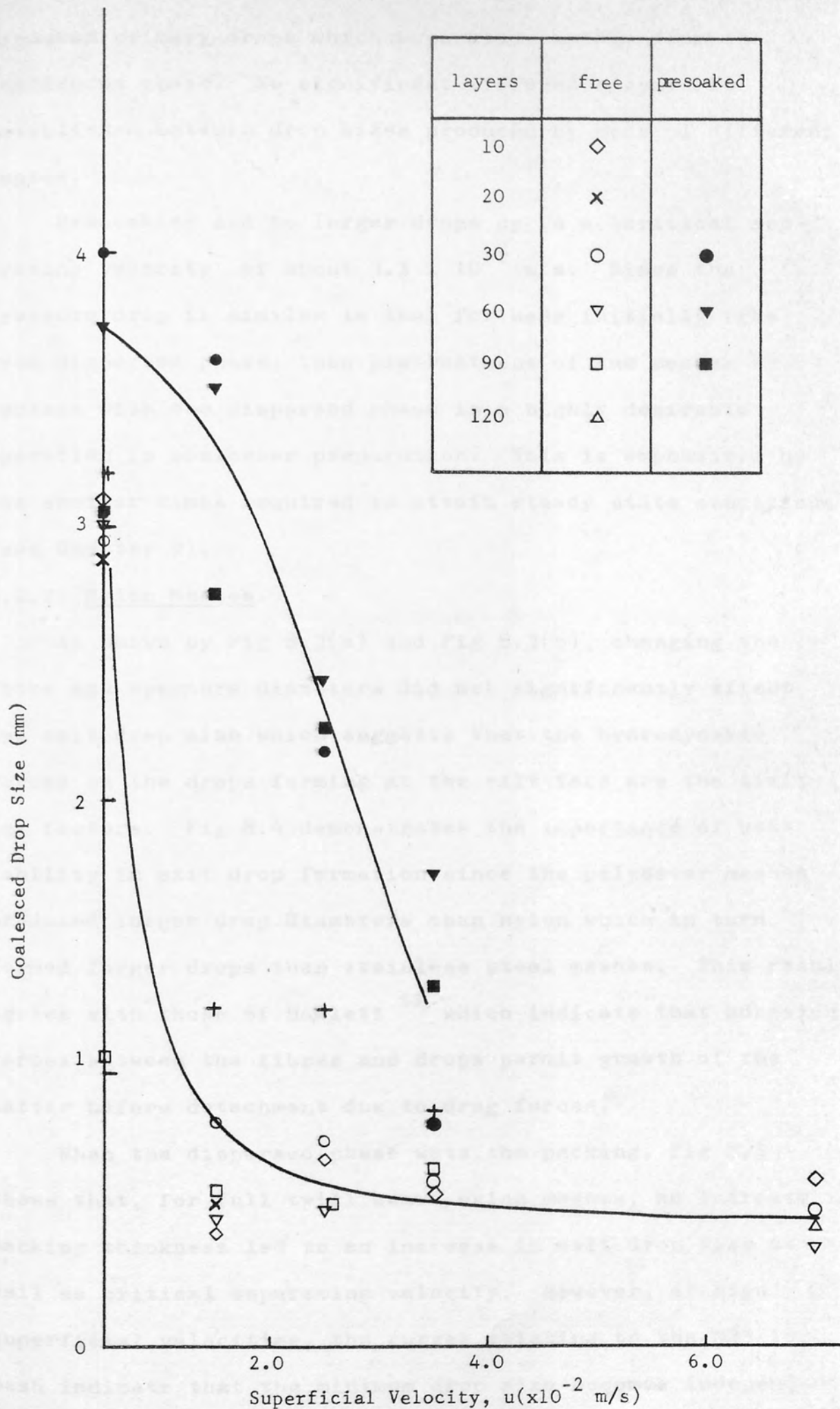


Fig.8.2. Variation of Coalesced Drop Size with Velocity.

produced primary drops which separated rapidly from the continuous phase. No significant difference could be established between drop sizes produced by beds of different depths.

Presoaking led to larger drops up to a 'critical separating velocity' of about  $3.5 \times 10^{-2}$  m/s. Since the pressure drop is similar to that for beds initially free from dispersed phase, then pretreatment of the meshes by contact with the dispersed phase is a highly desirable operation in coalescer preparation. This is emphasized by the shorter times required to attain steady state conditions (see Chapter 9).

#### 8.2.2. Nylon Meshes.

As shown by Fig 8.3(a) and Fig 8.3(b), changing the fibre and aperture diameters did not significantly affect the exit drop size which suggests that the hydrodynamic forces on the drops forming at the exit face are the limiting factors. Fig 8.4 demonstrates the importance of wettability in exit drop formation since the polyester meshes produced larger drop diameters than nylon which in turn formed larger drops than stainless steel meshes. This result agrees with those of Hazlett<sup>53</sup> which indicate that adhesion forces between the fibres and drops permit growth of the latter before detachment due to drag forces.

When the dispersed phase wets the packing, Fig 8.5 shows that, for full twill weave nylon meshes, an increase in packing thickness led to an increase in exit drop size as well as critical separating velocity. However, at high superficial velocities, the curves relating to the N25/18 mesh indicate that the minimum drop size becomes independent of bed depth. Increasing the velocity from a low value,

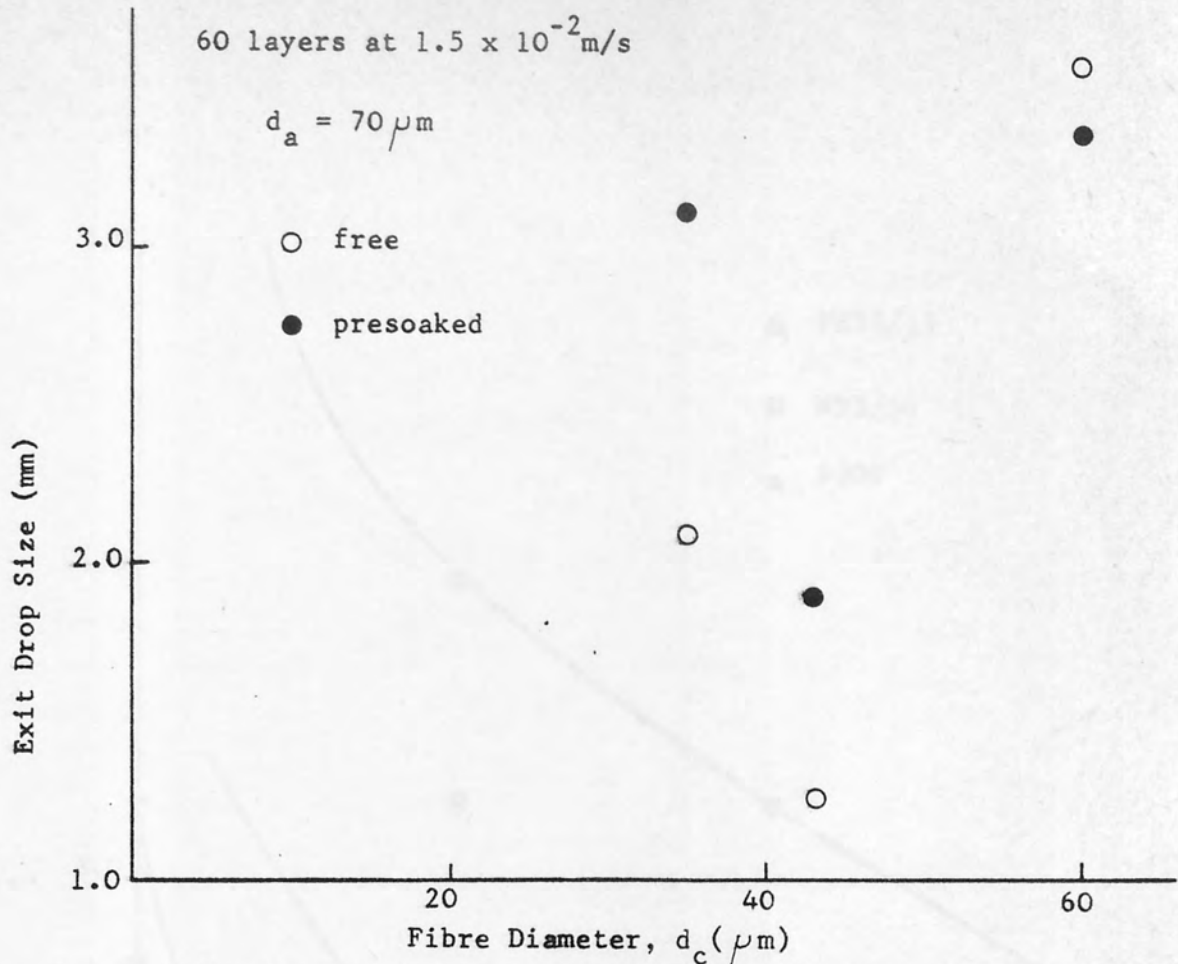


Fig 8.3(a) Effect of Fibre Diameter on Coalesced Drop Size

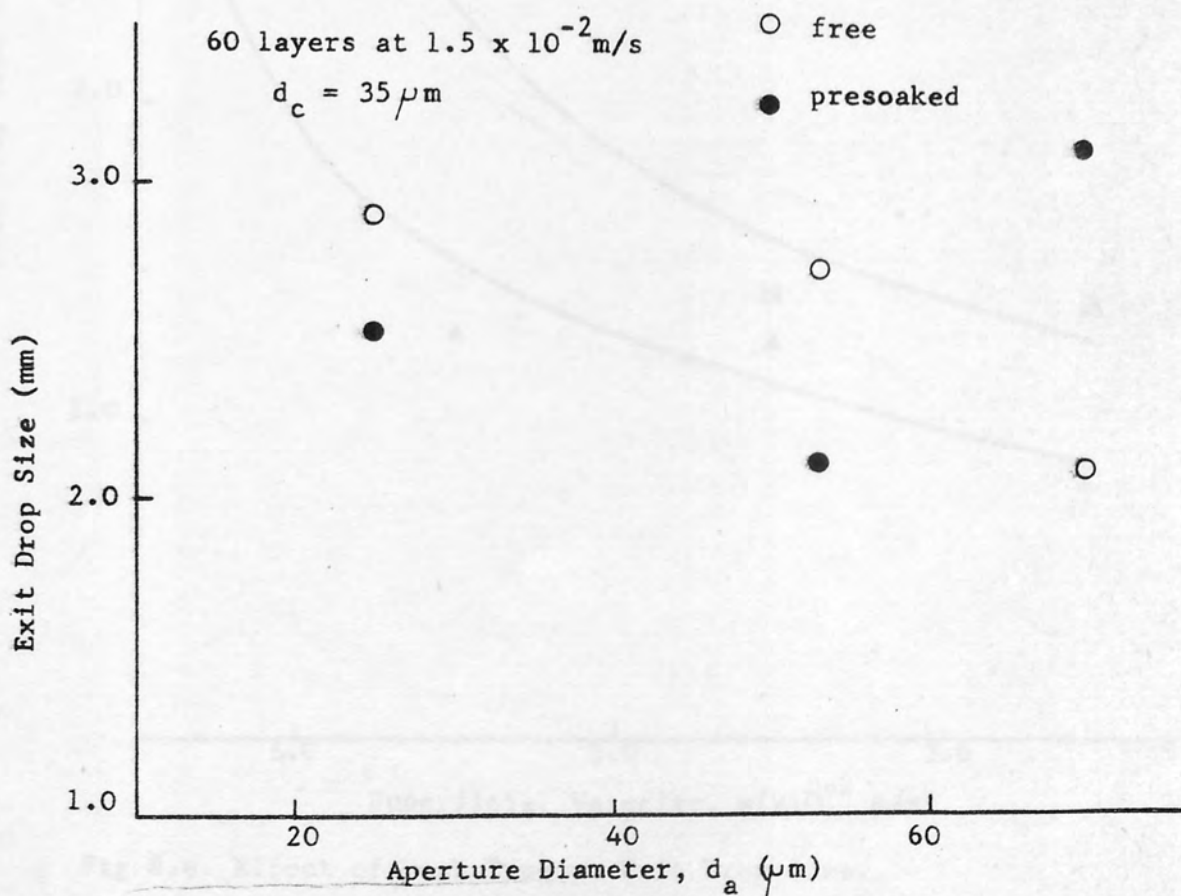


Fig 8.3(b) Effect of Mesh Aperture size on Coalesced Drop Size.

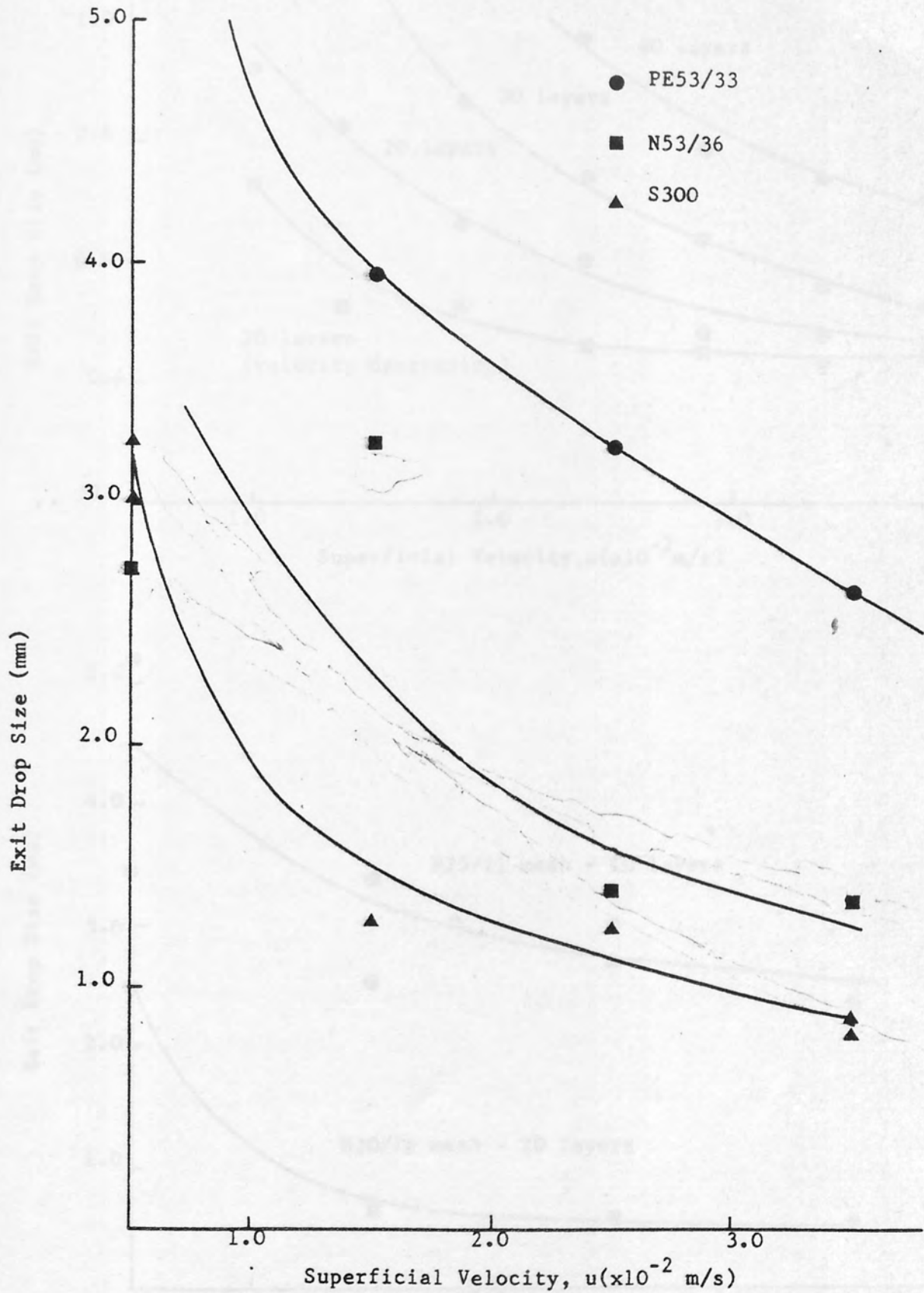


Fig 8.4. Effect of Mesh Type on Exit Drop Size.

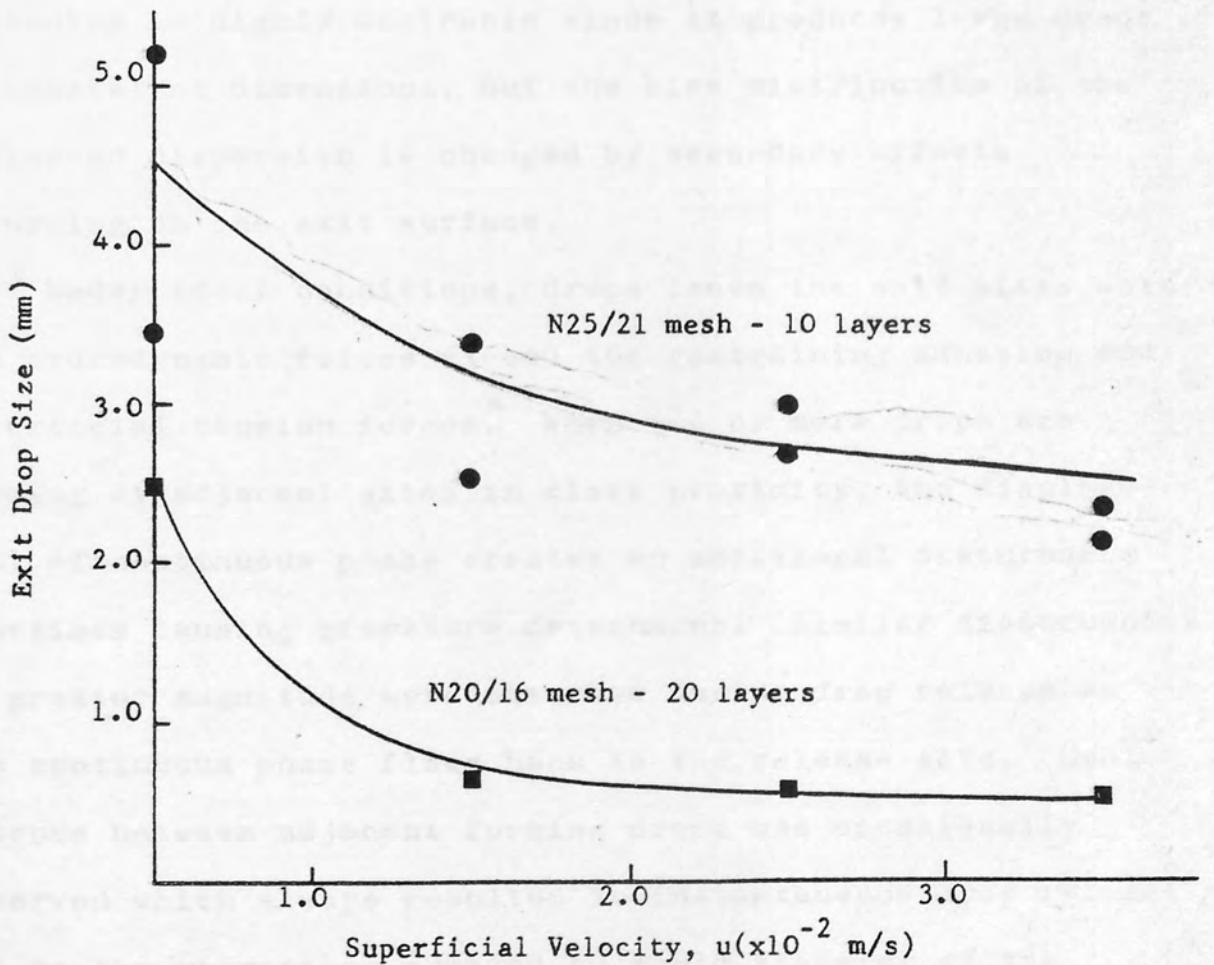
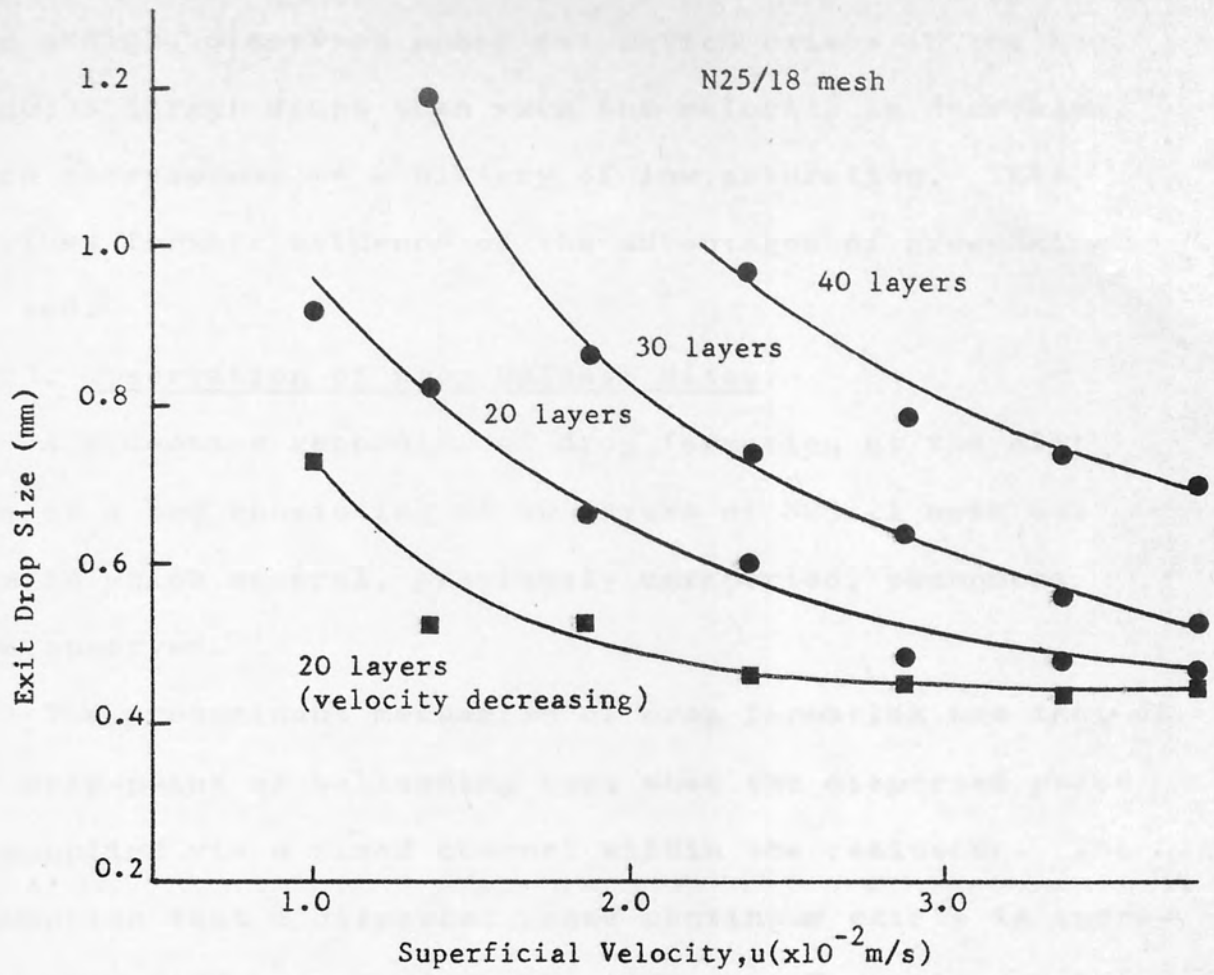


Fig 8.5 Variation of Exit Drop Size with Velocity for Nylon Meshes.

when a high, dispersed phase saturation exists in the bed, produces larger drops than when the velocity is decreased, which corresponds to a history of low saturation. This provides further evidence of the advantages of presoaking the bed.

### 8.2.3. Observation of Drop Release Sites.

A videotape recording of drop formation at the exit face of a bed consisting of 40 layers of N25/21 mesh was made in which several, previously unreported, phenomena were observed.

The predominant mechanism of drop formation was that of the drip-point or ballooning type when the dispersed phase is supplied via a fixed channel within the coalescer. The assumption that a dispersed phase continuum exists is therefore supported by experimental evidence. The drip-point mechanism is highly desirable since it produces large drops of consistent dimensions, but the size distribution of the coalesced dispersion is changed by secondary effects occurring on the exit surface.

Under ideal conditions, drops leave the exit sites when the hydrodynamic forces exceed the restraining adhesion and interfacial tension forces. When two or more drops are forming at adjacent sites in close proximity, the displacement of continuous phase creates an additional disturbance sometimes causing premature detachment. Similar disturbances of greater magnitude were observed during drop release as the continuous phase flows back to the release site. Coalescence between adjacent forming drops was occasionally observed which always resulted in instantaneous drop release due to the vibrations created by rapid transfer of the dispersed phase. Also due to their flexibility, the exit

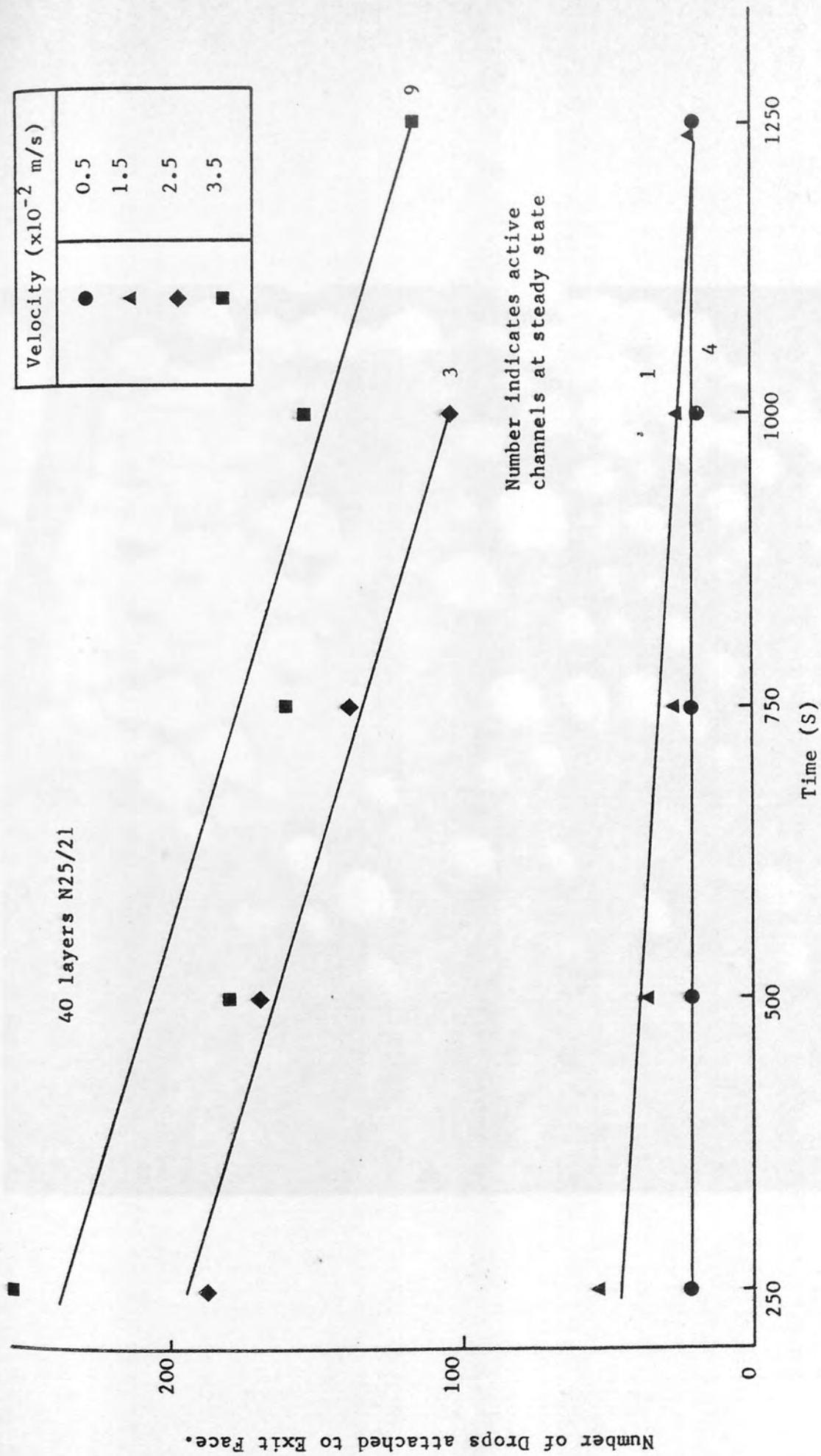


Fig 8.6. Variation in Number of Drops on Exit Face with Time of Operation.

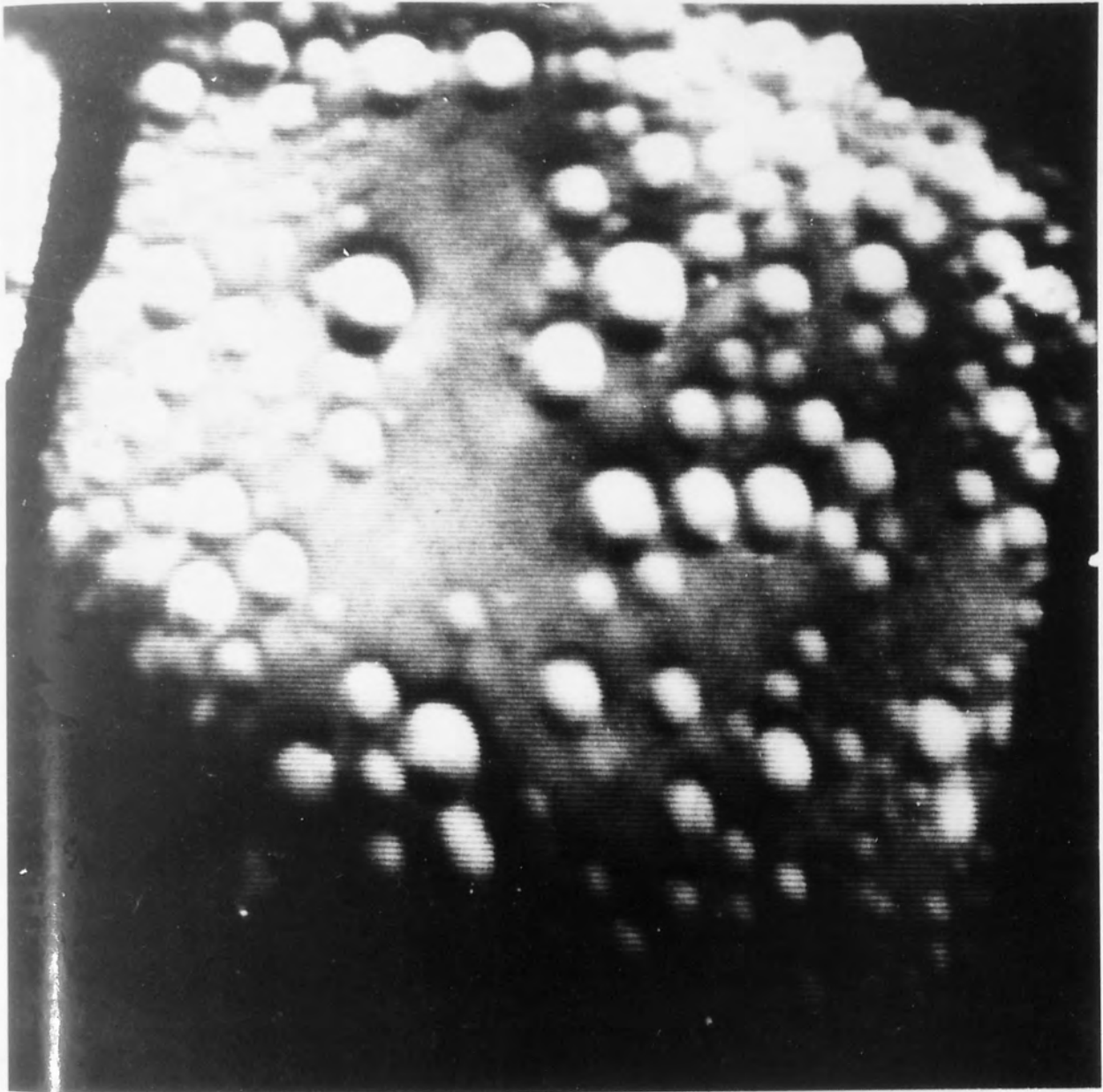


Fig. 8.6(b) Illustration of Drop Formation by 'Ballooning'  
from fixed channels

layers of the nylon beds were found to vibrate, especially at high velocities, causing considerable reduction of the mean drop size; metallic meshes were not susceptible to this detrimental effect.

At velocities less than  $1.5 \times 10^{-2}$  m/s, crude measurements of drop growth rate showed that the supply channels are fixed and intermittently active. But, at higher velocities, the same channels were not utilized after drop release, except when the mechanism of 'pointing' was observed, and drops were formed at apparently random positions on the exit face. There was evidence of spatial distribution of the release sites on the exit face as very few drops formed at the periphery.

Fig 8.6 shows the variation of the number of drops attached to the exit layer of the bed as a function of time for different velocities. Drops are formed from a large number of channels initially but as steady state conditions are approached, the dispersed phase flows in relatively fewer channels. Also, the number of drops observed at steady state is not indicative of the number of active channels since many of the drops remain attached to the packing when the associated channels are dormant. Typically, even for velocities up to  $3.5 \times 10^{-2}$  m/s, the drops of the exit primary dispersion are formed from less than ten active channels when steady state conditions are attained.

#### 8.2.4. Effluent Secondary Drops.

Uncoalesced secondary drops, whose mean diameter was determined by the holographic technique described in Chapter 7, are typically of  $30 \mu\text{m}$  diameter and are therefore quite distinguishable from coalesced drops of approximately 1 mm diameter. Results are presented for the stainless steel

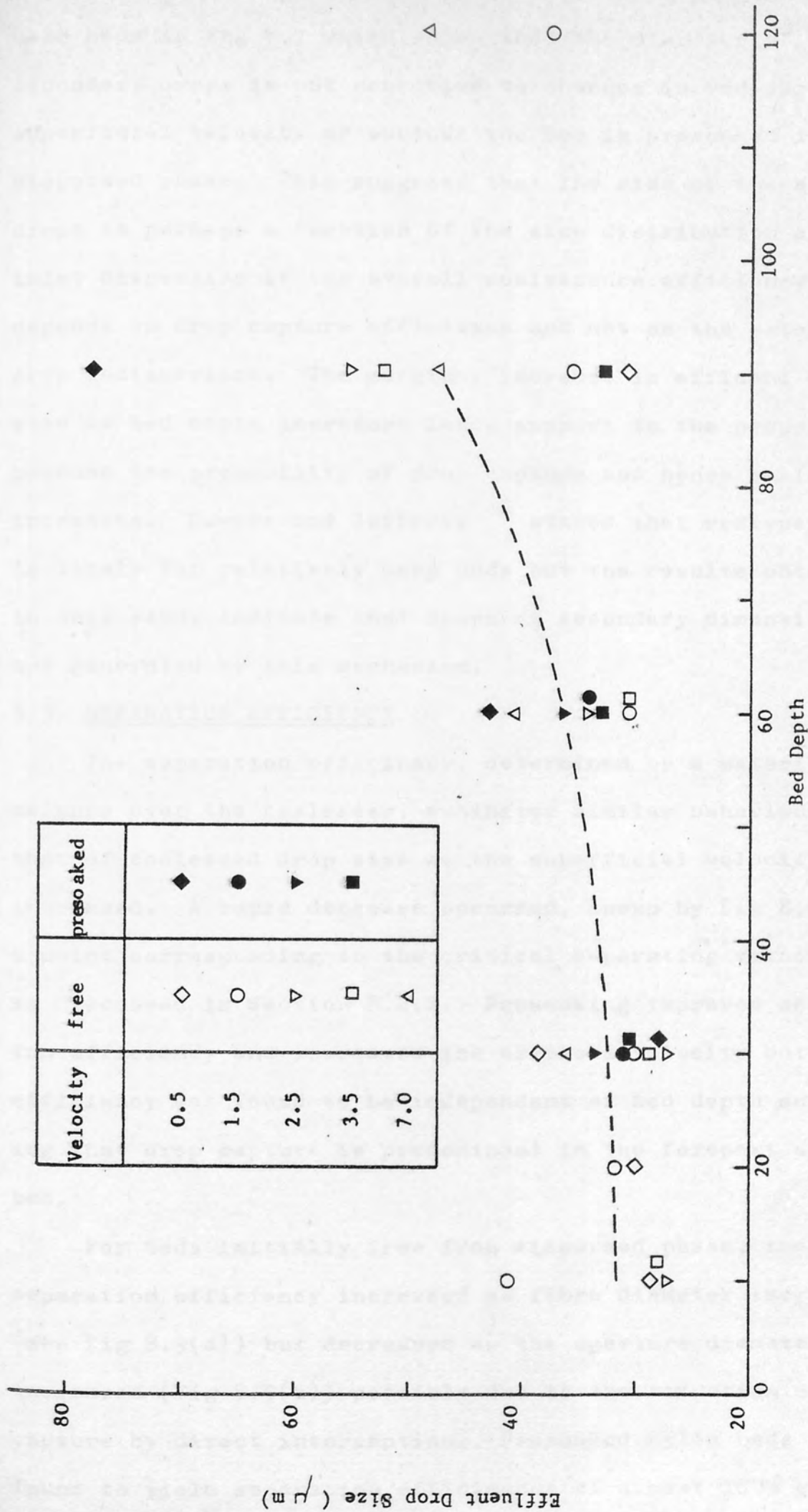


Fig.8.7 Variation of Effluent Drop Size with Bed Depth.

mesh beds in Fig 8.7 which shows that the diameter of the secondary drops is not sensitive to changes in bed depth, superficial velocity or whether the bed is presoaked in the dispersed phase. This suggests that the size of the effluent drops is perhaps a function of the size distribution of the inlet dispersion if the overall coalescence efficiency depends on drop capture efficiency and not on the extent of drop redispersion. The marginal increase in effluent drop size as bed depth increases lends support to the proposal because the probability of drop capture and hence coalescence increases. Davies and Jeffreys<sup>41</sup> stated that redispersion is likely for relatively deep beds but the results obtained in this study indicate that drops of secondary dimensions are not generated by this mechanism.

### 8.3. SEPARATION EFFICIENCY.

The separation efficiency, determined by a material balance over the coalescer, exhibited similar behaviour to that of coalesced drop size as the superficial velocity was increased. A rapid decrease occurred, shown by Fig 8.8, at a point corresponding to the critical separating velocity, as discussed in Section 8.2.2. Presoaking improved separation efficiency and increased the critical velocity but the efficiency was found to be independent of bed depth suggesting that drop capture is predominant in the forepart of the bed.

For beds initially free from dispersed phase, the separation efficiency increased as fibre diameter increases (see Fig 8.9(a)) but decreased as the aperture diameter was increased (Fig 8.9(b)) possibly due to the reduction of drop capture by direct interception. Presoaked nylon beds were found to yield separation efficiencies of almost 100% over the range of mesh dimensions investigated.

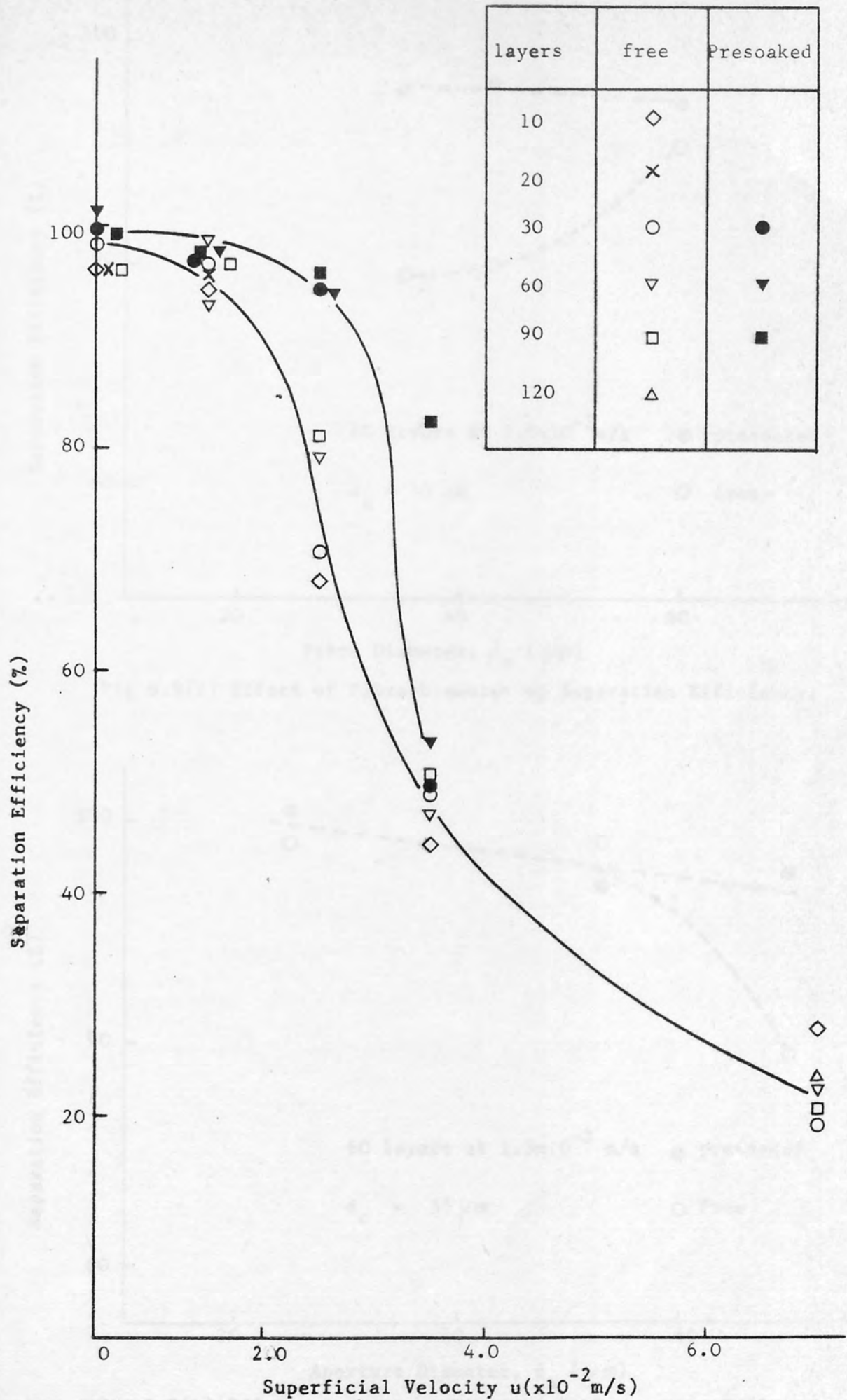


Fig 8.8 Variation of Separation Efficiency with Velocity.

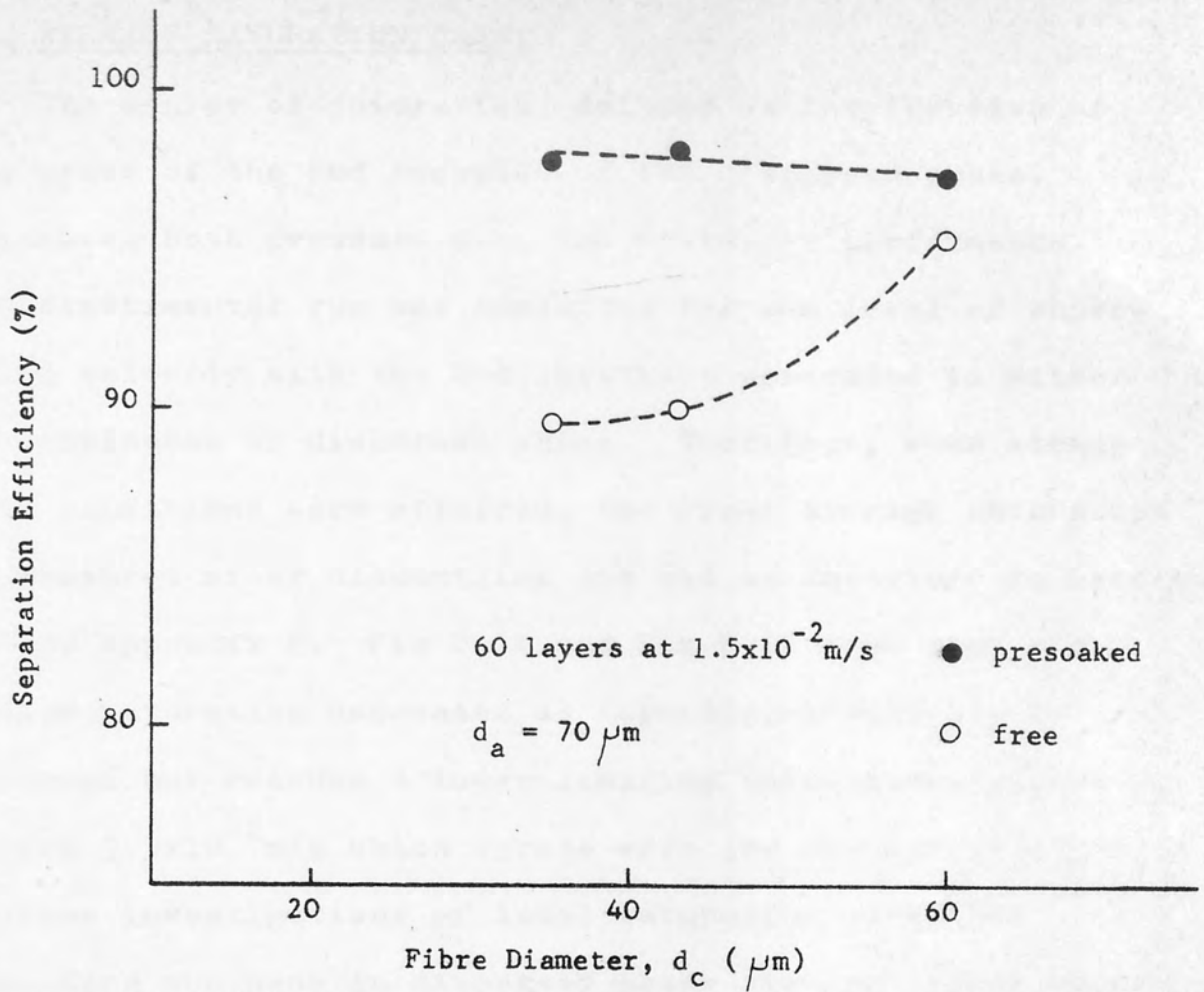


Fig 8.9(a) Effect of Fibre Diameter on Separation Efficiency.

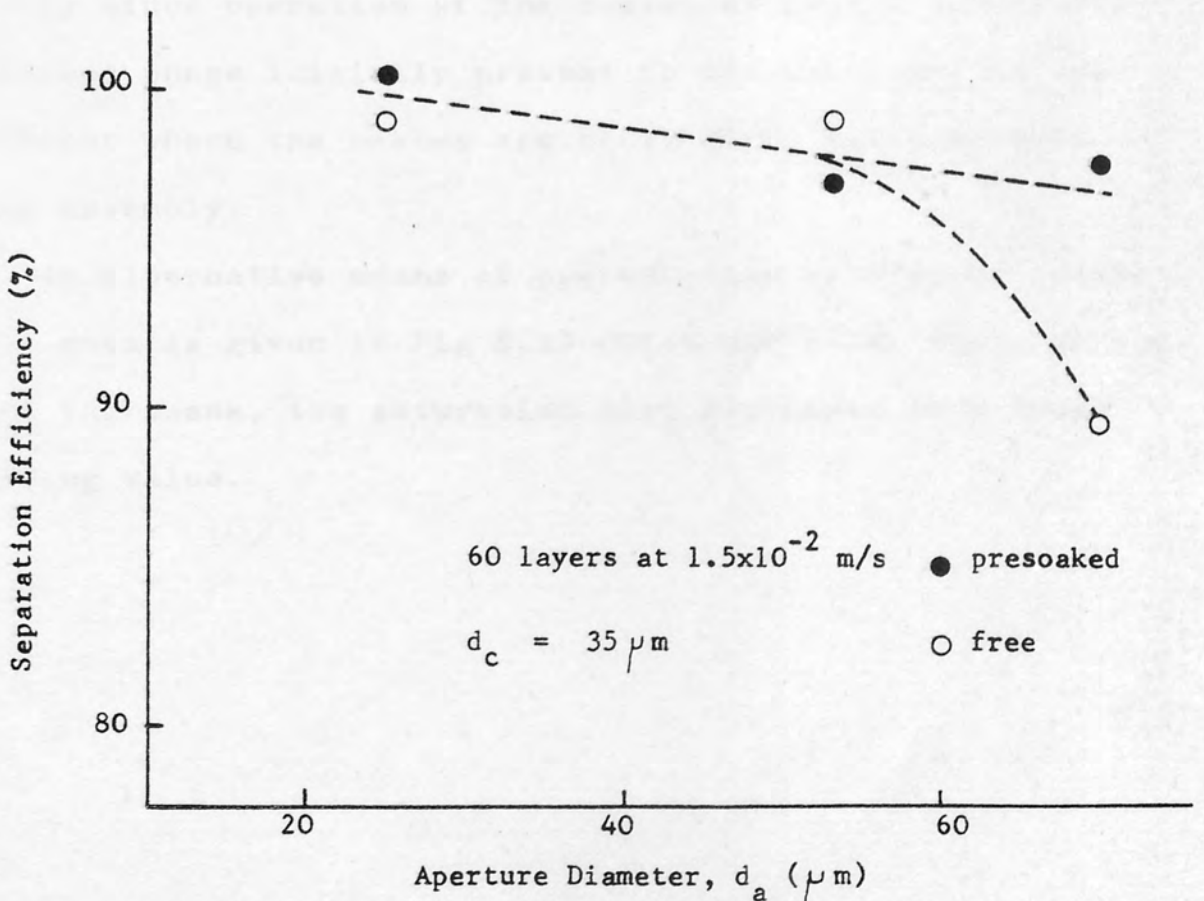


Fig 8.9(b) Effect of Aperture Diameter on Separation Efficiency.

#### 8.4. AVERAGE SATURATION DATA.

The degree of saturation, defined as the fraction of pore space of the bed occupied by the dispersed phase, influences both pressure drop and coalescer performance. Each experimental run was conducted for one level of superficial velocity with the bed initially presoaked in either the continuous or dispersed phase. Therefore, when steady state conditions were attained, the final average saturation was measured after dismantling the bed as described in Section 6.7 and Appendix F. Fig 8.10 and Fig 8.11 show that the average saturation decreases as superficial velocity is increased but reaches a lower limiting value above approximately  $3.5 \times 10^{-2}$  m/s which agrees with the results obtained in previous investigations of local saturation variation<sup>70,67,85</sup>

Presoaking the beds in dispersed phase yielded higher saturations but these measurements cannot be interpreted quantitatively since operation of the coalescer cannot remove the dispersed phase initially present in the periphery of the coalescer where the meshes are retained by the stainless steel assembly.

An alternative means of presentation of average saturation data is given in Fig 8.12 which indicates that, as bed depth increases, the saturation also decreases to a lower limiting value.



Fig 8.10. Variation of Saturation with Velocity for Beds presoaked in continuous phase.

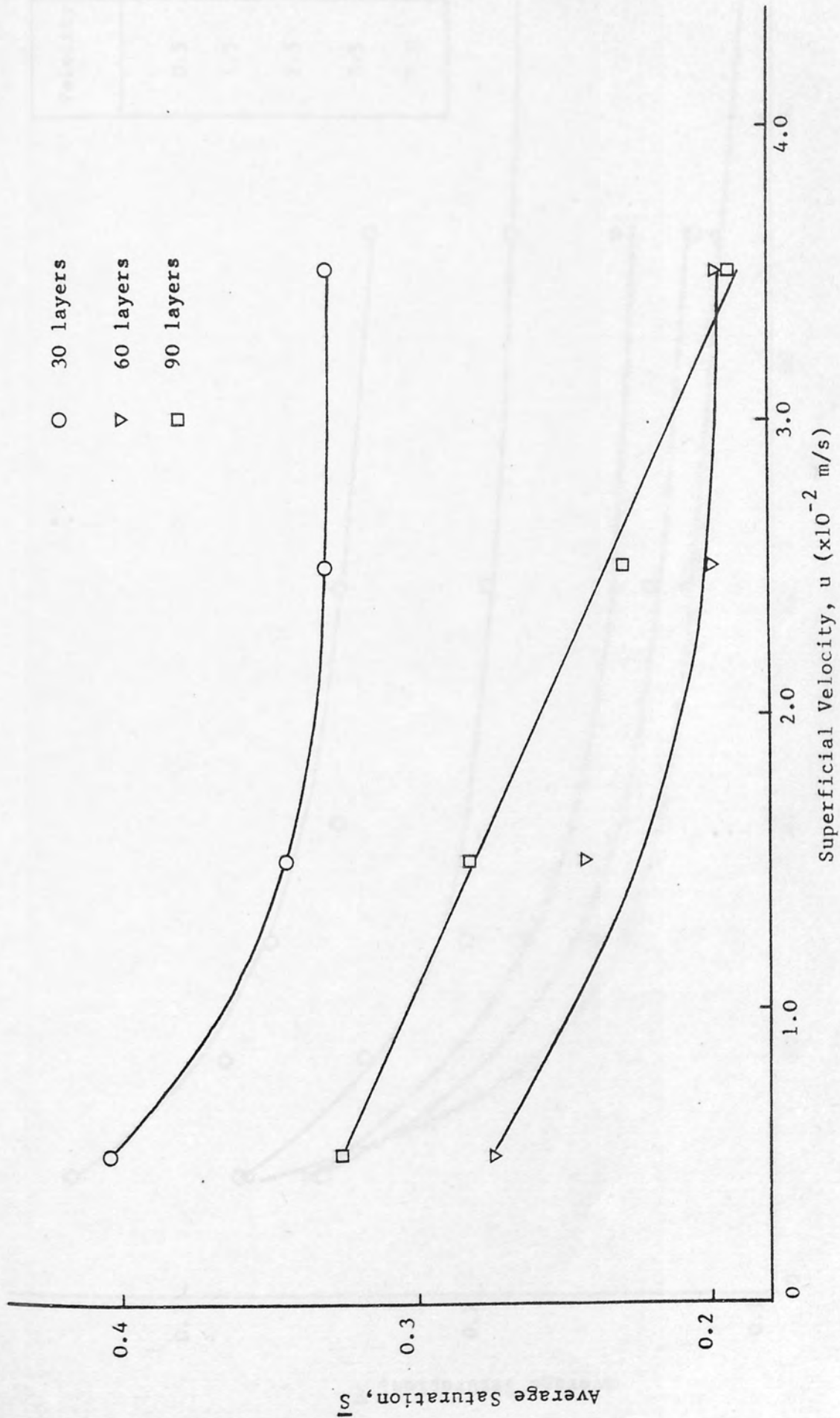


Fig 8.11. Variation of Saturation with Velocity for beds presoaked in dispersed phase.

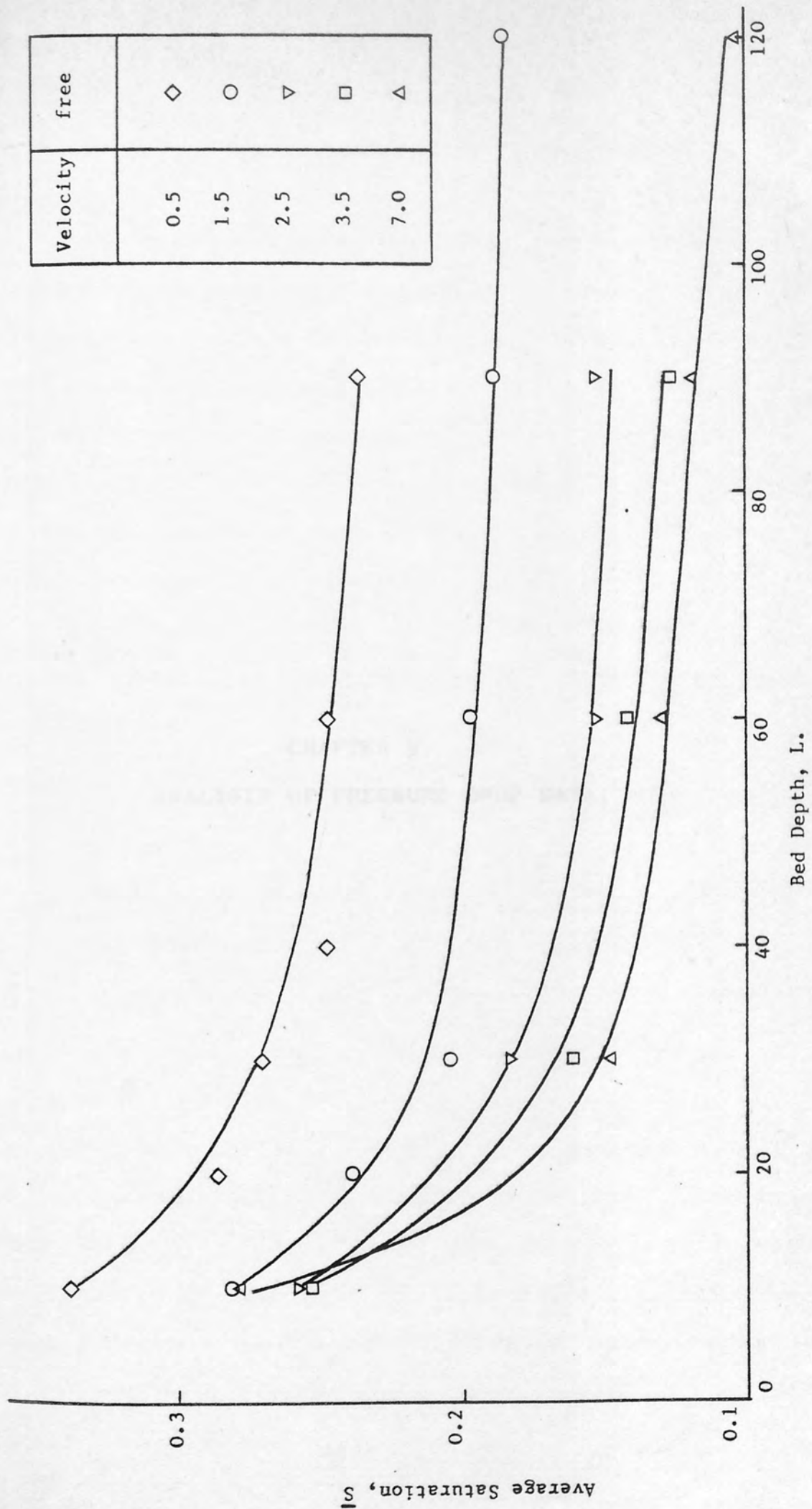


Fig 8.12. Variation of Saturation with Bed Depth for beds presoaked in continuous phase.



### 9.1 SINGLE PHASE FLOW PRESSURE DROP.

A study of the single phase pressure drop was made to determine the flow characteristics of the mesh media used for coalescence. Measurement of pressure drop during flow of the continuous phase alone serves to check the reproducibility of the packing technique and is used to detect ingress of air or particulate matter into the bed. Single phase pressure drop data also provides a basis for comparison with two phase flow during coalescence. Furthermore, flow characterisation may yield a more accurate description of the hydrodynamic function term, A which occurs in the drop capture efficiency equations presented in Chapter 5.

Of the many equations used to describe single phase flow in packed beds, the Ergun equation <sup>118</sup> is the most frequently applied,

$$\frac{\Delta P_1}{L} = \frac{150 \mu_c u (1-e_1)^2}{d_c^2 e_1^3} + \frac{1.75 \rho_c u^2 (1-e_1)}{d_c e_1^3} \quad 9.1$$

For low values of Reynolds number, i.e.

$$\text{when } N_{Re}'' = \frac{d_c \rho_c u}{\mu_c (1-e_1)} < 10,$$

the second term on the right hand side is negligible and equation 9.1 reduces to the Blake-Kozeny equation. Due to the low fibre diameters encountered in coalescers, the latter criterion is satisfied and therefore Sherony <sup>64</sup> and later, Shalhoub <sup>70</sup> applied this type of equation to fibrous bed coalescers. The value of the constant, 150 is equal to the product of the Kozeny constant, K and another constant which relates the characteristic particle diameter,  $d_c$  to the specific surface,  $a$ .

$$\text{For spheres, } d_c = \frac{6}{a} \quad \text{or} \quad d_c^2 = \frac{36}{a^2} \quad 9.2$$

The calculated value of the Kozeny constant, K is

$$\frac{150}{36} = 4.17, \text{ based on a packed bed of spheres. For cylinders}$$

$$d_c^2 = \frac{16}{a^2} \text{ and if fibre diameter is substituted into equation}$$

9.1, the value of the constant should be taken as 16K. Sherony<sup>64</sup> used this approach to calculate the Kozeny constant which varied between 7.45 and 9.65 for packings having void fractions between 0.924 and 0.946.

Sherony and Shalhoub used the Blake - Kozeny equation to determine the effective voidage of the packing during coalescence. This was done by substituting the experimental value of the two phase pressure drop into the following equation, which was then solved numerically to find the voidage.

$$\frac{\Delta P_2}{\Delta P_1} = \frac{e_1^3 (1-e_2)^2}{e_2^3 (1-e_1)^2} \quad 9.3$$

The dispersed phase saturation was then calculated by,

$$\bar{S} = 1 - \frac{e_2}{e_1} \quad 9.4$$

Unfortunately, the results can only be regarded as approximations since the method has a number of shortcomings. Firstly, although generally refuted by experimental evidence (see Section 5.5), it is assumed that saturation exhibits no spatial variation. Secondly, the Kozeny constant is assumed to be independant of voidage. However this is unlikely since the results of Sherony for high porosity packings are significantly different from the value of the Kozeny constant associated with the original Blake-Kozeny equation which is only valid for void fractions less than 0.5. The Kozeny constant, because it is a function of void fraction, will be different for two phase flow and therefore should be included in equation 9.2 expressed in terms of  $e_1$ .

9.2. FLUID FLOW EQUATIONS.

As discussed in Chapter 6, woven, monofilament meshes were selected as the packing media since their internal geometry is easier to define. Flow in single layers of media has received much attention but the different approaches fall into one of three basic categories. The flow in the screen is compared to,

- (a) An assembly of orifices
- (b) A random packed bed
- (c) An extension of the available analytical solutions for creeping flow over cylinders.

Armour and Cannon<sup>119</sup> combined (a) and (c) to describe turbulent and laminar flow regimes respectively, for flow of gases through screens of different weave types. The following equation was found by empirical fitting to the data,

$$f = 8.61 \frac{N''_{Re}^{-1}}{Re} + 0.52 \tag{9.5}$$

$$\text{where } f = \frac{\Delta P g_c e_1^2 d_a}{TB \rho_c u^2} ; \quad N''_{Re} = \frac{\rho_c u}{\mu_c a'^2 d_a}$$

The voidage,  $e_1$ , screen thickness,  $B$  and surface area per unit volume of screen,  $a'$  and pore diameter,  $d_a$  were all expressed in terms of the fibre diameter and mesh count. The tortuosity factor,  $T$  for each weave type was determined by regression analysis on the data. A similar approach was adopted by Ingmanson<sup>120</sup> to characterise flow of water through screens which produced the following equation,

$$f = 5.15 N''_{Re}^{-1} + 0.15 N''_{Re}^{-0.11} \tag{9.6}$$

$$\text{where } f = \frac{\Delta P g_c e_1^3}{Ba' \rho_c u^2} ; \quad N''_{Re} = \frac{\rho_c u}{\mu_c a'}$$

Rushton<sup>121</sup> tested the efficacy of several equations

to predict the resistance of various types of monofilament fabrics to water flow. He concluded that the analysis of Pedersen, which is based on the orifice assembly model, was successful especially for meshes of complex weave configuration. Pedersen, by geometrical analysis, characterised the orifices in terms of an effective fraction open area, and their perimeter  $W$  where the flow is most constricted. Rushton related his permeability data to this analysis using a discharge coefficient,

$$C = 0.17 N_{Re}''^{0.41} \quad 9.7$$

for  $1 < N_{Re}'' < 10$

$$\text{where } C = \left[ \frac{\rho_c u^2 (1 - \alpha^2)}{2 \Delta P g \alpha^2} \right]^{0.5}$$

$$N_{Re}'' = \frac{4 \rho_c u}{\mu_c W N_c^2}$$

$$\alpha = \frac{\phi \ln}{2} \left[ \frac{1 + (1 + \phi^2)^{0.5}}{\phi} \right] + \left[ \frac{(1 + \phi^2)^{0.5} - 1}{2 \phi} \right] - \frac{1}{4 \phi^2}$$

$$\left[ (2\phi - 1)^2 + 1 \right]^{0.5}$$

$$W = 2d_c \left[ (2\phi - 1)^2 + 1 \right]^{0.5} \mathcal{E} \left[ \left\{ 1 + \frac{1}{(2\phi - 1)^2} \right\}^{0.5}, \frac{\pi}{2} \right]$$

$$+ \frac{2}{N_c} \left[ 1 + \frac{1}{2\phi^2} \right]^{0.5}$$

where the elliptical integral,  $\mathcal{E}[k, \phi] = \int_0^\phi (1 - k^2 \sin^2 \theta)^{0.5} d\theta$

$$\text{and } \phi = (2d_c N_c)^{-1}$$

Drag theory was employed by Hutson in which the woven material is modelled by two perpendicular rows of equal parallel cylinders and an approximate solution of the

Navier-Stokes equation to give the following expression,

$$\frac{\Delta P}{B} = \frac{\mu_c r f(r) u}{d_c^2 (1-r)} \quad 9.8$$

where  $r = \frac{d_c}{d_c + da}$

$$f(r) = 8\pi \left[ 3.31571 - 2\ln 10r + 1.6449r^2 - 0.67644r^4 \right]^{-1}$$

for  $r < 0.6$

For plain square weave meshes, Rushton showed that the equation of Davies, which is based on the random packed bed analogy, satisfactorily predicted their permeability.

$$\frac{\Delta P}{L} = \frac{64 \mu_c (1-e_1)^{1.5}}{d_c^2} \left[ 1 + 56(1-e_1)^3 \right] u \quad 9.9$$

Equation 9.9 was developed empirically to account for the variation of the Kozeny constant in beds of porosities greater than 0.7.

Studies of pressure drops in fibrous aerosol filters have also attempted to express a dimensionless drag force,  $F^*$  in terms of the bed porosity. Kirsch and Fuchs<sup>122</sup> defined the dimensionless drag as,

$$F^* = \frac{\Delta P_1 \pi d_c^2}{4 u_I \mu_c (1-e_1)L} \quad 9.10$$

They reviewed the available correlations for  $F^*$ , which were developed by considering different arrangements of cylinders that constitute the fibrous filter. These correlations may be written in the following form,

$$F^* = \frac{4\pi}{A}$$

where A is the hydrodynamic function characterising the flow. Expressions for the hydrodynamic functions, including that derived by Spielman and Goren<sup>123</sup> are given in Table 9.1.

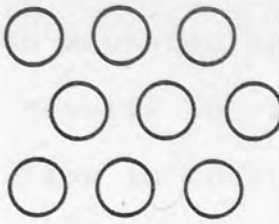
Investigator	Hydrodynamic Function, A.	Cylinder Configuration
Lamb 123	$2 - \ln N_{Re}$	Isolated Cylinder 
Happel 122	$-0.5 - 0.5 \ln(1-e_1) + \frac{(1-e_1)^2}{1 + (1-e_1)^2}$	Regular staggered rows 
Kuwabara 123	$-0.75 - 0.5 \ln(1-e_1) + (1-e_1) - 0.25(1-e_1)^2$	
Hasimoto 122	$-1.3105 - \ln \frac{r}{2} + \pi \left(\frac{r}{2}\right)^2$ where $r = \frac{d_c}{d_c + d_a}$	Regular square arrangement 
Tamada 122	$-1.33 - \ln \frac{r}{2} + \frac{\pi^2}{3} \left(\frac{r}{2}\right)^2$	Isolated row of parallel cylinders 
Keller 122	$\frac{8\sqrt{2}}{9} (1-r)^{2.5}$	Dense row of parallel cylinders 
Spielman 123	$\frac{K_o(Z)}{A K_1(Z)}$ where $(1-e_1) = \frac{Z^2}{8} \left[ \frac{K_1(Z)}{K_o(Z)} \right]$	Random orientation of cylinders with axes perpendicular to flow direction.

Table 9.1. Expressions for Hydrodynamic Function.

9.3. ANALYSIS OF SINGLE PHASE PRESSURE DROP DATA.

The Ergun equation was initially used to correlate the experimental results in view of its previous application to single phase flow in coalescers. The maximum value of the Reynolds number,  $N_{Re}$ , defined in Section 9.1, was calculated to be 7.1 for the range of variables investigated. The term involving  $u^2$  may therefore be neglected so that equation 9.1 reduces to the Blake-Kozeny form. An analysis of variance performed for quadratic regression on pressure-drop data for stainless steel meshes showed that the lack of fit and random errors were more significant than the second order term. This evidence, together with the high correlation coefficients obtained for linear regression analysis on the data, further justify sole consideration of a first order dependence on velocity.

. . From equation 9.1

$$\frac{\Delta P_1}{L} = \frac{16K \mu_c u (1-e_1)^2}{d_c^2 e_1^3} \tag{9.11}$$

Rearrangement of equation 9.11 gives,

$$\left[ \frac{\Delta P_1}{\mu_c} \right] \left[ \frac{e_1^3 d_c^2}{(1-e_1)^2 16N_L BT} \right] = K u \tag{9.12}$$

The first term,  $\left[ \frac{\Delta P_1}{\mu_c} \right]$  describing the pressure drop, contains the only property pertaining to the continuous phase, and therefore is independent of temperature fluctuations, which often occurred during acquisition of data. The viscosity of water was determined as a function of temperature using the correlation given in Appendix E.

The second term embodies all the properties of the packing which were evaluated using the equations of Armour and Cannon.

For a plain square weave mesh,

$$\text{Void fraction, } e_1 = 1 - \frac{\pi}{4} N_c d_c (N_c^2 d_c^2 + 1)^{0.5}$$

$$\text{Screen thickness, } B = 2 d_c$$

Then bed length,  $L = N_L B$  where  $N_L$  is the number of layers of mesh.

For single layers of plain square meshes, Armour and Cannon found that the Tortuosity factor,  $T = 1.0$ . However in this study, the beds were assembled by successively adding single layers of mesh so that coincidence of the apertures or fibre orientations would occur only by chance. Consequently, the fluid is likely to flow in a more tortuous path when the apertures of adjacent layers are not aligned. In Appendix I, an algorithm for the tortuosity factor is derived in terms of the relative positions of the aperture centres between two layers and the diameter ratio,  $\frac{d_c}{d_a}$ .

The co-ordinates of these mid points were determined using a random number generator and the tortuosity factor calculated within a computer program given in Appendix J. In this program, single phase pressure drop data was correlated against superficial velocity by linear regression analysis using equation 9.12. The results are presented in Table 9.2 for the different mesh types and the correlation obtained for stainless steel meshes illustrated in Fig 9.1 where the slope of the best fit line is equal to the Kozeny constant.

#### 9.4. COMPARISON OF SINGLE PHASE FLOW MODELS.

The equations presented in Section 9.2, with the exception of the Pedersen analysis, were rearranged into the form of equation 9.12 to enable comparison of the Kozeny constants. Expressions for  $K$  are given in Table 9.3. Although the

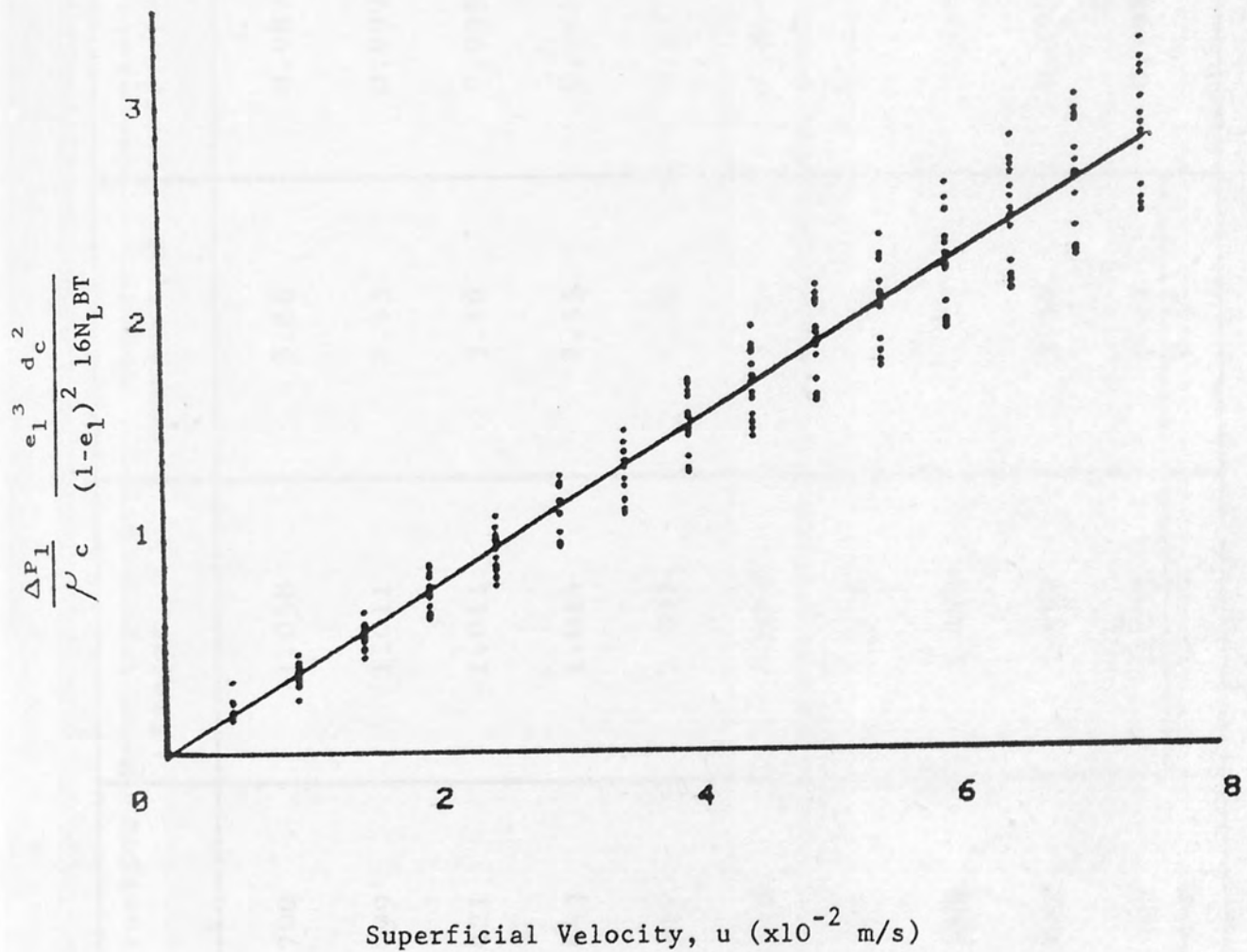


Fig 9.1. Correlation of Single Phase Pressure Drop Data for Stainless Steel Mesh, S300.

Mesh	Fibre diameter, $d_c$ ( $\mu\text{m}$ )	Void fraction, $e_1$	Mean tortuosity factor, T	Kozeny constant, K	Correlation coefficient, r	No. of data points
S300	30.5	0.700	1.058	3.86	0.983	345
N20/16	30.0	0.399	1.011	2.43	0.999	8
N25/18	35.0	0.421	1.011	3.16	0.999	15
N25/21	30.0	0.443	1.014	2.55	0.986	32
N50/35	35.0	0.540	1.041	2.32	0.977	32
N53/36	35.0	0.572	1.043	3.41	0.991	60
N69/38	43.0	0.521	1.050	2.31	0.999	15
N70/29	60.0	0.594	1.028	3.22	0.998	15
N70/45	35.0	0.612	1.077	3.54	0.999	15
PE/53/33	40.0	0.522	1.035	2.21	0.998	32
		Mean	1.037	2.90		

Table 9.2. Single Phase Pressure Drop Correlations.

Pedersen equation predicted pressure drops with less than 5% error for the stainless steel mesh data, it is difficult to present in terms of the Kozeny constant due to its complexity.

Source.	Kozeny Constant, K.
Blake/Kozeny.	4.17
Armour/Cannon.	$8.61e_1$
Ingmanson/Myers.	$\frac{5.15}{T}$
Davies	$\frac{4}{T} e_1^3 (1-e_1)^{-0.5} [1 + 56(1-e_1)^3]$
Hutson	$\frac{1}{16T} \frac{e_1^3}{(1-e_1)^2} \left[ \frac{r f(r)}{(1-r)} \right]$
Aerosol Filtration theory	$\frac{e_1^2}{T(1 - e_1) A}$

where the different expressions for A are given in Table 9.1.

Table 9.3. Expressions for the Kozeny Constant.

Using a mean tortuosity factor derived from experimental data (Table 9.2), the expressions listed in Table 9.3 were evaluated as functions of voidage and plotted in Fig 9.2. As expected, the models of Kuwabara and Happel predict very high values of the Kozeny constant since they were developed for high porosity beds (i.e.  $e_1 > 0.7$ ). In contrast the equations of Hasimoto and Tamada predict lower values but the variation does not exhibit a minimum point. The curve generated by Keller's expression shows excellent agreement with the experimental data points which is not surprising since the internal geometry of the meshes is entirely compatible with the physical model used to formulate the equation. The experimental values for the polymeric meshes were obtained using measured values of fibre diameter, bed depth and void fraction as dimensional changes occurred due to fibre expansion

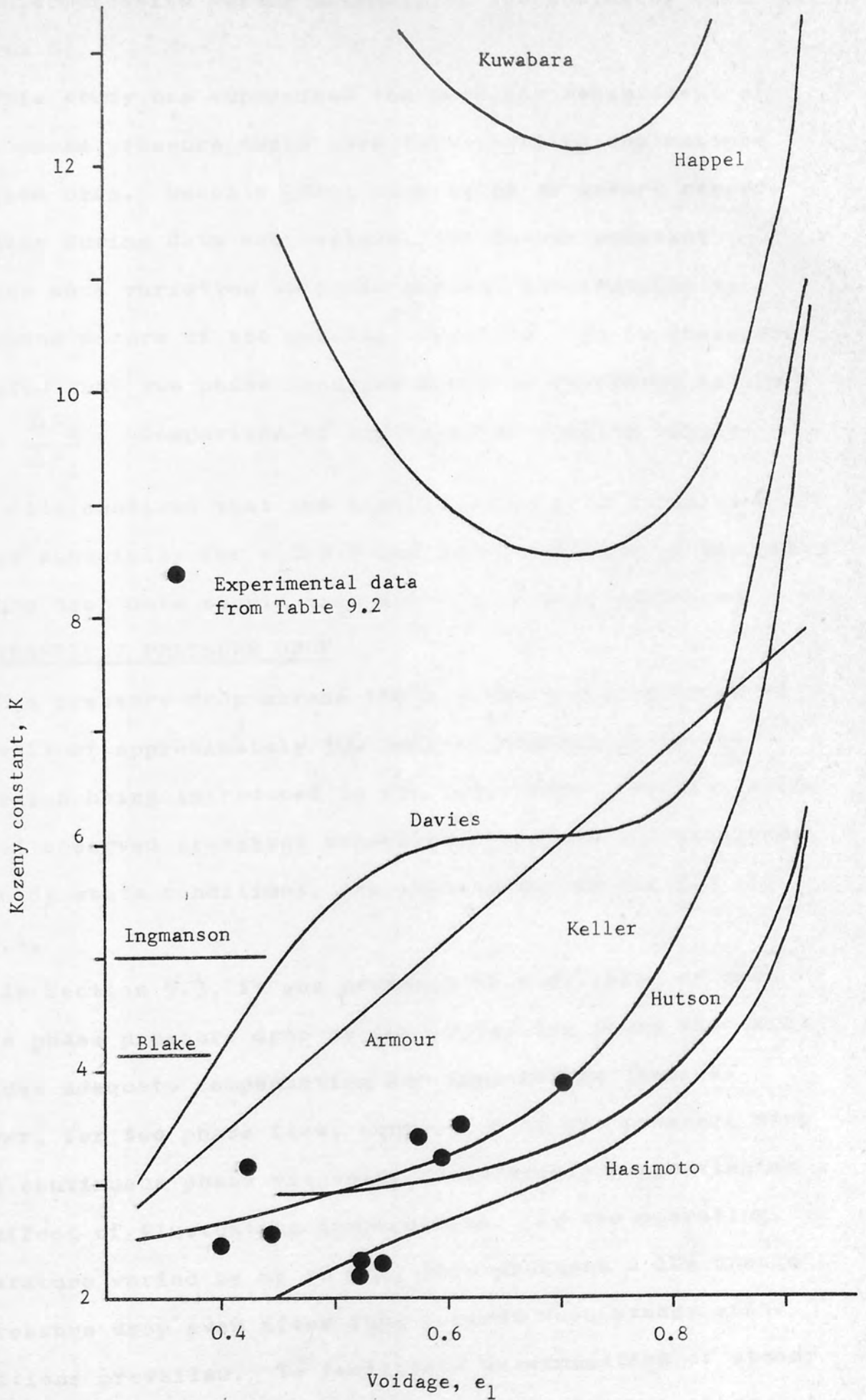


Fig.9.2. Variation of Kozeny constant with Voidage.

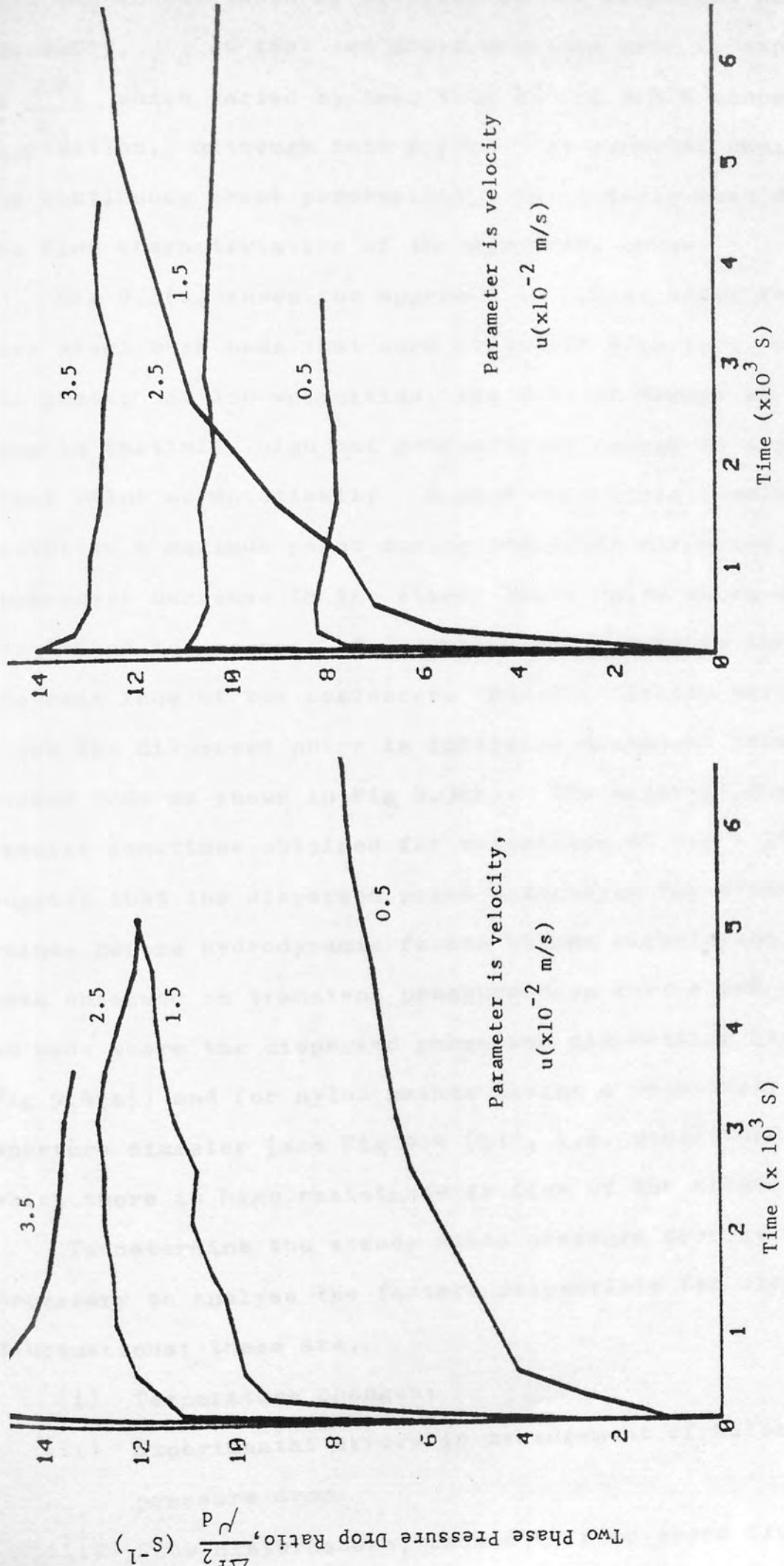
and bed compression during assembly of the coalescer (see Appendix D).

This study has emphasised the need for measurement of single phase pressure drops when investigating coalescence in packed beds. Despite great care taken to ensure reproducibility during data acquisition, the Kozeny constant exhibits some variation which is perhaps attributable to the random nature of the packing technique. It is therefore suggested that two phase pressure drops be expressed as the ratio,  $\frac{\Delta P_2}{\Delta P_1}$ . Comparison of equations describing single phase flow confirms that the Kozeny constant is a function of voidage especially for  $e_1 > 0.7$  and interpretation of two phase pressure drop data should take account of this variation.

#### 9.5. TRANSIENT PRESSURE DROP.

The pressure drop across the coalescer was recorded at intervals of approximately 500 seconds subsequent to the dispersion being introduced to the inlet face. Typical examples of observed transient behaviour, prior to the attainment of steady state conditions, are illustrated in Fig 9.3 and Fig 9.4.

In Section 9.3, it was proposed that division of the single phase pressure drop by the prevailing fluid viscosity provides adequate compensation for temperature changes. However, for two phase flow, correction of the pressure drop using continuous phase viscosity considerably overestimates the effect of fluctuating temperatures. As the operating temperature varied by up to 8 K, this produced a 10% change in pressure drop even after long periods when steady state conditions prevailed. To facilitate determination of steady state pressure drop and to compare the result with other data, it was essential to negate this temperature effect.



(a) Dispersed phase free initial condition. (b) Dispersed phase presoaked initial condition.

Fig 9.3. Two Phase Pressure Drop for 90 layers of S300 mesh - Transient Behaviour.

This was accomplished by dividing by the dispersed phase viscosity,  $\mu_d$  so that two phase pressure drop is expressed as  $\frac{\Delta P_2}{\mu_d}$  which varied by less than 1% for an 8 K temperature fluctuation. Although this approach is somewhat empirical, the continuous phase permeability, intuitively must depend on the flow characteristics of the dispersed phase.

Fig 9.3(a) shows the approach to steady state for stainless steel mesh beds that were initially free from the dispersed phase. At low velocities, the rate of change of pressure drop is initially high but gradually decreases to approach the final value asymptotically. Higher velocities sometimes exhibited a maximum point during transient operation with a subsequent decrease to the steady state value which may be attributed to progress of dispersed phase through and from the exit face of the coalescer. Similar effects were observed when the dispersed phase is initially displaced from pre-soaked beds as shown in Fig 9.3(b). The apparently anomalous results sometimes obtained for velocities of  $0.5 \times 10^{-2}$  m/s suggest that the dispersed phase saturation may attain high values before hydrodynamic forces become significant. The peak observed on transient pressure drop curves was accentuated in beds where the dispersed phase was non-wetting (see Fig 9.4(a)) and for nylon meshes having a relatively small aperture diameter (see Fig 9.4 (b)), i.e. conditions under which there is high resistance to flow of the dispersed phase.

To determine the steady state pressure drop it was necessary to analyse the factors responsible for short term fluctuations; these are,

- (i) Temperature changes.
- (ii) Experimental errors in measurement of velocity and pressure drop.
- (iii) Flow disturbances, caused by pump speed fluctuation:

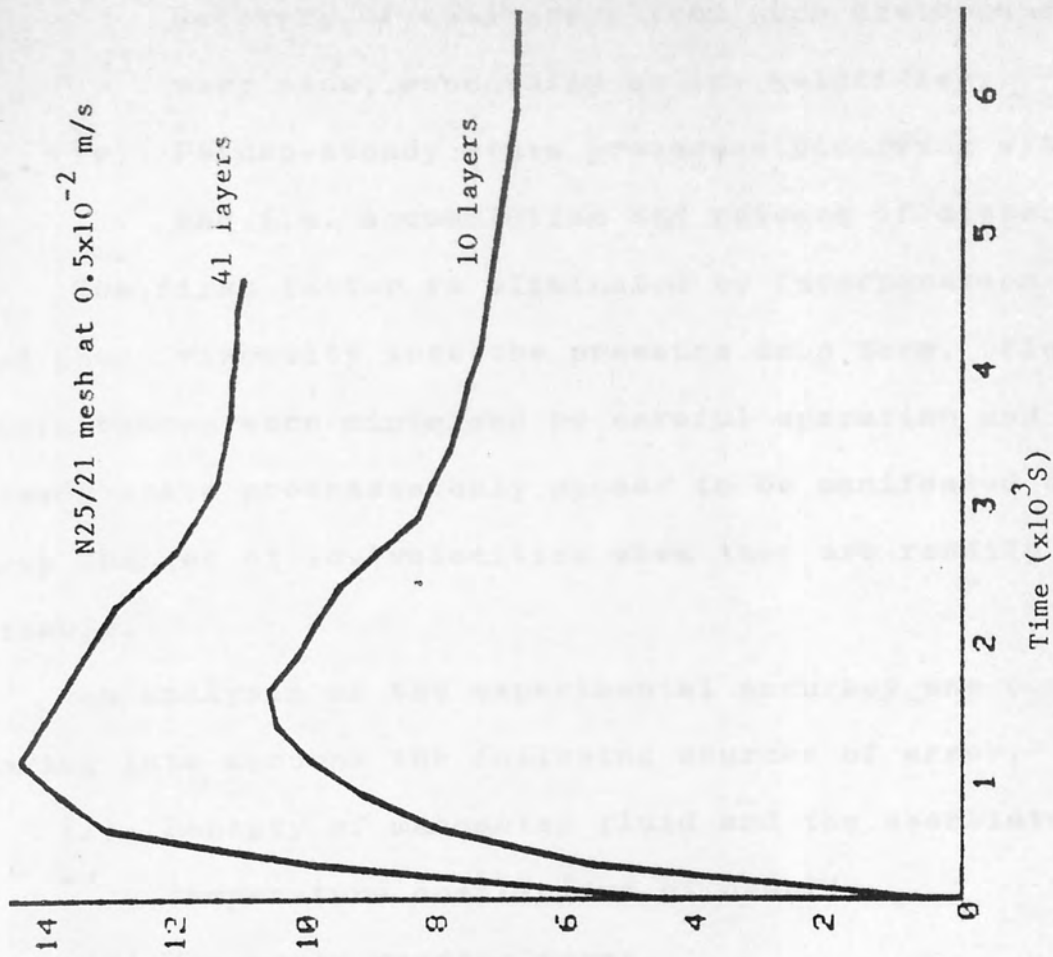


Fig 9.4.(b) Effect of Bed Depth on Two Phase Pressure Drop showing the transient peak.

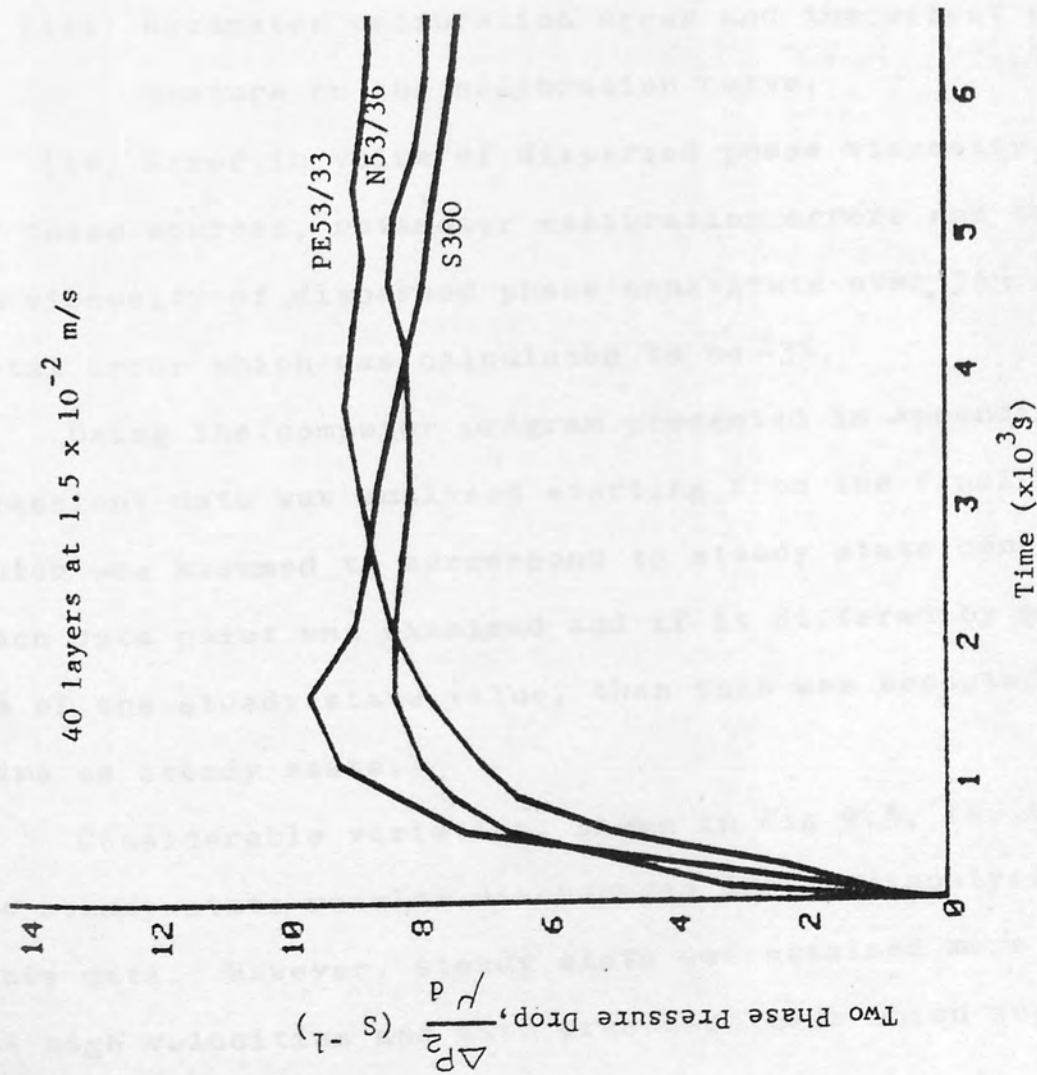


Fig 9.4.(a) Effect of Mesh Material on Two Phase Pressure Drop.

Recovery of coalescers from such disturbances is very slow, especially at low velocities.

- (iv) Pseudo-steady state processes occurring within the bed i.e. accumulation and release of dispersed phase.

The first factor is eliminated by incorporation of dispersed phase viscosity into the pressure drop term. Flow disturbances were minimised by careful operation and pseudo-steady state processes only appear to be manifested as pressure drop changes at low velocities when they are readily recognisable.

An analysis of the experimental accuracy was completed taking into account the following sources of error,

- (i) Density of manometer fluid and the associated temperature coefficient of density.
- (ii) Manometer reading error.
- (iii) Rotameter calibration error and the effect of temperature on the calibration curve.
- (iv) Error in value of dispersed phase viscosity.

Of these sources, rotameter calibration errors and the error in viscosity of dispersed phase constitute over 75% of the total error which was calculated to be  $\pm 3\%$ .

Using the computer program presented in Appendix K, the transient data was analysed starting from the final value, which was assumed to correspond to steady state conditions. Each data point was examined and if it differed by more than 3% of the steady state value, then this was accepted as the time to steady state.

Considerable variation, shown in Fig 9.5, for the time to steady state results discouraged detailed analysis of this data. However, steady state was attained more rapidly at high velocities and with presoaked beds which suggests that presoaking is a desirable preliminary operation.

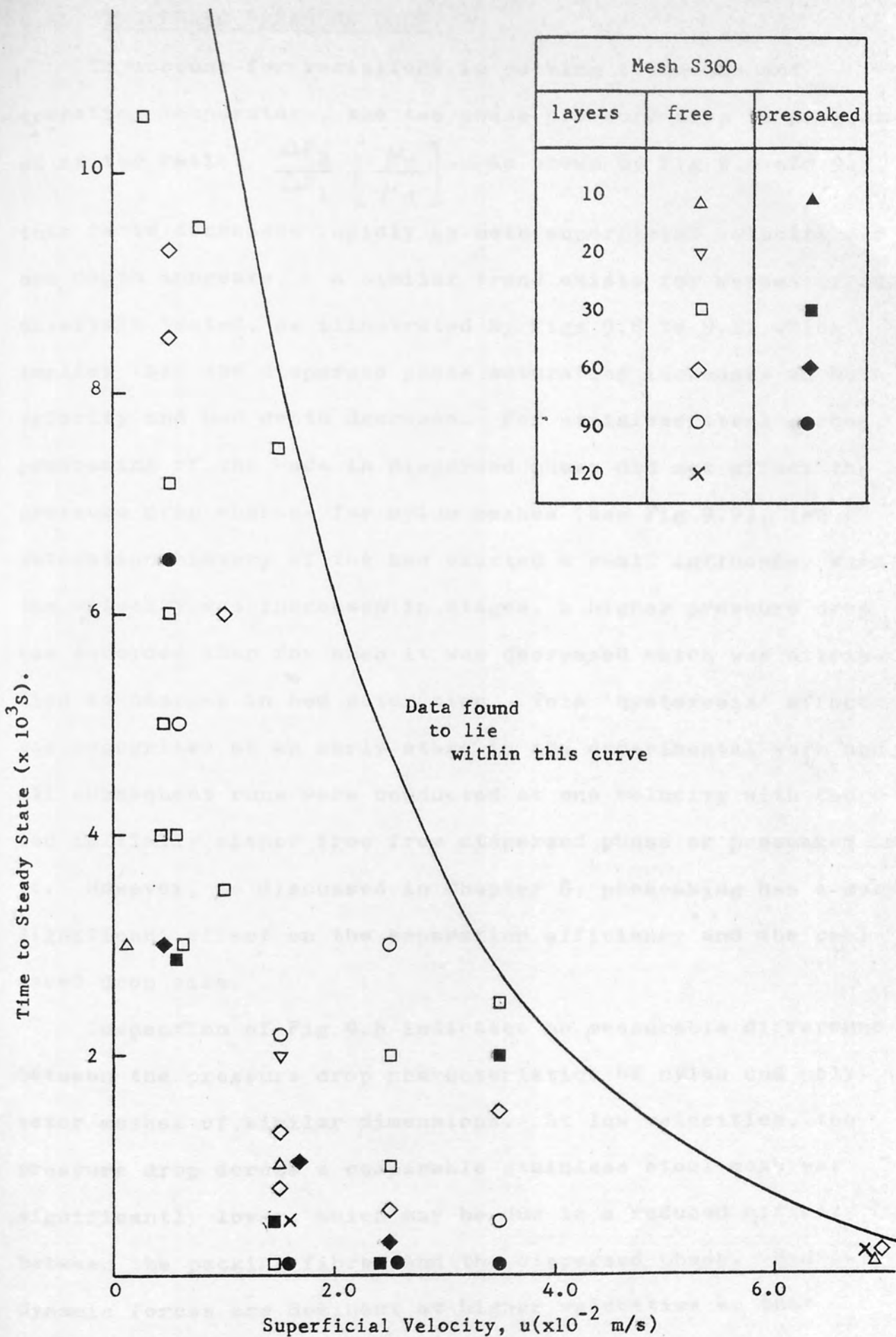


Fig 9.5. Length of Transient Periods for Stainless Steel Mesh Coalescers.

9.6. TWO PHASE PRESSURE DROP.

To account for variations in packing technique and operating temperature, the two phase pressure drop is presented as the ratio,  $\frac{\Delta P_2}{\Delta P_1} \left[ \frac{\mu_c}{\mu_d} \right]$ . As shown by Fig 9.6 and 9.7, this ratio decreases rapidly as both superficial velocity and bed depth increase. A similar trend exists for meshes of all materials tested, as illustrated by Figs 9.8 to 9.11 which implies that the dispersed phase saturation increases as both velocity and bed depth decrease. For stainless steel meshes, presoaking of the beds in dispersed phase did not affect the pressure drop whereas for nylon meshes (see Fig 9.9), the saturation history of the bed exerted a small influence. When the velocity was increased in stages, a higher pressure drop was recorded than for when it was decreased which was attributed to changes in bed saturation. This 'hysteresis' effect was recognised at an early stage in the experimental work and all subsequent runs were conducted at one velocity with the bed initially either free from dispersed phase or presoaked in it. However, as discussed in Chapter 8, presoaking has a more significant effect on the separation efficiency and the coalesced drop size.

Inspection of Fig 9.8 indicates no measurable difference between the pressure drop characteristics of nylon and polyester meshes of similar dimensions. At low velocities, the pressure drop across a comparable stainless steel mesh was significantly lower, which may be due to a reduced affinity between the packing fibres and the dispersed phase. Hydrodynamic forces are dominant at higher velocities so that wetting effects are less important.

Beds consisting of meshes of the full twill weave type exhibited similar trends (see Fig 9.10) but with reference

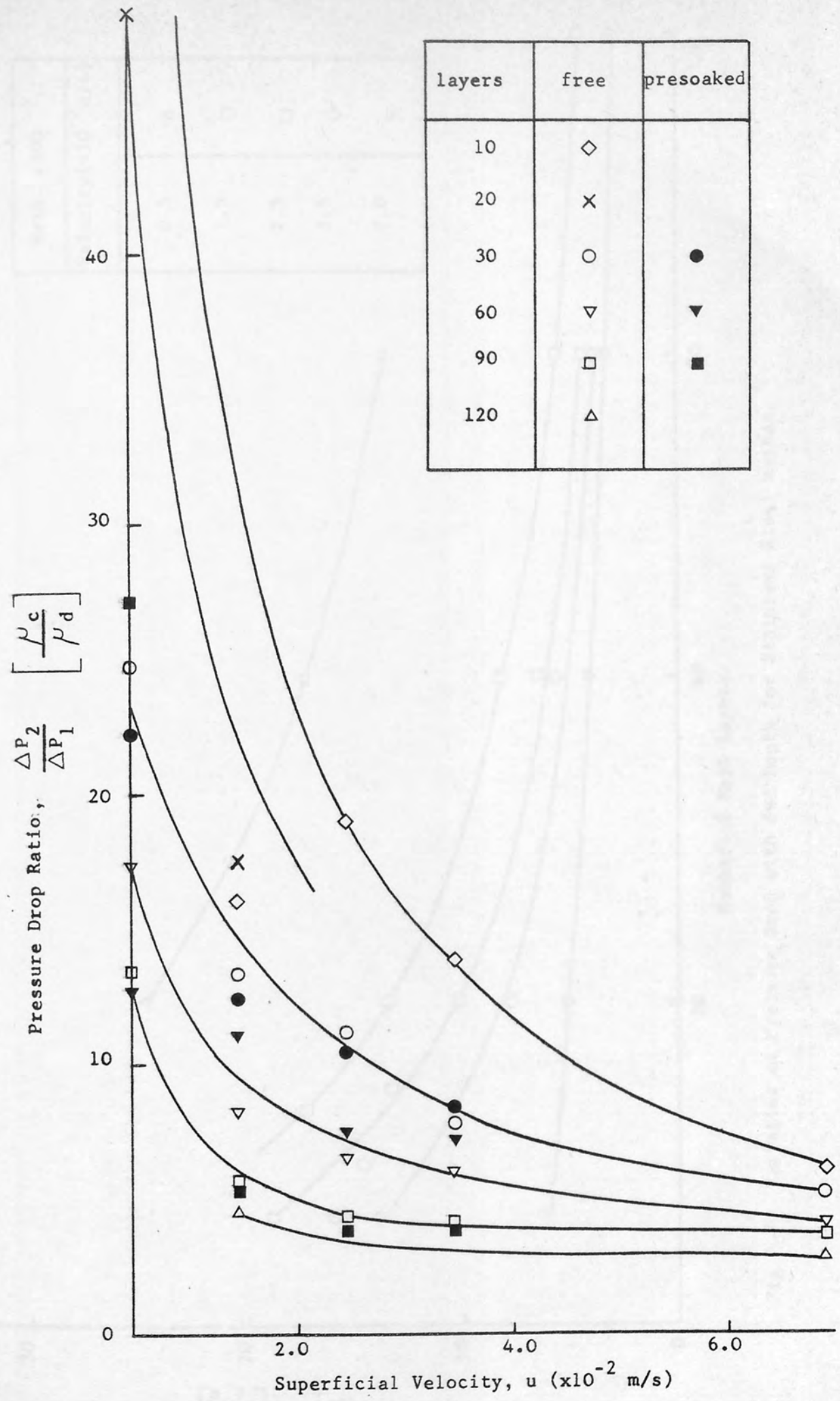


Fig 9.6. Variation of Pressure Drop with Velocity - Stainless Steel Mesh (S300).

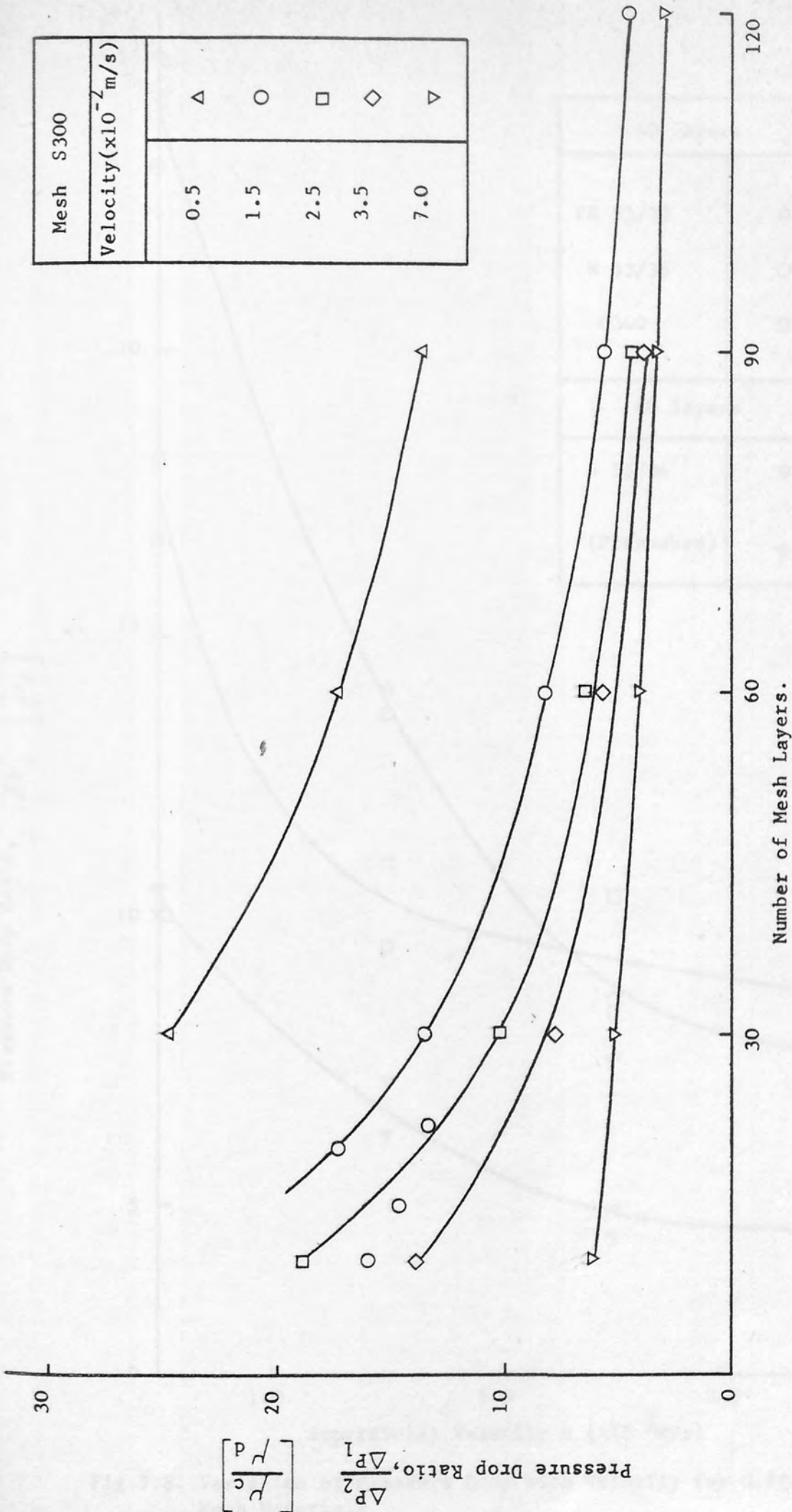


Fig 9.7. Variation of Pressure Drop with Bed Depth for Stainless Steel Meshes.

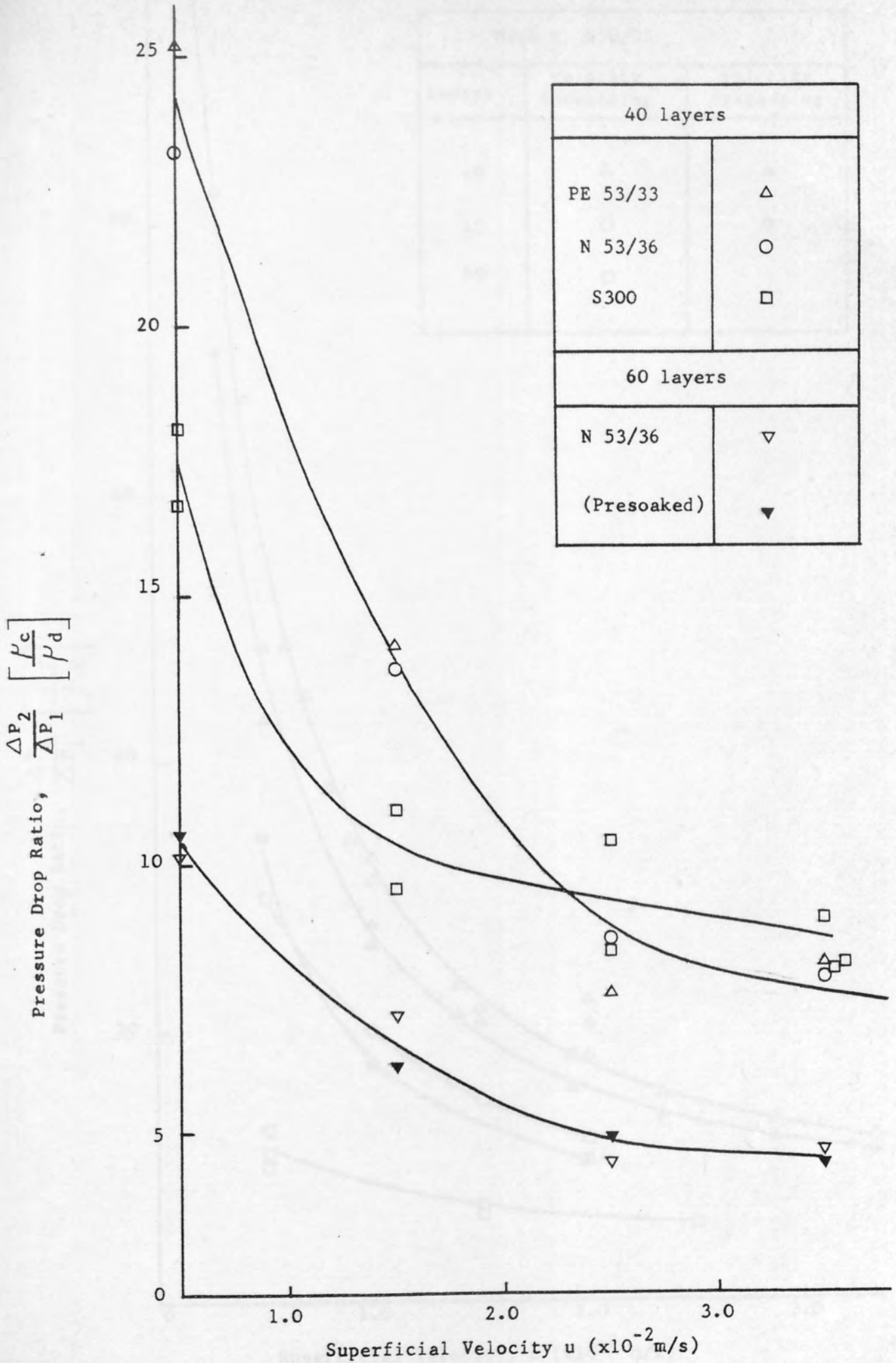


Fig 9.8. Variation of Pressure Drop with Velocity for different Mesh Materials.

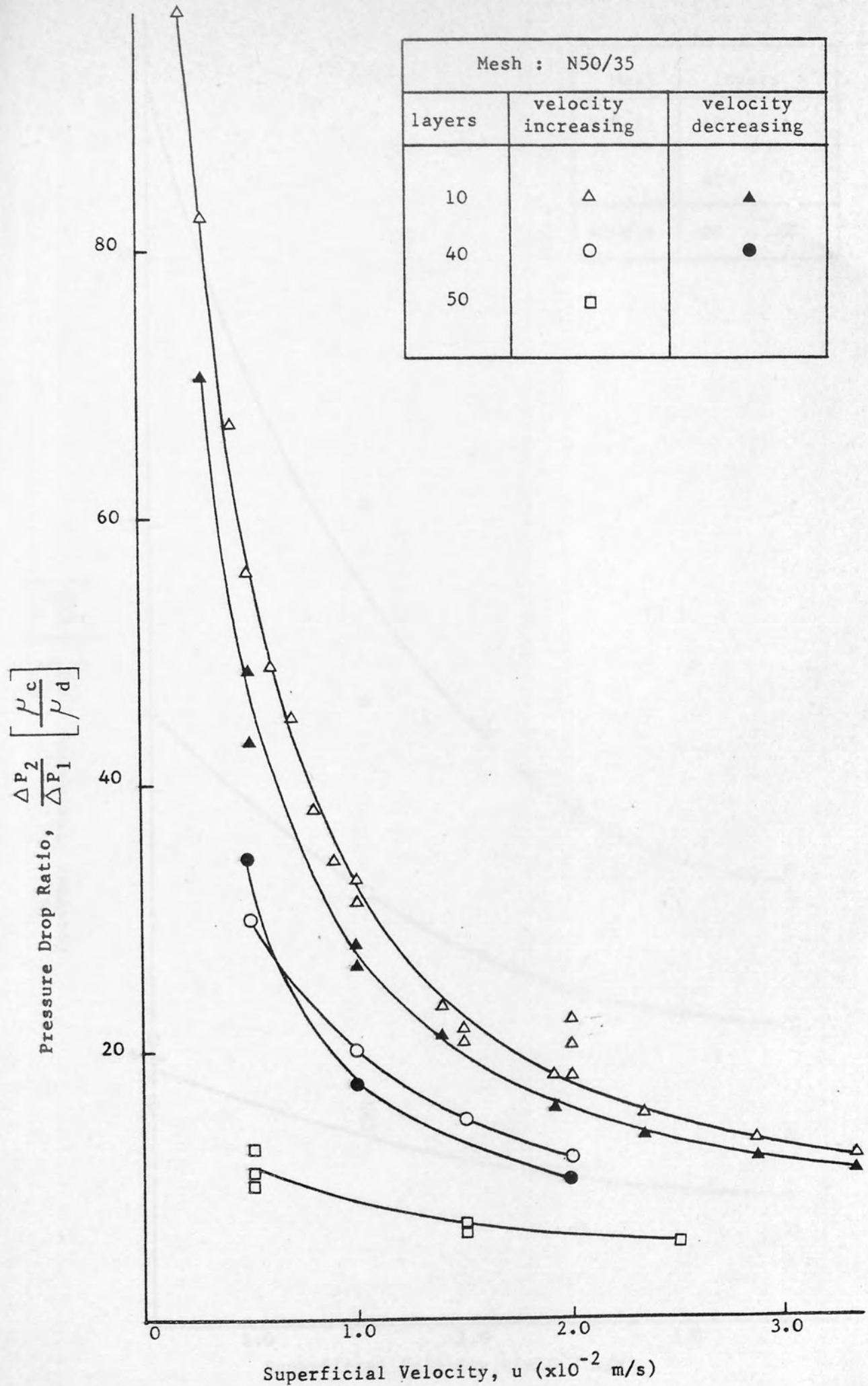


Fig 9.9. Variation of Pressure Drop with Velocity - Nylon Mesh.

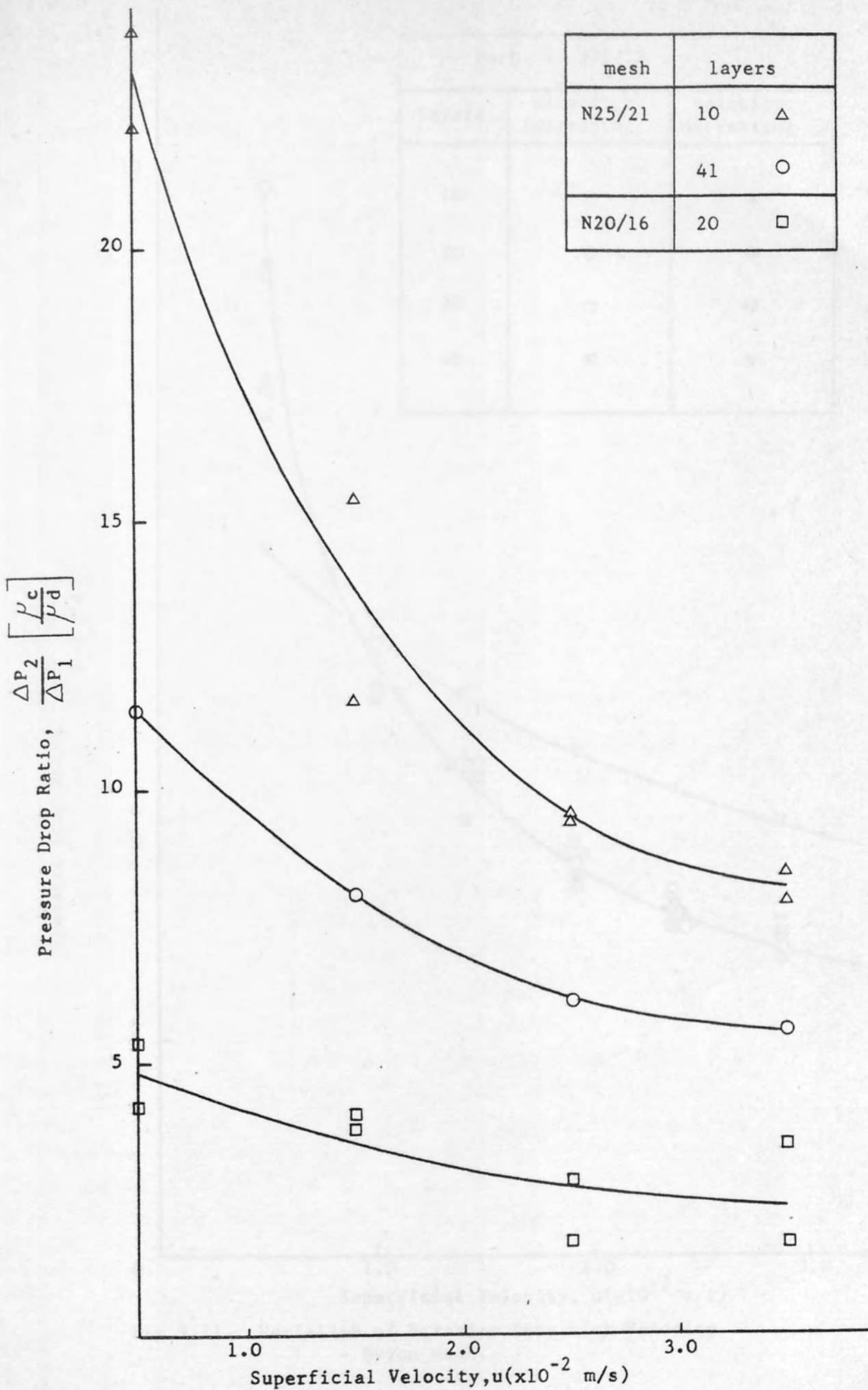


Fig.9.10 Variation of Pressure Drop with Velocity - Nylon Mesh.

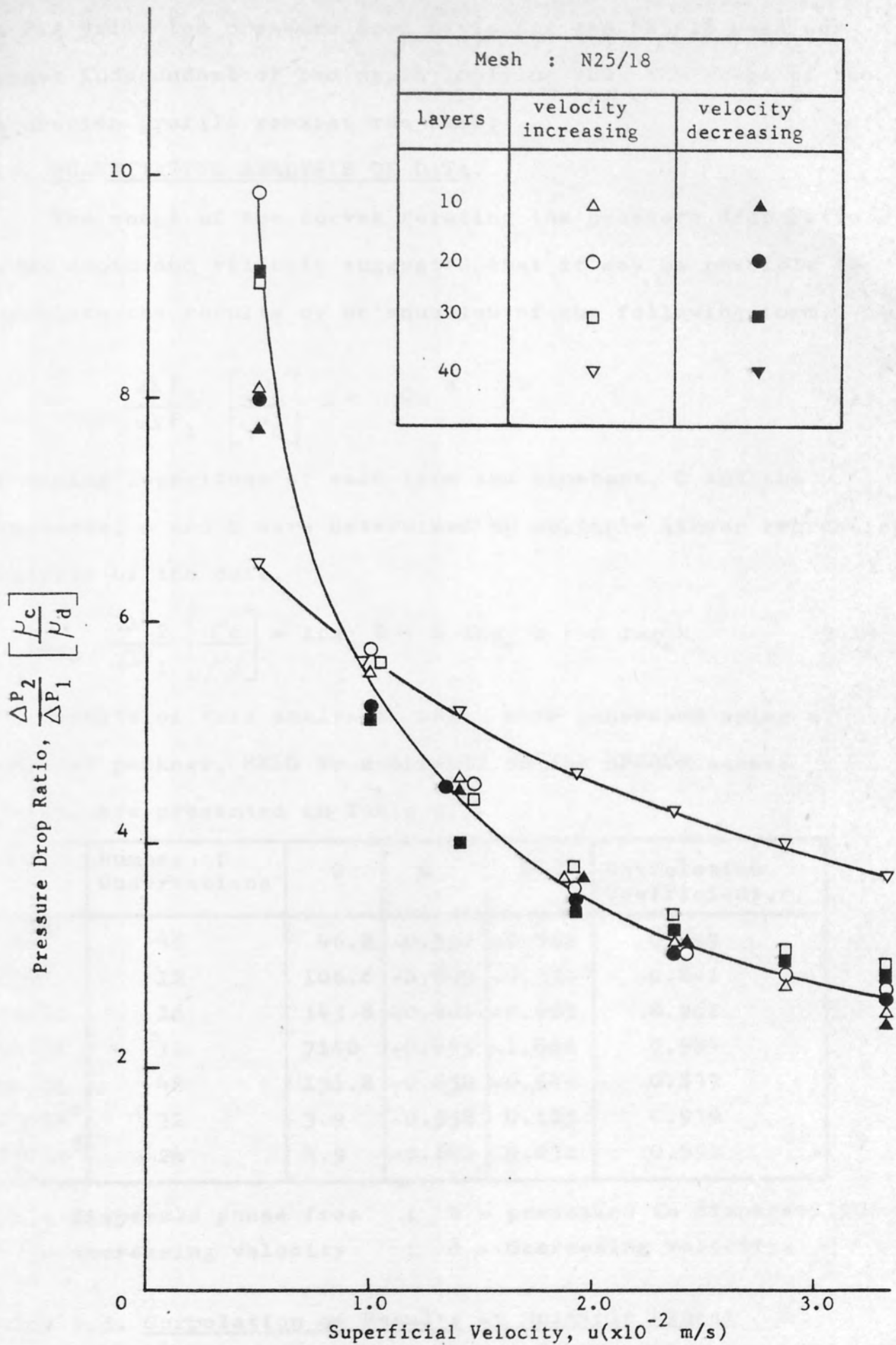


Fig 9.11. Variation of Pressure Drop with Velocity - Nylon Mesh.

to Fig 9.11, the pressure drop ratio for the N25/18 mesh was almost independent of bed depth implying that the shape of the saturation profile remains the same.

9.7. QUANTITATIVE ANALYSIS OF DATA.

The shape of the curves relating the pressure drop ratio to bed depth and velocity suggested that it may be possible to correlate the results by an equation of the following form,

$$\frac{\Delta P_2}{\Delta P_1} \left[ \frac{\mu_c}{\mu_d} \right] = C u^a L^b \tag{9.13}$$

By taking logarithms of each term the constant, C and the exponents, a and b were determined by multiple linear regression analysis of the data,

$$\log_e \frac{\Delta P_2}{\Delta P_1} \left[ \frac{\mu_c}{\mu_d} \right] = \log_e C + a \log_e u + b \log_e L \tag{9.14}$$

The results of this analysis, which were generated using a computer package, MREG 99 available on the HP2000 access system, are presented in Table 9.3.

Mesh	Number of Observations	C	a	b	Correlation Coefficient, r.
S300 <sup>a</sup>	46	46.8	-0.532	-0.362	0.899
S300 <sup>b</sup>	12	106.6	-0.609	-0.537	0.841
N25/21	16	143.8	-0.461	-0.965	0.962
N53/36	12	7140	-0.495	-1.666	0.984
N50/35	48	131.8	-0.652	-0.649	0.837
N25/18 <sup>c</sup>	32	3.9	-0.558	0.125	0.959
N25/18 <sup>d</sup>	24	4.9	-0.602	0.032	0.991

a - dispersed phase free ; b - presoaked in dispersed phase  
 c - increasing velocity ; d - decreasing velocity.

Table 9.3. Correlation of Results by Multiple Linear Regression.

It is quite clear from these results that correlation of the data for each mesh on an individual basis is the only

practicable approach since the value of the constant is extremely sensitive to the type of media used. Since a reasonable fit to the data was obtained, further investigation to ascertain the quantitative relationship between the constant, C and the type of mesh would be of value. The dependance on bed depth varied considerably which is likely to be a function of the saturation profiles prevailing within the bed, with a strong dependance indicating a considerable variation in local saturation.

A similar dependance of the pressure drop ratio on velocity was found for all meshes and this indicates that the two phase pressure drop is approximately proportional to  $\sqrt{u}$ .

Euzen<sup>124</sup> proposed that the two phase pressure drop was a function of the product of bed depth and velocity and found that the data could be represented by this equation,

$$\Delta P_2 = C(L u)^{0.86} \tag{9.15}$$

However, the value of the exponents determined in this study suggested that the two variables should be analysed separately.

The data of Shalhoub<sup>70</sup> indicated that the pressure drop ratio was independant of both bed depth and velocity for high porosity packings, which is consistent with the hypothesis of no spatial variation of saturation in the coalescer.

In the following chapter, a mathematical model, based on proposed forms of saturation profiles, is used to predict the two phase pressure drop, expressed as the ratio  $\frac{\Delta P_2}{\Delta P_1} \left[ \frac{\mu_c}{\mu_d} \right]$ ,

in terms of bed depth and velocity.

The filter coefficient is defined as the ratio of the number of particles removed to the number of particles entering the filter per unit area and unit time.

$$K = \frac{\log \left[ \frac{\text{Inlet concentration}}{\text{Outlet concentration}} \right]}{A \cdot t}$$

The number of particles removed per unit area and unit time is denoted by  $K$ . The filter coefficient  $K$  is defined as the ratio of the number of particles removed to the number of particles entering the filter per unit area and unit time. The filter coefficient  $K$  is defined as the ratio of the number of particles removed to the number of particles entering the filter per unit area and unit time.

### CHAPTER 10

### MODEL OF DISPERSION COALESCENCE.

For a bed consisting of 50 layers of 200 mesh each, the total thickness of the bed is 10 cm. The dispersion coefficient is  $1.5 \times 10^{-4}$  cm<sup>2</sup>/sec. The filter coefficient is  $K = 19.0 \text{ min}^{-1}$ .

#### 10.1.2. Equation of Motion

This model assumes that suspended drops are transported by the flow of liquid through the bed. The drops are assumed to be spherical and to coalesce into a larger drop when they collide. Under the action of hydrodynamic, gravitational and capillary forces, the dispersed liquid droplets are assumed to be spherical. The dispersed liquid droplets are assumed to be spherical. The dispersed liquid droplets are assumed to be spherical.

10.1 PREDICTION OF FILTER COEFFICIENT.

The filter coefficient provides a measure of the overall drop coalescence efficiency of a bed and is defined as,

$$\lambda = \frac{-\log_e \left[ \frac{\text{Outlet drop number density}}{\text{Inlet drop number density}} \right]}{L}$$

The majority of models for fibrous bed coalescers attempt to predict the filter coefficient and the equations developed are reviewed below. Also, to compare the values of  $\lambda$  obtained using these equations, the parameters presented in Table 10.1 provided a basis for this exercise.

10.1.1. Vinson and Churchill Equation.

This equation is not based on any theoretical model but was simply obtained by fitting experimental data for the system studied using photo-etched screens to simulate fibrous beds <sup>54</sup>,

$$\lambda = \frac{-\log_e \left[ 0.128 (u_i d_c \mu_c)^{-0.4} - 0.089 \right]}{L} \quad 10.1$$

For a bed consisting of 60 layers of S300 mesh used to coalesce a toluene/water dispersion at  $1.5 \times 10^{-2}$  m/s, equation 10.1 predicts that  $\lambda = 19.0 \text{ m}^{-1}$ .

10.1.2. Spielman and Goren Equation.

This model <sup>84</sup> assumes that suspended drops are transported to collectors and coalesce into a previously capture bulk of liquid. Under the action of hydrodynamic, gravitational and capillary forces, the coalesced liquid drains through the packing as a continuum. The immiscible liquids were assumed to flow within fixed microscopic channels with the non-wetting liquid flowing inside; each channel being described by Darcy's Law.

Parameter	Symbol	Value
Collector Diameter	$d_c$	30.5 $\mu\text{m}$
Aperture Diameter	$d_a$	53.0 $\mu\text{m}$
Dispersed Phase Density	$\rho_d$	866.9 $\text{kg}/\text{m}^3$
Continuous Phase Density	$\rho_c$	1000 $\text{kg}/\text{m}^3$
Dispersed Phase Viscosity	$\mu_d$	$0.58 \times 10^{-3} \text{Ns}/\text{m}^2$
Continuous Phase Viscosity	$\mu_c$	$1.00 \times 10^{-3} \text{Ns}/\text{m}^2$
Boltzman's Constant	$k'$	$1.38048 \times 10^{-23} \text{J}/\text{K}$
Absolute Temperature	T	293 K
Hamaker Constant	Q	$0.55 \times 10^{-20} \text{J}$
Hydrodynamic function	A	$2 - \log_e N_{\text{Re}}$

Table 10.1 Basic set of parameters used in comparison of capture mechanisms and filter coefficients.

Spielman and Goren<sup>84</sup> suggested that London-Van der Waal's forces are of sufficient magnitude to overcome any hydrodynamic retardation effects and were included in the evaluation of capture efficiency. Their equation, for continuous phase wetted beds, was obtained by correlation of experimental data with a modified Adhesion number,

$$\lambda = 0.29 \frac{d_p^2}{d_c^3} \left[ \frac{Q d_c^2}{\mu_c u d_p^4} \right]^{0.25} \tag{10.2}$$

This equation predicts  $\lambda = 195 \text{ m}^{-1}$  for similar conditions to those described in Section 10.1.1 and for a drop diameter,  $d_p = 25 \text{ }\mu\text{m}$ . But, equation 10.2 is not based on the model, and since a considerable amount of data is required to determine the constant and exponent, it is of limited use in coalescer design.

10.1.3. Sherony and Kintner Equation.

Sherony<sup>64</sup> was the first to develop a model for fibrous bed coalescence and to use it to derive a design equation. It was based on the 'travelling drop' model discussed in Section 5.4.2 and drop capture was assumed to occur by interception and inertial impaction. The final equation was expressed in terms of an overall coalescence efficiency,  $\eta_c$  and the average saturation,

$$\lambda = \frac{0.75}{d_c} \left[ \frac{\bar{s}}{1 - \bar{s}} \right] (1 - e_1) \left[ 1 + \frac{d_p}{d_c} \right] \eta_c \tag{10.3}$$

From the correlation between  $\eta_c$  and  $\frac{N_{Re}}{e_1}$  given in

Sherony's paper, using the data of Table 10.1,  $\eta_c = 0.15$ .

Also for a mean saturation of 0.25, equation 10.3 gives

$$\lambda = 672 \text{m}^{-1}.$$

10.1.4. Rosenfeld and Wasan Equation.

This model <sup>65</sup> also advocated the 'travelling drop' hypothesis but unlike Sherony's model, did not assume that when a drop detaches from a fibre, it is replaced by an identical one and that detachment occurs after a single coalescence event. Rosenfeld introduced an effective collector diameter,  $d_{ce}$  to account for held drops and introduced a factor,  $\beta$  to relate the collision frequency to coalescence efficiency,

$$\lambda = \frac{8 \beta (1-e_1) d_p}{\pi^2 d_c^2 e_1 (1-\bar{S})} \left[ \frac{2 d_{ce} + d_p}{d_{ce} + d_p} \right] \quad 10.4$$

where  $d_{ce} = d_c \left[ \frac{1-e_1(1-\bar{S})}{1-e_1} \right]$

A typical value of  $\beta$  was determined by Sherony <sup>64</sup> to be 0.41 which produces a filter coefficient,  $\lambda = 8486 \text{ m}^{-1}$ . Rosenfeld applied equation 10.4 to Spielman's data to discover that it was necessary to introduce another term to represent the filter coefficient for operation of the coalescer above a critical velocity. Since this critical velocity must be evaluated experimentally, the model is not adequate for design purposes.

The calculated values of filter coefficient using the above four equations vary over four orders of magnitude for the same operating conditions which alone illustrates the shortcomings of these models. However, this is not entirely surprising in view of possible interactions between operating parameters in the extremely complex coalescence process. Coalescence of secondary dispersions has been studied using different porous media with many systems under an extensive range of operating conditions but several basic principles have evolved. Both filter coefficient and pressure drop depend on the saturation in the bed and so

determination of the latter by theoretical or experimental methods is essential. In the following sections, a combined approach is discussed in an attempt to relate these parameters quantitatively.

## 10.2 THEORETICAL COMPARISON OF CAPTURE MECHANISMS.

Although many mechanisms have been suggested for drop capture, it is desirable to determine their relative contributions to the overall capture efficiency under practical operating conditions. This comparison was designed to produce an equation for estimation of the rate of drop capture in a coalescer.

The variables investigated in this experimental study included superficial velocity and drop diameter which both affect theoretical capture efficiency. Drop diameter may be treated as a variable since the inlet dispersion was polydisperse. Drop capture efficiencies due to interception, London-Van der Waal's forces, diffusion and sedimentation were determined employing a basic set of parameters, relevant to the experimental work, presented in Table 10.1. The equations for evaluation of the individual mechanisms were discussed in Section 5.2 and are summarised in Table 10.2. The calculations were performed for a range of values of drop diameter and superficial velocity using a computer program listed with the output in Appendix L. The comparison was made with Langmuir's expression characterizing the flow parameter,  $A$  for viscous flow over a cylindrical collector. Direct interception (pore catchment) was not included in the analysis since the efficiencies cannot be compared directly and this mechanism only becomes significant when the drop size exceeds the effective aperture diameter. Inertial impaction was also excluded since drop density is less than continuous phase

Mechanism	Characteristic Dimensionless Group	Equation for Capture Efficiency
Interception	Interception number, $N_R$	$\eta_I = \frac{1}{2A} \left[ 2(1+N_R) \log_e (1+N_R) + \frac{1}{(1+N_R)} - (1+N_R) \right]$
Direct Interception	Direct Interception number, $N_{RD}$	$\eta_{DI} = 1 (N_{RD} \geq 1) ; \eta_{DI} = 0 (N_{RD} < 1)$
Inertial Impaction	Stokes' number, $N_{Stk}$	$\eta_{II} = \frac{N_{Stk}^3}{N_{Stk}^3 + 0.77 N_{Stk}^2 + 0.22}$
Sedimentation	Gravity number, $N_G$	$\eta_G = N_G$
London Forces	Adhesion number, $N_{Ad}$	$\eta_L = \frac{N_R^2}{A} \left[ \frac{3\pi A N_{Ad}}{2} \right]^{1/3}$
Diffusion	Peclet number, $N_{Pe}$	$\eta_D = 2.16 (2A)^{-1/3} N_{Pe}^{-2/3}$

Table 10.2 Dimensionless Groups and Equations used in Capture Mechanism Evaluation.

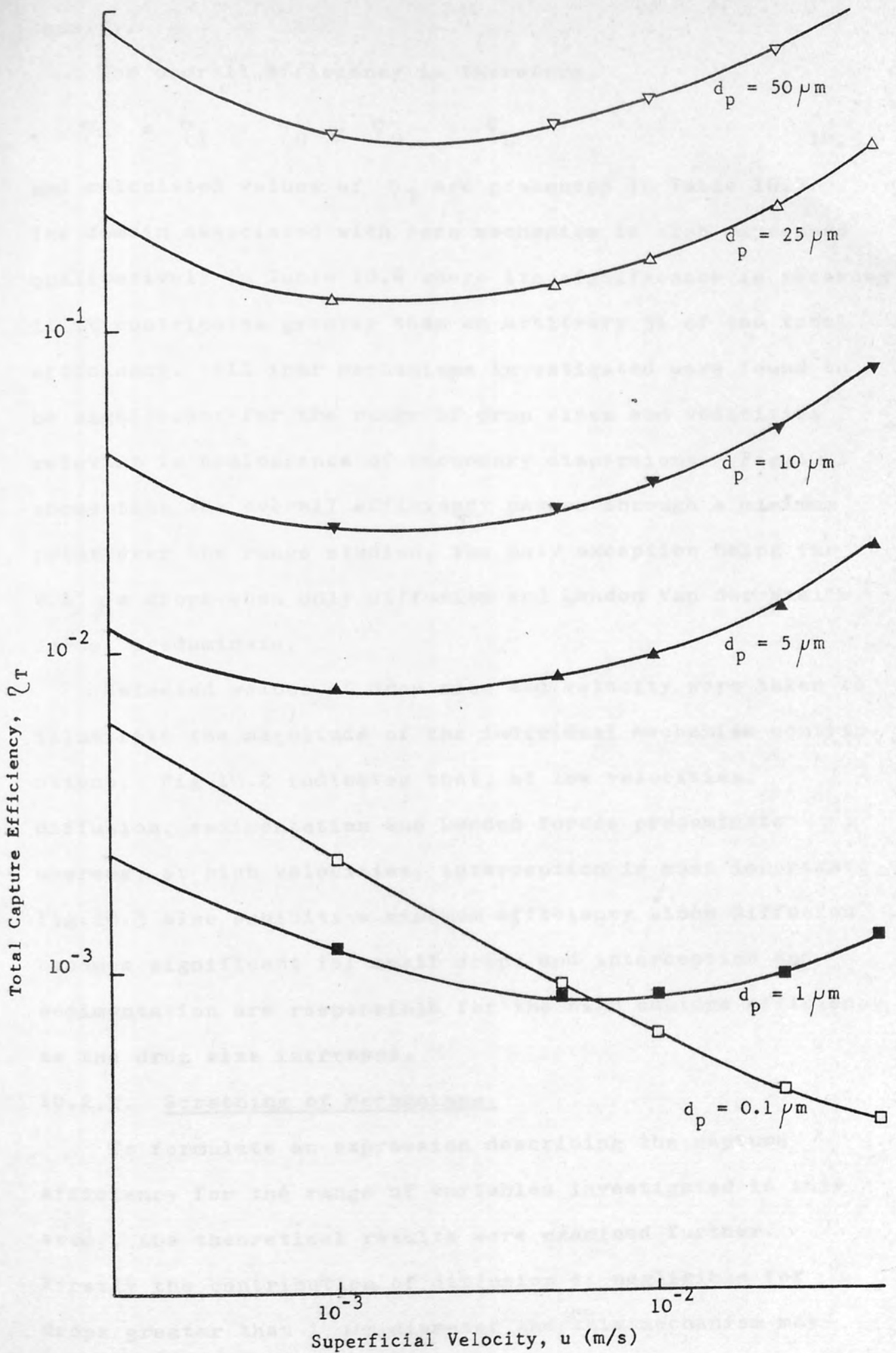


Fig 10.1 Variation of Total Capture Efficiency with Velocity for different Drop Sizes.

density.

The overall efficiency is therefore,

$$\eta_T = \eta_I + \eta_D + \eta_G + \eta_L \quad 10.5$$

and calculated values of  $\eta_T$  are presented in Table 10.3. The domain associated with each mechanism is also expressed qualitatively in Table 10.4 where its significance is recorded if it contributes greater than an arbitrary 5% of the total efficiency. All four mechanisms investigated were found to be significant for the range of drop sizes and velocities relevant to coalescence of secondary dispersions. Fig.10.1 shows that the overall efficiency passes through a minimum point over the range studied, the only exception being for 0.1  $\mu\text{m}$  drops when only diffusion and London Van der Waal's forces predominate.

Selected values of drop size and velocity were taken to illustrate the magnitude of the individual mechanism contributions. Fig 10.2 indicates that, at low velocities, diffusion, sedimentation and London forces predominate whereas, at high velocities, interception is most important. Fig.10.3 also exhibits a minimum efficiency since diffusion becomes significant for small drops and interception and sedimentation are responsible for the high capture efficiency as the drop size increases.

#### 10.2.1. Screening of Mechanisms.

To formulate an expression describing the capture efficiency for the range of variables investigated in this study, the theoretical results were examined further. Firstly the contribution of diffusion is negligible for drops greater than 1  $\mu\text{m}$  diameter and this mechanism may thus be eliminated. London-Van der Waal's forces are only significant when the overall efficiency is less than

Drop Diameter, $d_p$ ( $\mu\text{m}$ )	Superficial Velocity, $u$ ( $\times 10^{-2}$ m/s)						
	0.01	0.1	0.5	1.0	2.5	5	10
0.1	0.0089	0.0022	0.0009	0.0006	0.0004	0.0003	0.0003
1	0.0033	0.0012	0.0008	0.0008	0.0009	0.0012	0.0025
5	0.0190	0.0076	0.0083	0.0097	0.0137	0.0210	0.0475
10	0.0669	0.0248	0.0280	0.0336	0.0483	0.0747	0.1713
25	0.3854	0.1244	0.1384	0.1666	0.2414	0.3757	0.8657
50	1.4722	0.4123	0.4366	0.5230	0.7573	1.1798	2.7213

Table 10.3 Total Capture Efficiency for Range of Velocities and Drop Diameters encountered in Secondary Dispersion Coalescence (enclosed section describes range of variables encountered in this study).

Drop Diameter, $d_p$ ( $\mu\text{m}$ )	Superficial Velocity, $u$ ( $\times 10^{-2}$ m/s)						
	0.01	0.1	0.5	1.0	2.5	5	10
0.1	D	D	DL	DL	DL	DL	IDL
1	DGL	IDL	IDL	IDL	IDL	IL	IL
5	IGL	IGL	IL	IL	IL	I	I
10	IGL	IGL	IL	I	I	I	I
25	IG	IG	I	I	I	I	I
50	IG	IG	IG	I	I	I	I

Table 10.4 Significance of Different Capture Mechanisms at 5% Contribution Level for Range of Velocities and Drop Diameters encountered in Secondary Dispersion Coalescence (enclosed section describes range of drop diameter and velocity encountered in this study).